Development of A Continuous-Motion Piezoelectric Rotary Actuator for Mechatronics and Micropositioning Applications

by

Selcuk Gursan
B.Sc., Dokuz Eylul University, 1987

A Thesis Submitted in Partial Fulfillment of the
Requirements for the Degree of
MASTER OF APPLIED SCIENCE
in the
Department of Mechanical Engineering

We accept this thesis as conforming
to the required standard

[redacted]
Dr. Y. Stepanenko, Supervisor (Dept. of Mechanical Engineering)

[redacted]
Dr. S. Dost, Co-supervisor (Dept. of Mechanical Engineering)

[redacted]
Dr. Z. Dong, Departmental Member (Dept. of Mechanical Engineering)

[redacted]
Dr. P. Agathoklis, External Examiner (Dept. of Electrical and Computer Engineering)

Supervisors: Dr. Yury Stepanenko and Dr. Sadik Dost

Abstract

The main objective of this thesis is the development of high-precision positioning devices for a large range of displacements. As an actual representative of this class of devices, a piezoelectric rotary actuator was selected for the development. The basic principles of the design can, however, be easily applied to similar linear positioning devices. In addition to the high-resolution requirements, practicality of the design, reasonable-cost for manufacturing, suitability for commercialization, and good potential for further miniaturization are also among the other requirements.

Positioning devices with high accuracy and unlimited range of displacements are required by many industrial applications. High-precision micro machining, laser guidance systems, medical and physical instrumentation (for example, high-resolution microscopes) and microrobotics are some examples to mention.

The development of a piezoelectric rotary actuator with such targeted characteristics puts forward a number of theoretical and design problems. The most challenging components from a mechanical/dynamics point of view are the flexure hinge mechanisms. These mechanisms are intended for the magnification of piezoelectric displacements. They are of complex shape, and they work in dynamically intensive regimes. The development of an approach for stress analysis and the design of components with thin elastic bridges were the theoretical challenges of the work. The controller design for synchronization of multiple piezoelectric actuators in multi-micro-step regime constitutes the control part of the work. The last, but not the least challenges were the selection of the proper material for the piezoelectrics and flexure hinge mechanisms, and modelling the entire mechatronics system prior to the actual fabrication.

This thesis presents the entire process of the development from a novel idea to the

design, fabrication, implementation of the experimental prototype, and laboratory testing.

The actuator proposed in this thesis is of stepper type; it generates a continuous rotary motion by combining very small angular displacements. The main advantages of the proposed actuator over the existing ones can be summarized as follows:

- Compact and reliable design,
- Less number of multilayer piezoelectric devices[†] in the system,
- High resolution and better torque-speed characteristics,
- Simpler driving sequence that is achieved by a simple switching circuit,
- Suitability for further miniaturization.

The actuator consists of three functional subunits, namely clamping, clutching and rotational flexure units. While the clamping and clutching units accommodate two multilayer piezoelectric devices, the rotational flexure unit includes only one of them. Step-wise continuous rotary motion is generated by driving these piezoelectric devices in a predetermined logic and by employing very small displacements, 30 μm, and extremely high blocking forces, 10000 N, generated by the piezoelectric devices.

The results of this thesis work verify the potential of piezoelectric actuation for high-precision positioning devices. The developed actuator has been modelled and fabricated based on the design approach suggested in this thesis. The unique flexure amplification mechanisms of the actuator as well as the entire actuator itself have been tested, and the results have been found to be highly promising. The agreement between the results of the physical experiments and those of the simulations validates the practical modelling approach suggested and utilized in this thesis. The proposed

[†]The term *piezoelectric device* will be used hereafter to refer to a single piezoelectric unit itself.

actuator has potential to provide even better characteristics with the final suggestions presented in the thesis.

Examiners:

[redacted]

Dr. Y. Stepanenko, Supervisor (Dept. of Mechanical Engineering)

[redacted]

Dr. S. Dost, Co-supervisor (Dept. of Mechanical Engineering)

[redacted]

Dr. Z. Dong, Departmental Member (Dept. of Mechanical Engineering)

[redacted]

Dr. P. Agathoklis, External Examiner (Dept. of Electrical and Computer Engineering)

Table of Contents

List of Tables

List of Figures

Acknowledgements

I would like to thank my supervisors, Dr. Yury Stepanenko and Dr. Sadik Dost, for their continuous assistance and guidance throughout my program as well as for their financial support.

I also thank IRIS (*Institute for Robotics and Intelligent Systems*) for making this work come true with their financial support.

Discussions on potential designs and material selections with Dr. Mustafa Kaya helped so much; his help is greatly appreciated. Also, Nicholas Audet was there whenever he was needed; I acknowledge and appreciate his genuine help as well.

I thank Dr. Behrouz Tabarrok for his support that he provided when it was needed. I acknowledge Rodney Katz's genuine efforts while manufacturing the parts; I also thank him for being patient with me. I acknowledge Kevin Jones' efforts while designing and putting the driving circuit together; I also thank him for lending me some of his equipment. I thank Dean Addison, a dear friend, for his program that he wrote to correct some of the postscript images.

I thank Oktay and Yasemin Gursan, my brother and lovely sister, so much for believing in me.

Finally, Ibrahim Aytan and Dr. Ahmet Oztarhan will always be remembered; I wish I were able to find the right words to thank them enough...

To the most wonderful people of my life:

MY MOM AND DAD

Chapter 1

Introduction

1.1 Problem Statement

Piezoelectricity arises due to an interaction between the electrical and mechanical fields in solids. It was discovered by *Pierre Curie* and *(Paul) Jacques Curie* in the 1880s. They observed that certain types of crystals develop an electrical potential on their surfaces when an external mechanical force is applied. This is what is known as the *direct piezoelectric* or, in short, *piezoelectric effect.* They also showed that the same crystals experience a mechanical deformation when they are subjected to an electric field. This effect is called the *converse* or *reciprocal piezoelectric effect.*

Soon after the recognition of their discovery, many researchers were attracted to the theoretical formulation and practical applications of this phenomenon. The first practical application of piezoelectricity appeared during World War I as an underwater high frequency sound wave emitter and receiver. This was followed by many other significant applications which have utilized the piezoelectric effects successfully. Historical developments of piezoelectricity are summarized briefly in Chapter 2.

Evolving technology has led to numerous applications where the direct and converse piezoelectricity were used for sensing and actuation, respectively. Micropositioning devices having extremely good response characteristics and fine resolution have been the most promising applications over the last four decades. In fact, two of the breakthrough inventions namely *Scanning Tunneling Microscope* and *Atomic Force Microscope* utilize the converse piezoelectric effect in a scanning actuator making possible to see the atom. In addition, piezoelectricity has also been used in *mechatronics* and *microrobotics* as both actuators and sensors. The most promising applications of the converse piezoelectric effect are reviewed in Chapter 3.

Linear and rotary piezoelectric actuators have attracted great interest because of their advantages over conventional electromagnetic drives. Higher force/active area and torque/volume ratios, very good and controllable resolution, and the absence of any electromagnetic disturbances are the most significant advantages. Thus, the generation of a continuous linear or rotary motion by utilizing the converse piezoelectric effect has become one of the most attractive but challenging topics in the field. Many devices have been proposed for various applications such as mechatronics, adaptive optics and space devices over the last two decades. In such applications, the piezoelectric actuation became an alternative over the conventional actuation techniques.

Various linear and rotary actuators are discussed in Chapter 3, and their driving principles are presented. In general, the generation of a continuous linear or rotary motion by utilizing the converse piezoelectric effect is based on the following two main principles:

1. Generating a surface travelling wave in an elastic medium,

2. Combining small linear or angular displacements, created via piezoelectric actuation, to generate the step-wise continuous motion.

The first method constitutes the basis for what is known as *piezoelectric motors* or *ultrasonic motors* on which several patents have been issued in Japan and in the US since the 1980s. Although such actuators have found many applications, they introduce substantial problems because of their short life time. This is mainly because of the induced high alternating stresses in the piezoelectric medium.

The second method generates step-wise linear or rotary motion by combining very small linear or angular displacements at a high repeating frequency. A linear version of this type has already been patented and commercialized [1].

The review of the previously proposed rotary actuators given in Chapter 3 has revealed that some of these actuators could not go beyond being a laboratory set-up because of various problems involved. Such an actuator is not only required to move a shaft or rotate it but also to be confined in a compact and reliable package. These kinds of features would basically make a proposed design successful in applications. High resolution and torque-speed characteristics are also among the other parameters that the proposed actuator should be able to provide. A relatively simpler driving circuit and potential for further miniaturization should also come with the proposed development for a possible commercialization.

A new and unique piezoelectric rotary actuator is introduced in this thesis. The proposed actuator is a successful implementation of the converse piezoelectric effect. *3-D modelling*[†] of the proposed actuator prior to the actual manufacturing, finite element simulations for the developed amplification mechanisms, which are crucial to the success of the prototype, and, finally, some other key points for the process of generating step-wise continuous motion are all elaborated in this thesis.

Based on the approach explained in this thesis, a prototype of the proposed actua-

[†]The terms *3-D modelling* or *Solid modelling* will be used hereafter to refer to the physical modelling of the actuator.

tor has been built. Conceptual design has led to a working prototype through various steps, namely a carefully implemented 3-D solid modelling, preparation of the part drawings, finite element simulations, and a carefully carried out assembly process. Successful transition from the computer-generated images to the real prototype has been achieved without even any minor modifications during the implementation.

1.2 Thesis Outline

This thesis is divided into three main chapters. Following an introduction chapter, Chapter 2 begins with a brief historical background of piezoelectricity and introduces some fundamental concepts related to the phenomenon. Fundamental mechanism of piezoelectricity along with the linear constitutive equations are also given in this chapter. Definitions of various piezoelectric coefficients are also included.

Chapter 3 explains some of the concepts and definitions that are important in micropositioning applications. The most common and basic configurations of piezoelectric devices are also introduced in this chapter. Multilayer piezoelectric devices (or piezoelectric stack assemblies) are, in particular, discussed in detail since this configuration is utilized for the proposed rotary actuator. The need for amplification of piezoelectric actuation along with the common amplification techniques are discussed in this chapter as well.

Chapter 3 also presents a brief review of the applications of the converse effect. Brief discussions on basic operating principles for different piezoelectric devices are also given. Some previously proposed rotary actuators are discussed in terms of their basic driving principle, main advantages and drawbacks, and torque-speed characteristics. This review was essential for establishing the comparison criteria upon which the proposed rotary actuator of this work has been developed.

Chapter 4 is the main chapter in which the proposed actuator is discussed in detail. First, the basic operating principle of the proposed actuator is laid out schematically. Then, the actual design and its subunits are introduced. Important details involved in the process of generating step-wise continuous rotary motion are elaborated. Discussions given in this chapter are mainly based on the conducted research and the expertise developed throughout this thesis work. A summary of the characteristics of the multilayer piezoelectric devices, which were used to build the prototype, is also given in Chapter 4.

Finite element simulations of the developed flexure amplification mechanisms are also presented in Chapter 4. The results are presented in an easy-to-follow graphical and tabulated format for each flexure mechanism. §4.4 of Chapter 4 is completely allocated for the experiments performed. General methodology, the results and comparisons with the simulation results are presented and discussed. Finally, the switching frequency-speed characteristic (for zero load) and the torque-speed characteristic of the prototype are also presented in this chapter. A comparison with the previously proposed piezoelectric rotary actuators of the same nature is also made. The chapter is concluded with a brief discussion on the driving circuit.

A summary of the results is given in Chapter 5.

Appendices A and B contain some additional equations for index abbreviations and piezoelectric coefficients. Detailed technical drawings of the prototype are given in Appendix C. All these drawings were generated from the 3-D solid model of the proposed actuator, and they were proven to be successful having gone through various manufacturing processes. All required geometric and dimensional tolerances are specified on these drawings clearly. This appendix has been included hoping that it might help other researchers. Finally, Appendix D provides some supplementary illustrations and pictures of the experimental set-up and the prototype itself.

Chapter 2

Piezoelectricity

Piezoelectricity was first observed by *Pierre Curie (1859–1906)* and his elder brother, *(Paul) Jacques Curie (1855–1941)*, in the 1880s [2]. They showed that when certain types of crystals are deformed mechanically, they develop electrical potential. Conversely, when an electric field is applied to such crystals, they undergo a mechanical deformation. The former effect, in fact, is the basis for modern piezoelectric sensors and called *piezoelectric* or *direct piezoelectric effect* while the latter is the basis for modern piezoelectric actuators and called *converse* or *reciprocal* or, sometimes, *inverse piezoelectric effect.*

In this chapter, first, a brief review of historical developments will be introduced. This will be followed by a short section on the basic mechanism of piezoelectricity. Finally, the chapter will be concluded by discussing some common piezoelectric materials and the constitutive equations of piezoelectricity.

2.1 Historical Developments

Electrification in a heated tourmaline crystal had been known in Europe since about the eighteenth century. In 1824, Brewster introduced the name *pyroelectricity*[†] by observing the effect with various kinds of crystals. Then, the first definite theory of pyroelectricity was introduced by Lord Kelvin stating that pyroelectricity was the result of permanent polarization. Since then, the effect has been known as an interaction between electrical and thermal fields [3].

The Curie brothers showed that some crystals show positive and negative charges on certain portions of their surfaces when they are compressed in particular directions. The observed charges are proportional to the pressure, and they disappear when the applied pressure is removed. They were able to observe this effect by placing a weight on some particular crystals and measuring the induced charges on a Thomson electrometer [2].

This discovery was recognized by others soon; it was a "no-chance" discovery in Cady's own words [3]. Pierre Curie had previously studied the relation between pyroelectricity and crystal symmetry. This is, in fact, what led two brothers to looking for a similar relation between electrification and pressure as well. They looked into not only the relation between the electrification and applied pressure but also the relation between the induced electrification and the direction of the applied stress. The best explanation of the results of their investigation probably lies in their own words, translated from their paper announcing the discovery [2], [3]:

> "Those crystals having one or more axes whose ends are unlike, that is to say hemihedral crystals with oblique faces, have the special physical

[†]The prefix "pyro-" comes from a Greek word which means "fire."

> property of giving rise to two poles of opposite signs at the extremities of these axes when they are subjected to a change in temperature; this is the phenomenon known under the name of *pyroelectricity.*
>
> We have found a new method for the development of polar electricity in these same crystals, consisting in subjecting them to variations in pressure along their hemihedral axes.
>
> ...
>
> The effects produced are analogous to those produced by heat [pyroelectricity]: during a compression, the ends of the axis along which we are acting are charged with opposite electricities; when the crystal is brought back to the neutral state and the compression is relieved, the phenomenon occurs again, but with the signs reversed; the end which was positively charged by compression becomes negative when the compression is removed and reciprocally... In all these crystals, the effects produced by compression are in the same sense as those produced by cooling; those which result from relieving the pressure are in the same sense as those which come from heating."

The proposed discovery was, then, verified by Pierre and Jacques Curie with a series of experiments by using the following crystals: zinc blende, sodium chlorate, boracite, tourmaline, quartz[SiO_2], calamine, topaz, tartaric acid, cane sugar, and Rochelle salt[$(NaKC_4H_4O_6 \bullet 4H_2O)$]. In later papers, some other crystals having piezoelectric properties, the first quantitative measurements of the phenomenon in quartz and tourmaline, practical applications of piezoelectric crystals, and the verification of the converse effect were also described by the Curie brothers. In fact, explanation of converse effect, showing that quartz crystal has the same piezoelectric coefficients for both direct and converse effects, was based on Lipmann's discussion

of application of thermodynamic principles to reversible processes involving electric quantities. Lipmann's theory, on the other hand, was linked to some other studies done previously by Lord Kelvin in 1877. Finally, the name *Piezoelectricity*[†], a term which was accepted immediately by others including the Curie brothers themselves, was proposed by Hankel [4]. Similarly, since then, piezoelectricity has been known as an interaction between the electrical and mechanical fields in solids.

Electrostriction is another electromechanical interaction where strain is introduced with an applied electric field. In fact, the converse piezoelectric effect and electrostriction tend to be treated equally assuming that the converse piezoelectric effect is a special case of electrostriction. However, these two phenomena are essentially different in that deformations caused by electrostriction are proportional to the square of the applied field, that is independent of the direction of the applied electric field, whereas deformations caused by piezoelectricity are directly proportional to the applied electric field and dependent on the direction of the field. Electrostriction was mentioned here for the sake of completeness.

Based on the aforementioned studies, formulation of the piezoelectric phenomenon was studied by P. Duhem and F. Pockels, and, mostly, by Woldemar Voigt in 1894. Having remained silent for a long time, piezoelectricity found its first valuable practical application during World War I. Pierre Curie's student Paul Langevin (1872–1972) used the piezoelectric property of quartz to produce ultrasonic waves [2]. The device was used as an emitter and also a receiver for high frequency sound waves under water. The idea was developed further after the war, and it found extensive use in some other practical applications in many fields, such as chemistry, biology and industry during peacetime and as a submarine detector during World War II. In 1917, Bell Telephone Laboratories built loudspeakers, microphones and phonograph pickups us-

[†]The prefix "piezo-" comes from a Greek word which means "to press."

ing the piezoelectric properties of Rochelle salt. Some valuable theories were also developed by Max Born, Bragg and Gibbs in 1920 and 1925, respectively [4].

Walter Guyton Cady, whose famous book "*Piezoelectricity*" [3] has been one of the most valuable sources for the people working in this field, was attracted to the subject by Langevin's ultrasonic wave transducer. In 1921, he showed the use of quartz resonator as a filter which produces much more stable oscillations. This was a major application which was later used to control the frequency of military communication equipment during World War II. In later years, studies focused on finding new materials which are as stable and rugged as quartz and as good as Rochelle salt in terms of piezoelectric properties.

These materials were ceramics with desirable piezoelectric properties. In about 1947, the first commercial ceramic barium titanate, $BaTiO_3$, was on the market as phonograph pickups. There were three basic steps lied at the root of the discovery and understanding of the piezoelectric ceramics: the discovery of high dielectric constant, realization of the fact that the cause of high dielectric constant was ferroelectricity, and, finally, discovery of the poling process of ceramics [5]. In many publications and patent applications, it was mentioned that barium titanate showed both direct and converse piezoelectric effects. However, how that occurred was not made clear enough. The answer was the *poling process.* Poling process is described as applying a high voltage, which is high enough to reverse the electric moments of spontaneously polarized regions, to the ceramic. The first publication of poled piezoelectric barium titanate was made by S. Roberts. The first set of values for the piezoelectric coefficients of the same ceramic was studied and given by Hans Jaffe [5]. Rapid development of barium titanate followed to improve the temperature stability and voltage outputs. In 1952, piezoelectric lead niobate, having a different structure, was discovered. In 1954, very strong and stable piezoelectric effects were discovered

in *lead zirconate titanate (PZT)*†, $Pb(Ti, Zr)O_3$. Lead zirconate titanate with various additives became the dominant piezoelectric ceramic soon. *Polymers* also make up another class of materials having good piezoelectric properties. Piezoelectric polymers show excellent charge storage capabilities, and they are available as flexible thin films [2]. Polymers are, however, out of this thesis' scope.

Even today, many scientists all over the world are working independently to improve the piezoelectric characteristics of the ceramics mentioned above, especially lead zirconate titanate. Production of such ceramics with desired characteristics such as good temperature stability, low hysteresis, high electromechanical coupling factor and high linearity is the main challenge. These characteristics will be discussed later in this thesis.

2.2 Interactions of Electrical, Mechanical, and Thermal Fields in Solids

In this section, the interactions between the electrical, mechanical and thermal fields in solids are presented. Figure 2.1 [6] shows these interactions schematically. Vertices of the outer triangle show the intensive variables whereas the vertices of the inner triangle show the extensive variables. Commonly used intensive and extensive variable pairs are shown in Table 2.1.

A small change in one of these variables causes a corresponding change in the other. This is represented by the lines joining the circles. Each property shown on each line, on the other hand, is the property through which the interaction occurs.

†The acronym PZT has become a common term for lead zirconate titanate, and it will, also, be used hereafter in this thesis for brevity.

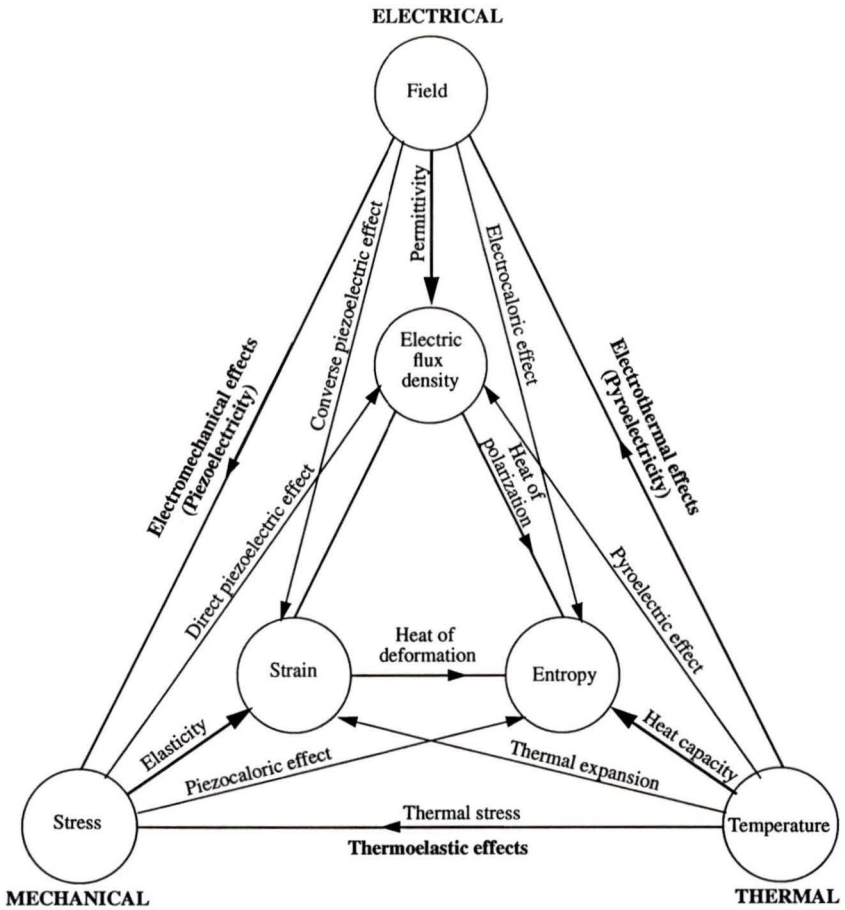

Figure 2.1: Interactions of mechanical, electrical, and thermal fields.

Dark lines represent the direct effects. These lines, connecting the thermal, elastic, and electrical variables, define the physical properties known as heat capacity, elasticity and electrical permittivity, respectively. A small increase in temperature, for example, causes an increase in entropy, and this change is proportional to the heat capacity. Coupled effects are also shown. These are represented by the lines joining different corners of the diagram. A change in temperature, for instance, will introduce an elastic strain which is proportional to the thermal expansion coefficient of the material. This is, in fact, what is known as thermal expansion.

Direct and converse coupled effects are also represented by the lines connecting

System	Intensive variable	Extensive variable
Thermal	Temperature	Entropy
Mechanical	Elastic stress	Elastic strain
Electrical	Electric field	Electric displacement

Table 2.1: Commonly used intensive and extensive variable pairs in mechanical, electrical and thermal interactions.

related variables. Physical relations between the changes in internal and external conditions and corresponding physical properties are summarized in Table 2.2.

Change in	has effect on		
	Entropy $\mathcal{S}$	Strain $\boldsymbol{S}$	Polarization $\boldsymbol{P}$
Temperature T	Thermal capacity $\div T$	Expansivity	Pyroelectric effect
Stress σ	Piezocaloric effect	Elastic compliance	Piezoelectric effect
Electric field E	Electrocaloric effect	Converse piezoelectric effect	Susceptibility

Table 2.2: Physical relations between intensive and extensive variables and corresponding physical properties.

Physical properties have values having the ratios of small changes in the parameters shown. Suspectibility, for example, is given by $\eta = d\boldsymbol{P}/d\boldsymbol{E}$. In general, the relations are not linear. Three of these properties, namely elastic compliance, dielectric permittivity (or susceptibility) and specific heat, are called principal properties since they relate the parameters of similar nature (thermodynamically conjugate), that is, both electrical, both mechanical or both thermal. As seen in the table, susceptibility relates the electrical parameters $\boldsymbol{E}$ *and* $\boldsymbol{P}$; elasticity relates the mechanical parameters $\boldsymbol{\sigma}$ *and* $\boldsymbol{S}$; and, finally, specific heat relates the thermal parameters T and $\mathcal{S}$. Other properties are called coupled properties since they relate the parameters of different nature. They are electrothermal (pyroelectric and electrocaloric) coefficients, thermoelastic (expansivities and piezocaloric) coefficients and electrome-

chanical (piezoelectric) coefficients. By examining the table given, one can see, for example, that piezoelectric effect is a measure of the change in polarization caused by an applied external stress, or vice versa.

2.3 Fundamental Mechanism of Piezoelectricity

Piezoelectricity is a sub-phenomenon of *Ferroelectricity.* This fact makes it almost impossible to explain the basic mechanism of piezoelectricity without giving the definitions of ferroelectricity itself as well as some others fundamental definitions of basic crystallography. These definitions are included to help readers understand the discussions given later in this section.

2.3.1 Ferroelectricity and Related Definitions

The term *Ferroelectric*[†] was first used by Valasek, in 1921, to show the analogy between ferromagnetic iron and Rochelle salt [7]. Analogy was made in terms of nonlinear hysteretic dielectric properties of Rochelle salt and magnetic behaviour of ferromagnetic iron.

By the most general definition, ferroelectrics are materials possessing a *spontaneous electric polarization (or electric dipole moment)* P_s which can be reversed, with no net change in magnitude, by an applied electric field E [8], [9]. This reversing process is called *switching*, and it is accompanied by *hysteresis*, which is a significant property of ferroelectrics. The dipoles are produced because the centres of positive and negative charges in each structural unit of the substance do not coincide. The

[†]Materials having ferroelectric properties are also called *Seignette-electrics* after P. de la Seignette, who first studied on Rochelle salt in the seventeenth century.

dipole moment may result from the charges of a simple array of ions in a primitive cell or a very complex arrangement in a multiple cell. Electrical polarization, called *spontaneous polarization*, occurs if the dipoles throughout the sample are aligned so that self-cancellation among these dipoles does not take place. The word *spontaneous* is used to emphasize that the polarization has a non-zero value even if an external electric field is not applied. Spontaneous polarization should be distinguished from induced polarization which takes place under an applied external electric field.

Polarization can be altered by changing the external conditions. In fact, the terms *dielectric, piezoelectric and pyroelectric* refer to the polarization changes caused by small changes in externally applied electric field, stress, and temperature, respectively. These changes can be detected as currents by using an appropriate circuit between the conductive electrodes placed on the surfaces of the substance.

Ferroelectrics are all solids and non-metallic materials. They are a distinct subgroup of pyroelectric materials. In general, all ferroelectrics are also pyroelectrics, and all pyroelectrics are also piezoelectric; *vice versa* cases, on the other hand, are not necessarily true for both cases. Being able to reverse the dipole moment is where ferroelectrics differ from pyroelectrics. Even though all pyroelectrics have a dipole, it is not necessarily possible to reverse the dipole by an externally applied electric field. It might be because the field needed to reverse the dipoles is greater than the electrical breakdown field of the substance, or dipoles might be due to an asymmetric and non-reversible arrangement of atoms. Thus, ferroelectricity is an empirical distinction separating ferroelectrics from non-ferroelectric subsets of pyroelectric substances on the basis of experimental observation [6].

Either *Polarization P* or *electric flux density (or electric displacement D)* is one of the variables in the theory of ferroelectricity. In fact, polarization is more suitable for theoretical treatment whereas electric displacement is usually preferred in prac-

tical analysis. Polarization is defined as the dipole moment per unit volume, which is also equal to the surface charge per unit area. As mentioned earlier in this section, ferroelectrics possess spontaneous dipole moment within a certain temperature range. Above this temperature range, ferroelectrics undergo a phase transition process, usually called *ferroelectric transition*, losing their spontaneous dipole moment. The phases with and without dipole moments are called *ferroelectric* and *paraelectric* phases, respectively. Once ferroelectric transition occurs, there is no spontaneous dipole moment and hysteresis loop. The temperature at which this transition takes place is called *Curie temperature.*

Nonlinearity and hysteresis are very fundamental to ferroelectricity. Thus, a couple of words about hysteresis might be very helpful at this point. As stated earlier in this section, in ferroelectric substances, there exist directions along which there is spontaneous polarization. The relation between the magnitude of the polarization and externally applied electric field is not linear, and it is given by a hysteresis loop. A typical hysteresis loop is shown in Figure 2.2.

As seen in Figure 2.2, as the hysteresis loop intersects the P-axis at a non-zero value, in the absence of an external electrical field; there still exists a finite value of polarization. This is, in fact, the spontaneous polarization described earlier. The direction in which spontaneous polarization occurs is called *ferroelectric axis.* The loop shown in Figure 2.2 does not have to be symmetrical with respect to any of the orthogonal axes. In fact, there is no such a symmetry in some ferroelectrics at all. As seen, the polarization is a double valued function of the applied electric field E, and it is determined by the past history of the system in a sense that the sign of the last applied electric field determines the response P.

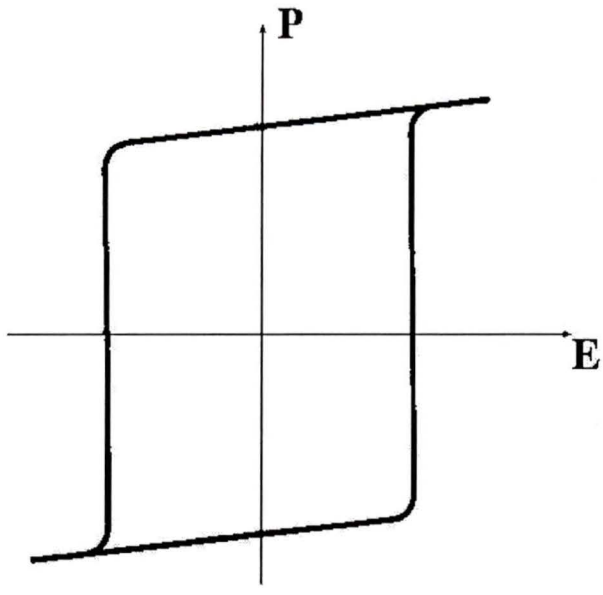

Figure 2.2: Typical dielectric hysteresis loop.

2.3.2 Perovskite Structure

A cubic *perovskite* structure, Figure 2.3, was one of the first simple structures representing the compounds that exhibit ferroelectric properties, and it is, probably, still the most important ferroelectric prototype [5], [7].

This structure can be described as a simple unit cell having a large lower-charged cations A on the corners, such as Na, K, Rb, Ca, Sr, Ba, Pb, etc; a smaller highly-charged cation B, such as Ti, Sn, Zr, Nb, Ta, W, etc, in the center of the cube; and, finally, oxygens in the centers of each face. For $BaTiO_3$, for example, $A = Ba^{+2}$, $B = Ti^{+4}$, and $O = O^{-2}$ constitute the structure.

The representation shown in the figure might be considered as an idealized representation since it is not a simple cubic in most cases. Also, the anions do not necessarily have to be oxygen in order for the structure to be called perovskite.

Although there exist simple ABO_3 compounds, such as $BaTiO_3$, $PbTiO_3$, $PbZrO_3$,

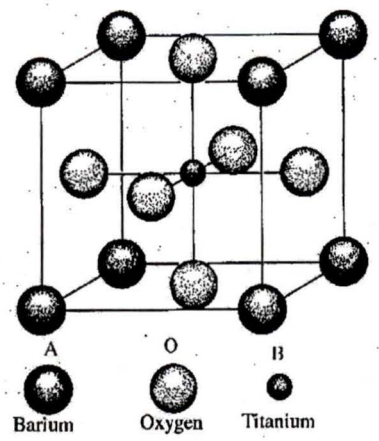

Figure 2.3: Cubic prototype structure of perovskite-type ABO_3 for $BaTiO_3$.

$NaNbO_3$, $KNbO_3$, $AgNbO_3$, WO_3, having interesting high temperature ferroelectric and anti-ferroelectric phases, more complex compounds can also be prepared. $BaTiO_3$ was, on the other hand, the first perovskite-type compound exhibiting ferroelectric properties as mentioned in §2.1.

Unlike single crystal piezoelectrics, ceramics to be piezoelectric must undergo a process called *poling*. Before poling, a ferroelectric ceramic is non-piezoelectric even though the individual crystals constructing the ceramic may be strongly piezoelectric. This is because the polarizations of randomly oriented individual crystals cancel each other. To make the ceramic piezoelectric, a strong electric field must be applied to the specimen above its characteristic Curie temperature. Above the Curie temperature of the ceramic and under applied strong electric field, the polar axes of the crystallites in the ceramic are switched to those directions allowed by the symmetry which are nearest to that of the applied electric field [5]. In other words, under these severe conditions, randomly oriented dipoles become aligned in the direction of applied electric field and remain partially aligned after the field is removed provided that the specimen is first cooled down well below its Curie temperature. This process

is called *poling*, and following this process, the ceramic is said to be *poled.*[†] After poling, the ceramic behaves like a pyroelectric crystal having a net dipole moment. Having being poled, the ceramic will respond to an applied electric field (converse effect) or mechanical stress (direct effect).

2.3.3 Mechanism of Piezoelectricity

Piezoelectric transducers are used to convert mechanical energy to electrical energy (direct effect) or electrical energy to mechanical energy (converse effect). Ferroelectric ceramics such as lead zirconate titanate, $Pb(Ti, Zr)O_3$ or PZT as a common acronym, and barium titanate, $BaTiO_3$, become piezoelectric when they are poled.

During cooling, ferroelectrics undergo a displacive phase transformation and gain spontaneous polarization. $BaTiO_3$ would be a good example to explain this process briefly.

Above its Curie point, which is 120 $°C$, barium titanate is paraelectric having a cubic perovskite structure as shown in Figure 2.3. Below its Curie temperature, the structure becomes tetragonal having shifted Ti^{+4} and Ba^{+2} relative to O^{-2} framework which also becomes distorted. At room temperature, the shifted structure can be represented by Figure 2.4.

Figure 2.4 is a projection view on the (100) plane, and the cell centre coincides with the intersection point of the lines connecting the O^{-2} ions. As seen in the figure, both Ti^{+4} and Ba^{+2} ions are shifted in the same direction, upward in this representation, by different amounts. In the mean time, the top and bottom O^{-2} ions are, also, shifted, downward in this representation, by a certain amount. The

[†]Analogy can be made between poling process and magnetizing of magnets.

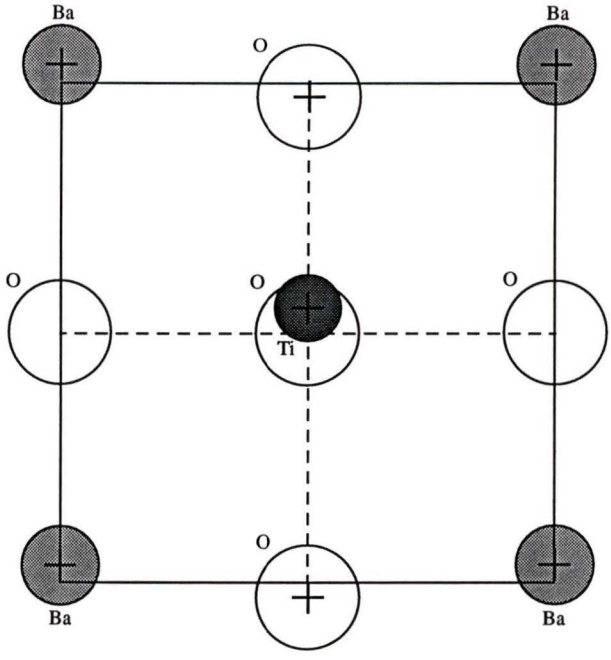

Figure 2.4: A projection on the (100) plane of the tetragonal unit cell of barium titanate having shifted Ba^{+2}, Ti^{+4} and O^{-2} ions.

cubic cell itself has peculiar dimensions in shifting direction and the other orthogonal directions at this temperature.

After shifting takes place, the center of gravities of the positive and negative charges do not coincide anymore, and the cell gains a permanent dipole moment. Integration of this dipole moment over the macroscopic volume of the crystal gives the spontaneous polarization P_s. The temperature derivative of P_s at constant electric field and elastic stress is the pyroelectric coefficient, which was mentioned earlier. An applied sufficiently strong electric field on the ceramic can reverse the direction of atomic displacements that is the sign of P_s. As emphasized earlier, this dipole reversibility is a peculiar property which distinguishes the ferroelectrics from the non-ferroelectric subsets of pyroelectric materials. Having a permanent spontaneous polarization, ceramic, now, can exhibit piezoelectricity following a poling process.

Based on the discussion given above, mechanism of piezoelectricity can be elaborated now. Before explaining the mechanism of piezoelectricity, it might be useful to give a simple definition of *piezoelectric coefficient*, d.

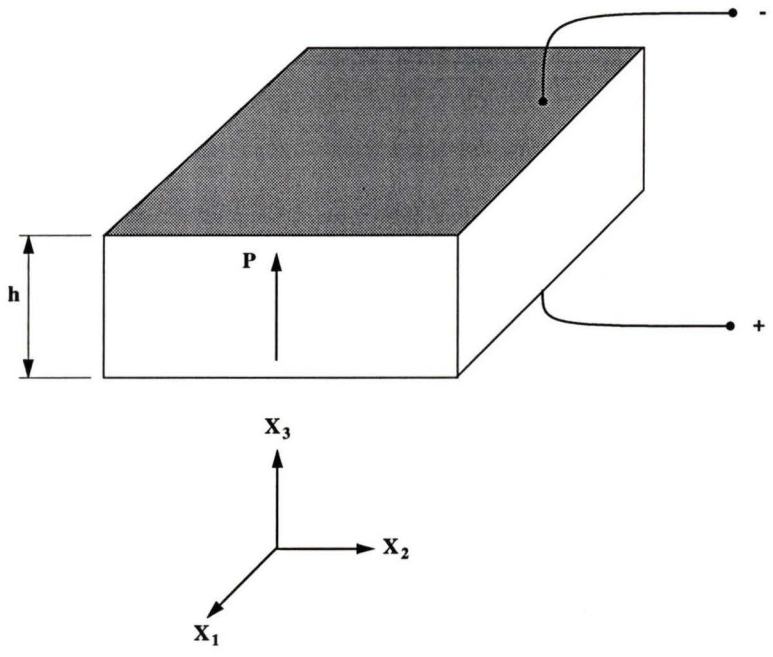

Figure 2.5: A sample piezoelectric ceramic block having electrodes on its surfaces.

Figure 2.5 shows a simple block of piezoelectric ceramic having electrodes on its top and bottom surfaces. By convention, the X_3 axis is chosen along the polarization direction of the ceramic. Orthogonal axes X_1 and X_2 are determined by applying right hand rule. For direct piezoelectric effect, the piezoelectric coefficient d_{ij}, for example, relates the stress-induced polarization to the applied mechanical stress. P_1, P_2 and P_3 are the components of the stress-induced polarization along the X_1, X_2 and X_3 axes, respectively. For converse piezoelectric effect, the piezoelectric coefficients relate the induced strain to the applied electric field. Here, d_{ij} is a second order tensor being identical for both direct and converse piezoelectric effects. For direct piezoelectric effect, the first subscript on the elements of d_{ij} tensor indicates the direction of the

induced polarization whereas the second is the direction of the applied mechanical stress. For converse effect, on the other hand, the first and second subscripts indicate the direction of the applied electric field and induced strain, respectively. More about piezoelectric coefficients will be given later in this chapter.

Having introduced the piezoelectric coefficient, d_{ij}, the basic mechanism of piezoelectricity can be given. As mentioned earlier, when electric field is applied to the poled piezoelectric ceramic in the direction of polarization, the aligned dipoles in the ceramic respond collectively and produce a macroscopic expansion along the poling axis and contraction along the axes which are perpendicular to the poling axis. This has, in fact, been described as converse piezoelectric effect earlier. In direct effect, on the other hand, an applied mechanical stress to the piezoelectric ceramic results in electrical potentials on the surfaces of the ceramic.

Simple mechanism of direct piezoelectric effect is shown in Figure 2.6. In Figure 2.6 and in the theory of piezoelectricity in general, P_1, P_2 and P_3 are the components of stress-induced polarizations along the X_1, X_2 and X_3 axes, respectively. Also, tensor elements T_1, T_2 and T_3 are the applied tensile stresses along the X_1, X_2 and X_3 axes whereas T_4, T_5 and T_6 are the shear stresses applied about the X_1, X_2 and X_3 axes, respectively.

Again, a projection on the (100) plane of the tetragonal unit cell of $BaTiO_3$ at a temperature below its Curie temperature is shown in Figure 2.6. As seen in the figure, tetragonal $BaTiO_3$ is *non-centrosymmetric* with the titanium ion displaced from the centre of the unit cell. The atomic displacements shown cause the ceramic to exhibit a spontaneous polarization and piezoelectric coefficients with respect to this polarization direction. When a tensile stress is applied in the X_3 direction, which is the upward direction in the figure plane, the Ti^{+4} ion displaces further creating a positive polarization in this direction. If a tensile stress is applied along one of the

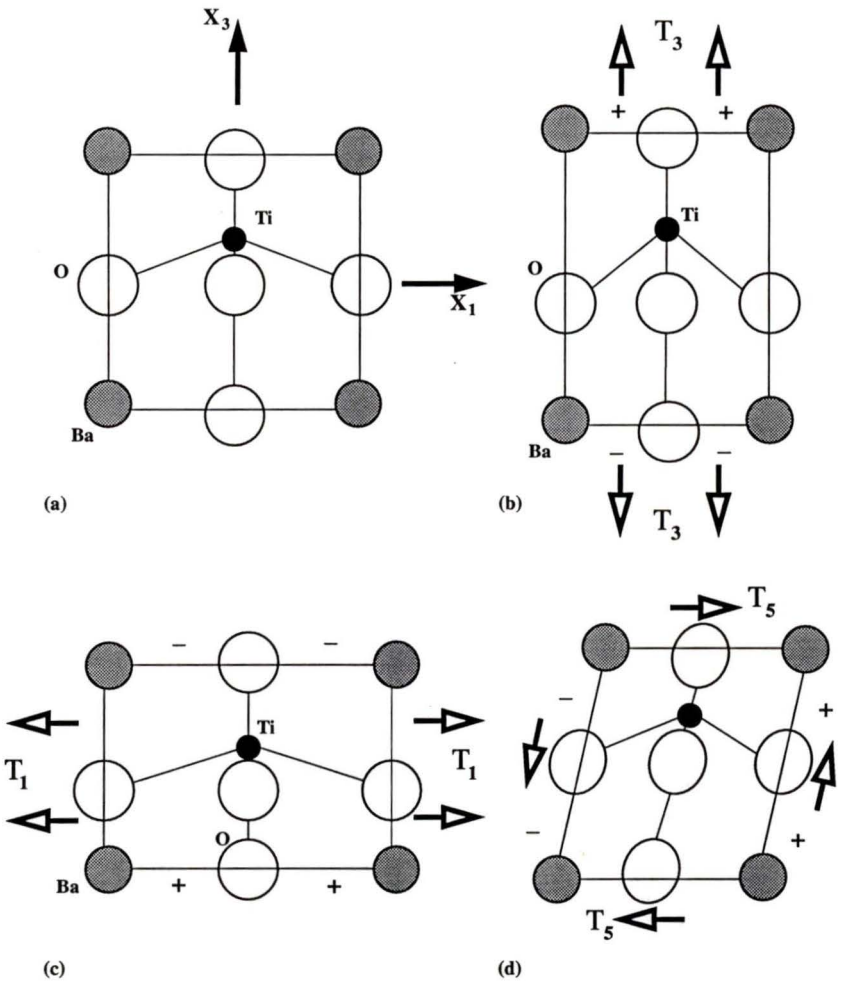

Figure 2.6: Illustration of direct piezoelectric effect on a projection on the (100) plane of the tetragonal unit cell of barium titanate.

directions which are perpendicular to the X_3 direction, direction X_1 for example, the dipole moment of the unit cell decreases and a negative polarization is created. Hence, the piezoelectric coefficient for an applied stress along this direction appears to be always negative while it is always positive for X_3 direction, which is the polarization direction of the ceramic. In other words, d_{31} is always negative while d_{33} is always positive. Finally, for an applied shear stress about the X_2 axis, the dipole moment is tipped, and polarization in X_1 direction is introduced [10]. Detailed formulation of

piezoelectricity will be covered in §2.4.

The converse piezoelectric effect can also be elaborated in the same manner. In this case, when the poled ceramic is subjected to a small electric field in the same direction as that of polarization, which is X_3 as mentioned earlier, the dipoles of the specimen will respond collectively producing a small expansion in this direction and contractions in other orthogonal directions. This is in fact, the basis of piezoelectric actuators whereas the former is the main principle of piezoelectric sensors.

2.4 Fundamental Equations of Piezoelectricity

In this section, various forms of the fundamental equations of piezoelectricity will be introduced. Derivations and detailed elaboration of these equations are not given here. Derivations of two common forms of piezoelectric constitutive equations, however, are included for the sake of completeness.

Mechanical and electrical dissipation, and nonlinear effects are not included in the equations introduced in this section. The equations given here are all based on the linear theory, and the elastic, piezoelectric and dielectric coefficients are treated as constants.

In linear piezoelectricity, linear elasticity equations and charge equations of electrostatics are coupled through piezoelectric coefficients. To be able to introduce a simple methodology for the derivation of two of the common equations of piezoelectricity, it is useful to give the relevant mechanical and electrical field variables briefly. Definitions of different piezoelectric coefficients will, also, follow before the equations are introduced.

2.4.1 Nomenclature

The following summarizes the notation used for the fundamental quantities in the theory of piezoelectricity.

c_{ijkl}, c_{pq}	Elements of stiffness tensor and matrix, respectively.
d_{ijk}, d_{ip}	Elements of piezoelectric constant tensor and matrix, respectively.
D_i	Elements of electric displacement vector.
D (superscript)	Measured at constant electric displacement.
e_{ijk}, e_{ip}	Elements of piezoelectric constant tensor and matrix, respectively.
E_i	Elements of electric field vector.
E (superscript)	Measured at constant electric field.
g_{ijk}, g_{ip}	Elements of piezoelectric constant tensor and matrix, respectively.
H	Electromechanical enthalpy density.
h_{ijk}, h_{ip}	Elements of piezoelectric constant tensor and matrix, respectively.
I	Electric current.
s_{ijkl}, s_{pq}	Elements of elastic compliance tensor and matrix, respectively.
S_{ij}, S_q	Elements of mechanical strain tensor and matrix, respectively.
S (superscript)	Measured at constant strain.
T_{ij}, T_q	Elements of mechanical stress tensor and matrix, respectively.
T (superscript)	Measured at constant stress.
t	Time.
u_i	Infinitesimal displacement.
β_{ij}	Elements of dielectric impermeability matrix.
ϵ_{ij}	Elements of dielectric constant matrix.

2.4.2 Variables of Mechanical Systems

As stated in §2.2, the condition of a material is described by intensive and extensive parameters. The external conditions are described by the intensive parameters such as electric field $\boldsymbol{E}$, temperature, and stress $\boldsymbol{T}$. The corresponding internal conditions are the extensive parameters namely polarization $\boldsymbol{P}$, or electric displacement $\boldsymbol{D}$, entropy $\mathcal{S}$, and the shape and volume which is represented by strain $\boldsymbol{S}$.

Variables in mechanical systems are strain S_{ij} and stress T_{ij}, both of which are tensors of second-order. The linear strain tensor components are given by

$$S_{ij} = \frac{1}{2}\left(\frac{\partial u_i}{\partial x_j} + \frac{\partial u_j}{\partial x_i}\right) \tag{2.1}$$

The most generalized form for linear stress-strain relation is given by *Hooke's Law* as follows:

$$T_{ij} = c_{ijkl} S_{kl} \tag{2.2}$$

or inversely

$$S_{ij} = s_{ijkl} T_{kl} \tag{2.3}$$

where

T_{ij} = elements of stress tensor

S_{ij} = elements of strain tensor

c_{ijkl} = constants of material stiffness tensor

s_{ijkl} = constants of material elastic compliance tensor.

In Equation (2.2) and Equation (2.3), c_{ijkl} and s_{ijkl} are both fourth-order tensors since T_{ij} and S_{kl} are both second-order tensors. In general, there are $(3)^4 = 81$ constants for such fourth-order tensors. However, since T_{ij} and S_{kl} are both symmetrical, the number of independent constants in c_{ijkl} and s_{ijkl} tensors can be reduced to 36

due to the following symmetry conditions [11]:

$$c_{ijkl} = c_{jikl} = c_{ijlk} = c_{jilk} \tag{2.4}$$

and

$$s_{ijkl} = s_{jikl} = s_{ijlk} = s_{jilk} \tag{2.5}$$

By utilizing such symmetry conditions and being able to reduce the number of independent constants, these tensors can be written in simple matrix forms. This is done via index abbreviations which will be mentioned briefly later in this chapter.

2.4.3 Variables of Electrical Systems

In linear piezoelectric theory, not all the electromagnetic equations are needed. In other words, magnetic field effect can be assumed to be negligible compared to electrical effects [7]. In electrical theory, the Cartesian components of the electric field and electric displacement (or flux density) are denoted by E_i and D_i, respectively. As mentioned earlier in this chapter, the polarization P_i is usually more suitable for theoretical treatments where electric displacement D_i is more convenient in practical analyses [4].

The constitutive relations between electric displacement and electric field are given by

$$D_i = \epsilon_{ij} E_j \tag{2.6}$$

or

$$E_i = \beta_{ij} D_j \tag{2.7}$$

where ϵ and β are dielectric constant and dielectric impermeability, respectively, and they are both second-order tensors.

2.4.4 Piezoelectric Coefficients

Piezoelectricity is represented by four different relations, namely $d\mathbf{D}/d\mathbf{T}$, $d\mathbf{D}/d\mathbf{S}$, $d\mathbf{E}/d\mathbf{S}$ and $d\mathbf{E}/d\mathbf{T}$. Each of these relations contains 18 constants, and their names and definitions are given below:

d piezoelectric strain coefficient

e piezoelectric stress coefficient

h piezoelectric stress constant

g piezoelectric strain constant

$$d = \left(\frac{\partial \mathbf{D}}{\partial \mathbf{T}}\right)_E \qquad d^* = \left(\frac{\partial \mathbf{S}}{\partial \mathbf{E}}\right)_T \tag{2.8}$$

$$e = \left(\frac{\partial \mathbf{D}}{\partial \mathbf{S}}\right)_E \qquad e^* = -\left(\frac{\partial \mathbf{T}}{\partial \mathbf{E}}\right)_S \tag{2.9}$$

$$h = -\left(\frac{\partial \mathbf{E}}{\partial \mathbf{S}}\right)_D \qquad h^* = -\left(\frac{\partial \mathbf{T}}{\partial \mathbf{D}}\right)_S \tag{2.10}$$

$$g = -\left(\frac{\partial \mathbf{E}}{\partial \mathbf{T}}\right)_D \qquad g^* = \left(\frac{\partial \mathbf{S}}{\partial \mathbf{D}}\right)_T \tag{2.11}$$

In Equations (2.8), (2.9), (2.10) and (2.11), the suffixes show the parameters to be held constant while measuring these coefficients. The coefficients having $*$ superscripts are the coefficients for converse piezoelectric effect indicating the mechanical response to an externally applied electric field. Direct and converse effect piezoelectric coefficients are identical for each definition given above.

2.4.5 Linear Piezoelectricity

The conservation of energy for piezoelectric medium leads to the first law of thermodynamics which can be written as

$$\dot{U} = T_{ij}\dot{S}_{ij} + E_i\dot{D}_i \tag{2.12}$$

where U is the stored energy density. The electric enthalpy density H, on the other hand, is given by

$$H = U - E_i D_i \tag{2.13}$$

Substitution of Equation (2.12) in Equation (2.13) leads to

$$\dot{H} = T_{ij}\dot{S}_{ij} - D_i\dot{E}_i \tag{2.14}$$

Then, it can be written that

$$H = H(S_{ij}, E_i) \tag{2.15}$$

By differentiating and taking the time derivative of Equation (2.15), and comparing the resultant equation with Equation (2.14), one can write

$$T_{ij} = \partial H/\partial S_{ij} \tag{2.16}$$

$$D_i = -\partial H/\partial E_i \tag{2.17}$$

In linear piezoelectricity, enthalpy equation is given in the following form [7]:

$$H = \frac{1}{2}c^E_{ijkl}S_{ij}S_{kl} - e_{kij}E_kS_{ij} - \frac{1}{2}\epsilon^S_{ij}E_iE_j \tag{2.18}$$

where c^E_{ijkl}, e_{kij} and ϵ^S_{ij} are the elastic, piezoelectric and dielectric constants, respectively.

From Equation (2.16), (2.17) and (2.18) the following equations can be derived:

$$T_{ij} = c^E_{ijkl}S_{kl} - e_{kij}E_k \tag{2.19}$$

$$D_i = e_{kij}S_{kl} + \epsilon^S_{ik}E_k \tag{2.20}$$

Equations (2.19) and (2.20) are the two forms of constitutive equations of linear piezoelectricity, known as *e-form*, having strain and electric field as independent variables.

As mentioned earlier in §2.4.2, index abbreviations are used to write the constitutive equations of piezoelectricity in matrix form which makes the tensorial equations easy to handle. Rules for index abbreviation are given in Appendix A. Matrix notations of the tensorial quantities appeared in the piezoelectric constitutive equations can also be found in Appendix A.

By applying index abbreviations explained in Appendix A, Equations (2.19) and (2.20) can be rewritten in matrix form as follows:

$$T_p = c_{pq}^E S_q - e_{kp} E_k \tag{2.21}$$

$$D_i = e_{iq} S_q + \epsilon_{ik}^S E_k \tag{2.22}$$

Other forms of the constitutive equations of piezoelectricity, including the two forms introduced already in Equations (2.21) and (2.21), are given below. It should be noted that they are all written in matrix forms by applying index abbreviations. Also, even the indices in compressed matrix notation are omitted for further brevity in the equation sets given below.

$$\mathbf{T} = \mathbf{c}^{\mathbf{D}}\mathbf{S} - \mathbf{h}\mathbf{D} \tag{2.23}$$

$$\mathbf{E} = -\mathbf{h}\mathbf{S} + \beta^{\mathbf{S}}\mathbf{D} \tag{2.24}$$

$$\mathbf{S} = \mathbf{s}^{\mathbf{E}}\mathbf{T} + \mathbf{d}\mathbf{E} \tag{2.25}$$

$$\mathbf{D} = \mathbf{d}\mathbf{T} + \epsilon^{\mathbf{T}}\mathbf{E} \tag{2.26}$$

$$\mathbf{S} = \mathbf{s}^{\mathbf{D}}\mathbf{T} + \mathbf{g}\mathbf{D} \tag{2.27}$$

$$\mathbf{E} = -\mathbf{g}\mathbf{T} + \beta^{\mathbf{T}}\mathbf{D} \tag{2.28}$$

$$\mathbf{T} = \mathbf{c}^{\mathbf{E}}\mathbf{S} - \mathbf{e}\mathbf{E} \tag{2.29}$$

$$\mathbf{D} = \mathbf{e}\mathbf{S} + \epsilon^{\mathbf{S}}\mathbf{E} \tag{2.30}$$

Equations (2.23) and (2.24) are known as *h-form* piezoelectric constitutive equations while the other sets are called *d-form*, *g-form* and *e-form*, respectively, in the same order as the equations are given. In these four forms of equations, **S** and **D**, **T** and **E**, **T** and **D** and, finally, **S** and **E** appear as independent variables.

The use of given equations depends on the specific geometrical, mechanical and electrical conditions. For a piezoelectric rod vibrating at low-frequency, for example, either Equations (2.25) and (2.26) or Equations (2.27) and (2.28) would be preferred. The reason is that under these conditions, all stress components vanish, either exactly or approximately, except for the extensional stress along the rod. However, whether to use the first or the second set of equations is determined by the given specific information regarding the shape of the cross section and the placement of the electrodes [7].

The coefficients appeared in Equations (2.23)—(2.30) are somehow related to each other. The relations between these coefficients are given in Appendix B for completeness.

2.4.6 Simple Application of Constitutive Equations to A Poled Piezoelectric Ceramic Block

Four common forms of constitutive equations of piezoelectricity have been presented in §2.4.5. Also, in §2.3.3, a simple block of poled piezoelectric ceramic has been illustrated in Figure 2.5 to describe the direct and converse piezoelectric effect. A

simple application of these equations can be shown on this piezoelectric ceramic block for a final clarification.

To illustrate the direct piezoelectric effect, it is assumed that the piezoelectric ceramic block shown in Figure 2.5 is subjected to an externally applied mechanical stress while there is no externally applied electric field. Equation (2.26) can be used to find the induced electric displacement (or flux density) as a result of the externally applied mechanical stress. General matrix forms of the terms which appear in Equation (2.26) are given in Appendix A. Induced electricity as a result of direct piezoelectric effect can be found simply by substituting those matrices in Equation (2.26).

Before the substitution, an important clarification regarding the piezoelectric coefficients in poled ceramics should be made. For poled ferroelectric ceramics, conical symmetry dictates that all piezoelectric coefficients except $d_{31} = d_{32}$, d_{33}, and $d_{15} = d_{24}$ are zero. In general, some other elements in the other matrices, appeared in the constitutive equations, are zero while there are equalities between the others. These zero elements and equalities result from the crystal symmetry as studied and shown in the earliest years of piezoelectric phenomenon [3], [12]. For $BaTiO_3$, for instance, the matrices for dielectric, piezoelectric and elastic coefficients in the tetragonal state below the Curie point appear to be as follows [12]:

$$\mathbf{d} = \begin{bmatrix} 0 & 0 & 0 & 0 & d_{15} & 0 \\ 0 & 0 & 0 & (d_{24} = d_{15}) & 0 & 0 \\ d_{31} & (d_{32} = d_{31}) & d_{33} & 0 & 0 & 0 \end{bmatrix} \quad \epsilon = \begin{bmatrix} \epsilon_{11} & 0 & 0 \\ 0 & \epsilon_{22} & 0 \\ 0 & 0 & \epsilon_{33} \end{bmatrix} \tag{2.31}$$

$$\mathbf{s} = \begin{bmatrix} s_{11}^E & s_{12}^E & s_{13}^E & 0 & 0 & 0 \\ s_{12}^E & s_{11}^E & s_{13}^E & 0 & 0 & 0 \\ s_{13}^E & s_{13}^E & s_{33} & 0 & 0 & 0 \\ 0 & 0 & 0 & s_{44}^E & 0 & 0 \\ 0 & 0 & 0 & 0 & s_{44}^E & 0 \\ 0 & 0 & 0 & 0 & 0 & s_{66}^E \end{bmatrix} \tag{2.32}$$

By substituting **d**, Equation (2.31), in Equation (2.26),

$$\begin{bmatrix} D_1 \\ D_2 \\ D_3 \end{bmatrix} = \begin{bmatrix} 0 & 0 & 0 & 0 & d_{15} & 0 \\ 0 & 0 & 0 & (d_{24} = d_{15}) & 0 & 0 \\ d_{31} & (d_{32} = d_{31}) & d_{33} & 0 & 0 & 0 \end{bmatrix} \begin{bmatrix} T_1 \\ T_2 \\ T_3 \\ T_4 \\ T_5 \\ T_6 \end{bmatrix}$$

From the above substitution, one can conclude

$$\begin{aligned} D_1 &= d_{15}T_5 \\ D_2 &= d_{15}T_4 \\ D_3 &= d_{31}(T_1 + T_2) + d_{33}T_3 \end{aligned}$$

Therefore, polarization along X_1 in a such a poled piezoelectric ceramic can be generated by an externally applied shear stress about X_2. For hydrostatic pressure p, $T_1 = T_2 = T_3 = -p$ and $T_4 = T_5 = T_6 = 0$, the resulting electric displacement can be observed along the X_3 axis only, and it can be written as

$$D_3 = (2d_{31} + d_{33})(-p) \tag{2.33}$$

Going even one step further, one can calculate the electric current generated as a result of direct piezoelectric effect by applying the following fundamental equation at

constant stress and electric field conditions [6]:

$$I = \frac{dQ}{dt} = A\frac{dD}{dt} \tag{2.34}$$

where A, I, Q are the electrode area normal to the polarization direction, piezoelectric current and charge, respectively.

Similar substitutions can also be made for Figure (2.6) presented in §2.3.3. For this case, it can be easily seen that such substitutions will result in $D_3 = d_{33}T_3$, $D_3 = d_{31}T_1$ and $D_1 = d_{15}T_5$ for Figure (2.6) (b), (c) and (d), respectively.

Chapter 3

Applications of Converse Piezoelectric Effect

In this chapter, first, brief definitions of some common properties regarding piezoelectric actuation will be introduced. Then, primitive configurations for piezoelectric devices will follow. Finally, the most common applications will be discussed following a brief discussion of the need for amplification of piezoelectric actuation. Since the piezoelectric actuation is the main interest of this thesis, applications of piezoelectric sensing will not be included.

3.1 Some Important Properties of Piezoelectric Actuation

3.1.1 Hysteresis

As mentioned in §2.3.1, all piezoelectrics exhibit hysteresis to a certain degree since it is inherent in their ferroelectric properties. In piezoelectric actuation, the magnitude of hysteresis is simply defined as the ratio, expressed in percentage form, of the maximum difference in expansion at a particular point on the voltage-expansion curve to the maximum expansion value at that particular point [13].

A common and the most generalized classification of piezoelectric ceramics is given as *hard* and *soft* piezoelectric materials [7]. The determining parameter in this classification scheme appears to be the characteristic Curie temperature of the material. In general, hard piezoelectric ceramics exhibit better hysteresis and linearity, and they have Curie temperatures above 300 $°C$. Therefore, high temperatures are needed during the poling process as discussed in §2.3.2. They have relatively smaller piezoelectric constants producing small expansions. Typical hysteresis values for hard piezoelectrics can be less than 2% [13]. Soft piezoelectric materials, on the other hand, have relatively lower Curie temperatures, below 200 $°C$, and relatively larger piezoelectric constants producing larger expansions at the expense of worse hysteresis and linearity. Because of their lower characteristic Curie temperatures, they can be poled even at about room temperatures with strong applied electric fields. Magnitude of hysteresis for soft piezoelectric ceramics can be as high as 20% [14]. In general, these materials also have large dissipation factors, which will be described later in this chapter, introducing limitations in high frequency applications. Typical hysteresis curves for hard and soft piezoelectrics are shown in Figure 3.1.

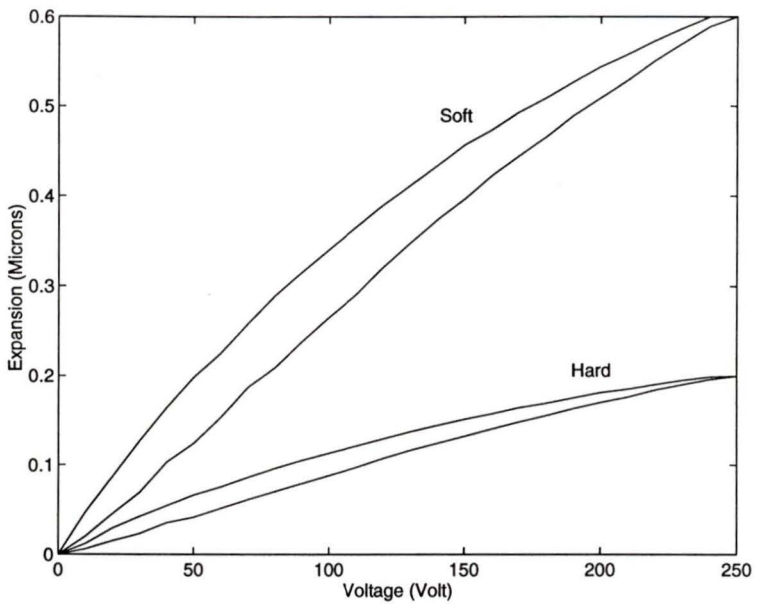

Figure 3.1: Typical hysteresis curves for soft and hard piezoelectric ceramics.

3.1.2 Linearity

The relation between strain and applied voltage for piezoelectrics is not actually linear as it was given in §2.4. Linearity is usually specified for the lower portion (increasing voltage) of the hysteresis curve only, and it is defined as the maximum deviation from the best straight line fit for this portion of the curve. Hard piezoelectrics exhibit better linearity at the expense of lower expansions. Linearity for hard piezoelectrics can be as low as 1% whereas it can range from 2% to 10% for soft piezoelectrics [13].

3.1.3 Creep

Piezoelectric actuation is known for its rapid response to an applied electric field in general. Piezoelectrics respond to any step change in the applied voltage in the fraction of milliseconds. However, following such a quick response, there is still some

time needed for a short time dimensional stabilization. In other words, there is still a slower actuation following a rapid response to reach the total expansion value of the actuation. This is simply shown in Figure 3.2.

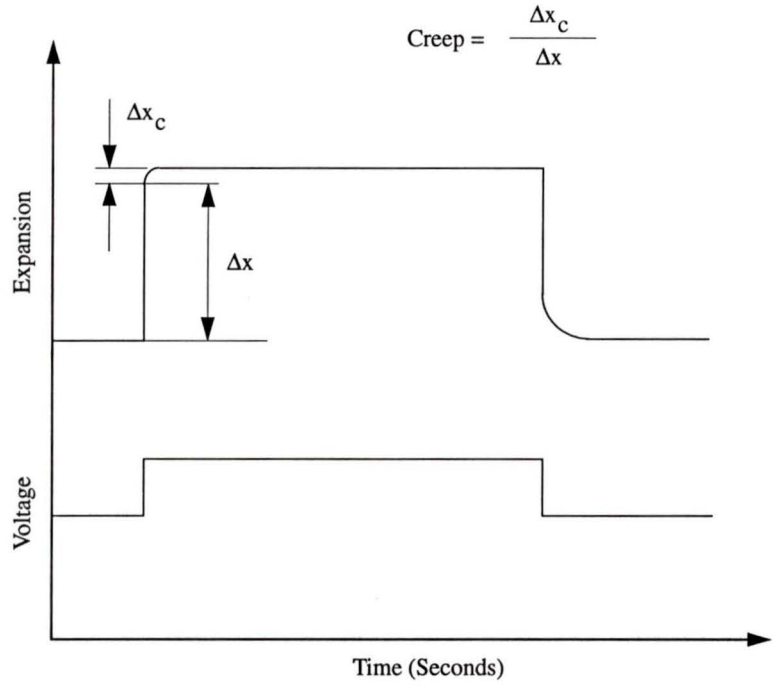

Figure 3.2: Typical creep curve.

Creep is the delay in actuation, and it happens for both increasing and decreasing voltages having usually larger values for decreasing voltages. The value of the creep is given as the ratio of the mentioned additional small expansion (or contraction for decreasing voltage) value to the initial rapid response, and it is expressed with the associated time constant as shown in Figure 3.2. Typical values for creep may range from 1% to 20% with the time constants from 1 to 100 *seconds* for both hard and soft piezoelectrics showing no peculiar distinction in neither of these classes [14].

3.1.4 Elastic Compliance

Elastic compliance has been discussed in §2.4.2. It should be added that elastic properties of piezoelectrics are not isotropic; they take different values in polarization direction and in the other orthogonal directions.

In actuators, piezoelectric materials are generally used in certain configurations, which will be elaborated later in this chapter, where piezoelectrics constitute a unit by interacting with some other type of materials such as adhesive layers or some other ceramics. In such cases, elastic properties of the whole unit cannot be represented by a single linear model, and they are usually determined experimentally.

3.1.5 Thermal Properties and Extension Under Load

The response of piezoelectrics to temperature changes is also anisotropic. Their thermal expansion coefficients take different values in different directions as well. Thermal stability is a crucial aspect in micropositioning applications. Also, piezoelectrics should be operated at temperatures well below their characteristic Curie temperatures since they can be partially depoled and lose their piezoelectric properties at temperatures near their Curie temperatures. Therefore, hard piezoelectric ceramics make a better choice for high temperature applications. Piezoelectric constants also change with changing temperatures, and that should be taken into account in applications where the temperature changes during the operation.

In most cases, thermal behaviour of the piezoelectric devices are mostly determined by the design and basic configuration of the piezoelectric units. In such cases, it is a common practice to determine the thermal properties of the overall structure experimentally.

It has been shown experimentally that piezoelectrics can be operated under constant preload, and the preload does not have a substantial negative effect on their overall expansion characteristics. Besides, it is very common to manufacture the piezoelectric subunits with a built-in preload to avoid any undesired additional compliance.

3.1.6 Dissipated Power

Piezoelectric devices are nothing but capacitors from electrical point of view. Even though ideal capacitors do not dissipate energy during charging and discharging, piezoelectric units do dissipate energy by heat conversion. Dissipated energy is proportional to the dissipation factor $tan\delta$, which is also defined as the loss angle, of the material [9]. The dissipation factor indicates the dielectric loss which is inherent in piezoelectrics. Dissipated energy is also proportional to the capacitance of the piezoelectric device, operational frequency and the applied voltage.

The breadth of the hysteresis curve can give an idea about the dissipation factor of the material; the greater the breadth the larger the dissipation factor. To be able to compare different materials in terms of dissipation factor, it is a common convention to specify the dissipation factor for low applied electric fields at 1000 Hz frequency. Hard piezoelectric ceramics may have dissipation factors as low as 0.005 at 1000 Hz, whereas it may range from 0.02 to 0.04 for soft piezoelectrics [14]. It should be noted that in high frequency applications, dissipated heat should be removed by using a heat sink to protect the piezoelectric device.

3.1.7 Ageing

The dielectric constant of a piezoelectric ceramic exhibits *ageing* following the firing or any other sudden thermal change, application of a strong electric field or mechanical stress. Ageing process is a logarithmic function of time and usually shows good linearity. Each ageing process started by one of the aforementioned sudden effects may exhibit a different ageing cycle [5].

Piezoelectric coefficients, coupling coefficient, which will be discussed next, and resonant frequency values can also be affected by ageing.

Ageing process for hard piezoelectric ceramics can be neglected over short time periods whereas this is not always true for soft piezoelectric ceramics. They can exhibit severe loss of their piezoelectric properties even over short time periods. Such loss of polarization, however, can always be recovered easily by repoling the ceramic as explained in Chapter 2.

3.1.8 Electromechanical Coupling Coefficient

In piezoelectric actuation, certain amount of mechanical energy is stored in the material as a result of dimensional changes. In fact, in the linear representation, the stored mechanical energy is equal to the closed area bounded by stress-strain curve and orthogonal axes on the stress-strain diagram. This stored energy is due to an applied electric field. Therefore, there is a certain effective energy conversion ratio between the electrical and mechanical fields during the interaction, and this is expressed by *electromechanical coupling coefficient* or simply *coupling factor* of the piezoelectric transducer.

There are a number of physical representations of the electromechanical coupling coefficient in the literature. However, the following two definitions, given by

Mason [4], are included here since they are more appropriate for practical applications of the piezoelectric actuation.

$$k^2 = \text{(stored mechanical energy)/(supplied electrical energy)} \tag{3.1}$$

or

$$k^2 = \text{(stored electrical energy)/(supplied mechanical energy)} \tag{3.2}$$

3.2 Common Configurations for Piezoelectric Actuation

Based on the discussions given in Chapter 2, one can easily see that the converse piezoelectric effect depends on the applied electric field and the piezoelectric coefficients, mostly d_{33} and d_{31}. Magnitude of the applied electric field is given by:

$$E = \frac{V}{h} \tag{3.3}$$

where V and h are the applied voltage and thickness of the plate, respectively, as shown in Figure 2.5.

Maximum expansion of the piezoelectric transducer for a certain applied voltage is desirable in most applications. In order to achieve this, either the piezoelectric coefficient of the material or the magnitude of the applied electric field must be increased. However, for a given material, there is not much to do about the piezoelectric coefficients. Development of new ceramics may offer better piezoelectric coefficients. In this thesis, only the commercially available piezoelectric ceramics will be considered. More about new ceramics can be found in [15], [16], [17], [18], [19], [20], [21], [22], and [23].

The piezoelectric coefficients of one of the most common commercial piezoelectric ceramics, PZT-5, are given as follows [24]:

$$\begin{aligned} d_{33} &= 550\text{x}10^{-12} \quad (m/V) \text{ or } (C/N) \\ d_{31} &= -200\text{x}10^{-12} \quad (m/V) \text{ or } (C/N) \end{aligned}$$

Mechanical deformation per unit applied voltage for this ceramic is very small. Larger deformations require very high voltages which may introduce a number of disadvantages such as increased risk of accident, higher cost, and limitations in terms of electrical breakdown voltage of the ceramic. The second option is to decrease the ceramic thickness to obtain larger magnitudes of applied electric field for small voltages. However, there are manufacturing limitations in terms of obtainable ceramic thicknesses without introducing structural cracks. Thickness of each layer can be as thin as 0.1 mm [13].

Based on the foregoing discussion, one may ask *"What can be done to obtain larger displacements associated with reasonably high actuation forces?"* Answers to this question will be addressed in the following subsections in which common configurations for piezoelectric devices are introduced.

3.2.1 Unimorph and Bimorph Designs

In a unimorph configuration, a thin layer of piezoelectric material is bonded to a thin metal strip as shown in Figure 3.3. In bimorph configurations, on the other hand, two thin layers of piezoelectric material are bonded together as shown in Figure 3.4.

In bimorph structures, two thin layers of piezoelectric material are bonded back to back in such a way that one of them expands in one direction while the other one contracts in the same direction when the system is subjected to a voltage. This is

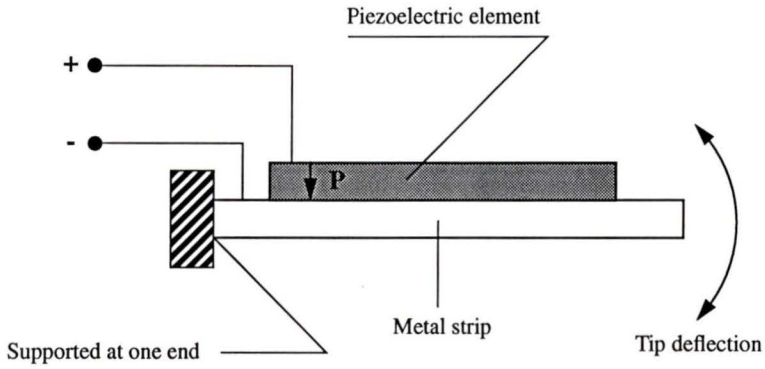

Figure 3.3: Unimorph design.

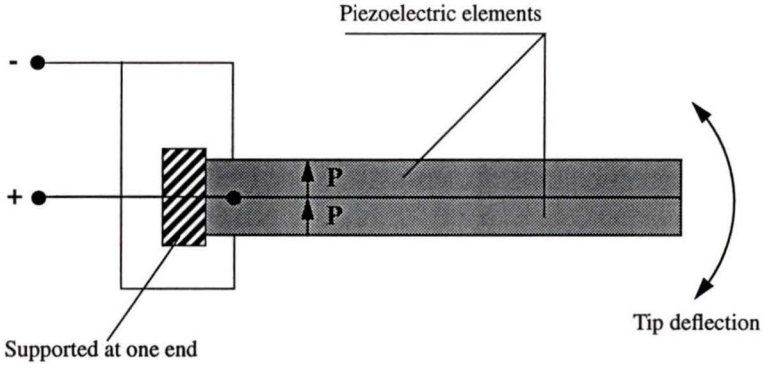

Figure 3.4: Bimorph design.

done by a proper arrangement of the polarization directions and wiring. Figure 3.4 shows the most common and basic bimorph arrangement.

Both unimorph and bimorph configurations can produce large usable tip displacements at the expense of low tip force when supported at one end. Tip displacements can be as high as 100 μm. Although unimorph and bimorph arrangements are not very common due to lack of mechanical stiffness and low resonant frequencies, there are applications in which they are utilized successfully. Phonograph pickups are the earliest examples for the utilization of the direct piezoelectric effect in bimorph piezoelectric transducers [25]. They are also one of the first solutions to servo fluid microvalve applications [13].

Mechanical stiffness can be increased by supporting the unimorph and bimorph structures at both ends and using the center displacement of the structure. Structures of circular shape, supported at their periphery, are also used. Such structures form a cone when deformed and can produce displacements as high as 1 mm [13]. Application of unimorph arrangements to telephone sets and a mobile microdevice are investigated in [26] and [27], respectively.

Microfabricated flow control systems, especially for medical applications, are also among the other promising applications where unimorph and bimorph arrangements are utilized successfully [28], [29], [30], and [31].

More about theoretical and experimental investigations of piezoelectric bimorph structures for various applications can be found in [32], [33], [34], [35], [36], [37], and [38].

3.2.2 Piezoelectric Tubes and Tube Segments

A piezoelectric tube electroded on its inside and outside surfaces and polarized in radial direction is a common structure as a single piezoelectric element. This simple structure has found many applications in tilting and translating optical mirrors where its structural simplicity and rigidity, and very high resonant frequency are utilized. Such structures are polarized through the wall thickness as shown in Figure 3.5, and they elongate axially while contraction occurs in the radial direction.

The displacement along the axis of the tube is given by the following simple equation [39]:

$$\Delta Z = d_{31} V l / h \tag{3.4}$$

where V, l, and h are the applied voltage, the length of the piezoelectric tube, and wall thickness, respectively.

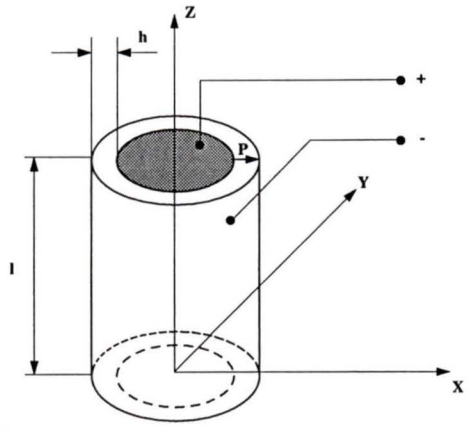

Figure 3.5: Piezoelectric tube polarized through its wall.

Since the segments cut from a whole piezoelectric tube have identical piezoelectric properties, tilting about the X and Y axes and elongation along the Z axis can be realized by combining such segments in one structure and activating them separately. Such translators have potential applications in optical mirror alignments [25]. The scanning tunneling microscope (STM), half recipient of the 1986 Nobel Prize in Physics, utilizes a partially electroded single piezoelectric tube as a scanning actuator [40]. Detailed information on piezoelectric tube translators can be found in [39], [41], [42], [43], and [44].

3.2.3 Stack (Multilayer) Assemblies

Stacking thin piezoelectric ceramic layers on top of each other to overcome the limitations mentioned in §3.2 is one of the most common solutions. A schematic illustration of a stacked piezoelectric assembly is shown in Figure 3.6.

If Equation (2.25) is applied to the stack assembly shown in Figure 3.6 for zero applied external stress, the total expansion of the stack can be expressed as follows:

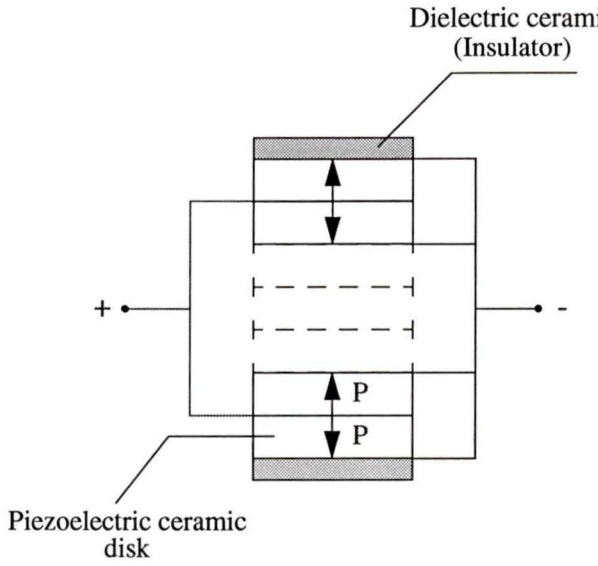

Figure 3.6: Stack (multilayer) assembly.

$$\Delta h = n d_{33} V \tag{3.5}$$

where Δh, V, and n are the total expansion of the piezoelectric stack, applied voltage, and the number of piezoelectric layers in the stack, respectively.

Each piezoelectric layer in the stack is electroded and poled before stacking. Adjacent layers are stacked in such a way that the polarization directions are faced opposite to each other. Such arrangement makes it possible to have a common electrode between the adjacent layers. As a result, only two electrical leads are needed to apply voltage to each layer of the stack simultaneously. Finally, insulators are added to the final assembly to isolate the end electrodes. In multilayer arrangement, the thinner the layer the greater the total displacement. However, the thickness of the layers is limited by the manufacturing capabilities. More information on multilayer piezoelectric actuator fabrication can be found in [45], [46], [47], [48], [49], [50], and [51].

One of the advantages of the stack design over other configurations discussed earlier in this section is that they can provide very large blocking forces, up to 30000 N, and reasonably large displacements, up to 100 μm, [52]. Therefore, they have found numerous applications in optical mirror and and fiber optics alignment devices, translating stages having more than one degree of freedom, micromanipulators for biomedical applications, and various types of linear and rotary continuous motion generation. Commercial pushers are usually provided in steel cases with a built-in preload spring. Preload is usually needed to avoid unnecessary compliance by ensuring proper mating between each layer of the stack.

Multilayer piezoelectric translators are composed of piezoelectric layers, dielectric insulators, electrodes, and various adhesives between the layers. Such composite nature makes it difficult to estimate the mechanical behaviour of the assembled stack for different loading conditions and temperature variations; therefore, the response of the stack is usually determined experimentally. There exist, however, various modelling techniques, and they can be found in [53], [54], [55], [56], [57], and [58].

3.3 Amplification of Piezoelectric Actuation

With the advent of effective fabrication techniques of multilayer piezoelectric translators, piezoelectricity has found numerous applications in micropositioning and microrobotics in recent years.

Piezoelectric actuation offers many advantages over the conventional electromagnetic drives [59]; however it requires proper amplification of small displacements. Various amplification techniques have been utilized in different applications so far. One or a combination of the following techniques is used [60]:

1. Hydraulic amplification,

2. Mechanical amplification by utilizing flexure hinge mechanisms,

3. Impulse transfer systems,

4. Generation of travelling wave in an elastic medium, and

5. Integration method.

Hydraulic displacement amplifiers utilize two hydraulic cylinders of different diameters [52]. The idea of hydraulic amplification in piezoelectric applications introduces some major problems such as sealing, compressibility of the fluid and seals which result in large drifts and low bandwidth [25].

One of the most common amplification techniques for piezoelectric actuation is the utilization of *flexures or flexure hinges.* The idea has been used successfully in numerous applications since flexure hinges provide zero structural backlash and friction. Flexure hinges are basically mechanical members which are compliant in bending about one axis but rigid about the other axes. They are simple in shape and operation, but they require a complex mathematical analysis [61].

Impulse transfer systems utilize peak inertia forces resulting from the rapid deformation of piezoelectric devices. Switching a piezoelectric device at a certain frequency can generate enough peak inertia forces to drive, for instance, a slider or activate a printing head. Translators of this sort are sometimes called *inertial sliders.* There have been many translators offered for micropositioning applications, and they will be discussed briefly later in §3.4.

Surface acoustic waves (SAW) can be generated in an elastic medium by superimposing two standing waves of equal amplitude but different phase by $\pi/2$ with respect to both time and space. The waves are due to a combination of longitudinal and shear motions, and the particles of the surface layer of the elastic medium move along an

elliptical trajectory as a result of this generated surface travelling wave. Standing waves, on the other hand, are generated by piezoelectric actuation. Once the travelling wave is generated, linear or rotary motion is created by driving a contacting slider. Such devices are operated at ultrasonic frequencies to achieve the maximum power output and noise emission, and, therefore, they are often called *resonant piezoelectric motors* or *ultrasonic motors*. Several patents have been issued on the use of travelling waves in a rotary motor in Japan since 1980. A short historical development of piezoelectric wave motors can be found in [59].

The integration method is the most popular technique in which very small displacements of piezoelectric actuation are used to create a step-wise linear or rotary motion. One of the well-known commercial products, Inchworm Motor†, and some other research studies, which will be summarized in §3.4, have used the same idea in different designs to generate a step-wise continuous linear or rotary motion having very fine controllable resolution. In fact, the piezoelectric rotary actuator proposed in this thesis employs the same idea in a unique design by converting the small displacements of piezoelectric actuation into step-wise continuous rotary motion. The actuators of this sort will be referred as *stepper piezoelectric motors* hereafter.

3.4 Review of Applications

Relatively recent applications and those which are currently under research will be covered briefly in this section. The discussions will focus on only those applications in which converse piezoelectric effect, not direct effect, is utilized.

The review will be given under four different subsections, and only some of the

†Inchworm Motor is a trademark of Burleigh Instruments, Inc.

major and relevant applications will be covered in terms of their basic operating principles. Related bibliography will also be included.

3.4.1 Micropositioners

Micropositioning is one of the most common applications where piezoelectricity offers a great potential. Micropositioning with nanometer resolutions can be achieved with piezoelectric actuators.

A multilayer piezoelectric device, mentioned in §3.2.3, is a micropositioner itself. Such devices are commercially available and can be used to drive any micropositioning set-up independently. They can even be purchased as micropositioners mounted on a mechanical amplification stage or even equipped with a feedback controller to eliminate the hysteresis effect and nonlinearities [14], [62].

Besides commercially available piezoelectric micropositioners, there are research studies at various research institutions on more sophisticated micropositioners for specific applications. For instance, a piezo-driven micropositioning stage with sub-nanometer resolution was developed by Scire et al. for optical and electron microscopes [63]. The stage combines a piezoelectric driving element with flexure amplification mechanisms to achieve a compact and vacuum compatible micropositioning with a resolution of 0.001 μm over a range of 50 μm. Overall design problems and possible solutions, fabrication techniques for such devices, analytical and experimental discussions on flexure hinge designs, and different material options for hinge mechanisms are also given in this work. Simple design rules, derived partly from finite element analysis, and design formulae, material and manufacturing tolerance considerations for monolithic high precision translation mechanisms employing flexure hinges were also studied by others [64]. A piezoelectrically-controlled rotary micropositioner for

surface finish metrology has been presented recently [65]. A translation device for X-Ray interferometric scanning has been proposed by Alemanni et al. in [66] where discussions on flexure hinge design, material selection, finite element modelling and experimental results are presented.

A different and novel approach was presented by Jones et al. in a very recent work [67]. In this article, self-sensing actuation was presented as a control technique and applied to a soft piezoelectric multilayer actuator. The presented approach is unique in that it reduces the need for costly feedback sensors, used in closed-loop applications, to eliminate nonlinearity and hysteresis effects of the piezoelectric actuation. The same piezoelectric material was utilized as both an actuator and a sensor in this approach. A more economical open-loop compensation technique with better potential was also presented in [68] to improve the dynamic response and position resolution of a piezoelectrically-driven micropositioner.

An active micro-position control technique using piezoelectric actuators has also been proposed in [69]. In this article, a general theory for piezoelectric actuators subjected to mechanical excitations and feedback voltages has been given. Bergamin et al. presented a macroscopic one-axis micropositioner with picometer resolution [70]. The proposed micropositioner utilizes a piezoelectric actuator in a feedback loop. Maximum travel distance up to 0.1 mm with a 1 pm resolution has been achieved experimentally by employing the proposed feedback control.

Following a 3.5″-disk drive unit tracks with a piezoelectric micropositioning device having a high track density and bandwidth is among the recent applications as well [71]. A proposed dual-stage micropositioner utilizing a piezoelectric actuator was a typical solution to such a challenging problem. Mechanical design and dynamic response of such a device as well as the control system used are given in detail in the presented work.

3.4.2 Inertial Sliders

Rapid deformation of piezoelectric devices can provide large inertia forces which can be used to move a mass on a slide or surface. Since the deformation speed of the piezoelectric device can be controlled with the input signal, the generated inertia force resulting from the acceleration can be controlled as well. Consequently, the produced small movements of the mass can also be controlled. The idea is, basically, to simulate a caterpillar motion with small movements of the mass or slider. At the end of each step, clamping the moving mass or slider might be necessary for safety reasons [72].

Bending mode of a bimorph piezoelectric actuator has been used to implement the same basic idea [73]. The proposed slider can move in two different directions at a maximum moving speed of 1 mm/s with about 2 nm/V sensitivity. Clamping the translation device is also possible in any desired position.

A piezoelectrically-driven $XY\theta$ table, developed for submicron lithography systems, offers one more degrees of freedom [74]. Positioning accuracies of less than 1 μm in X and Y directions, and 7.5×10^{-6} rad in θ direction have been achieved by using four piezoelectric actuators in the set-up.

A high frequency translator with light weight, rapid response and controllability characteristics has been proposed as a precise positioning translator [75]. Precision of 1 μm was achieved by driving two multilayer piezoelectric actuators at 20 KHz frequency.

Another proposed translator of the same type was equipped with both force and position sensing capabilities and was able to provide a high resolution up to 0.6 μm [76]. A stepper linear motor based on the same idea is able to climb slopes of up to 12° and has found applications in electron microscopy, alignment of optical fibers, and magnetic recording [77]. This linear stepper motor offering sub-micrometer resolution

and large travel distances was achieved by employing one single piezoelectric ceramic actuator in a unique design.

Many other inertial sliders utilizing piezoelectric actuation have been proposed for different applications [27], [78], [79], [80]. Each of these translators has unique characteristics for the intended application. Another linear device of the same class was able to perform in vertical orientation with a translator moving against gravity [81]; overall translation speed of 0.25 mm/s with an extremely small step size was achieved with this device.

3.4.3 Travelling Wave Piezoelectric Motors

The use of travelling waves in a rotary motor has been patented and commercialized already. Piezoelectric motors utilizing travelling surface waves have found many commercial applications such as positioning motors in vehicles, office devices, satellites, medical equipment, window winders, gearless windshield wiper drives, seat adjusters, heating and ventilation flap operations, paper feeders, printers and auto focus cameras. Schematic structure of a rotary piezoelectric wave motor is shown in Figure 3.7.

In a rotary piezoelectric wave motor, the stator consists of a metal ring as the elastic medium and a segmented piezoelectric ceramic ring that are bonded to each other. As shown in Figure 3.7, adjacent segments of the piezoelectric ceramic are polarized in opposite directions. The spatial phase between the mentioned standing waves results from the $3\lambda/4$ and $\lambda/4$ gaps between the poled sectors of the piezoelectric ceramic as shown. The time phase, on the other hand, is created by applying voltages which are out of phase by 90° to the sectors of the piezoelectric ceramic layer. If the applied voltages are assumed to be $U_0 \sin(\omega t)$ and $U_0 \cos(\omega t)$, then the generated

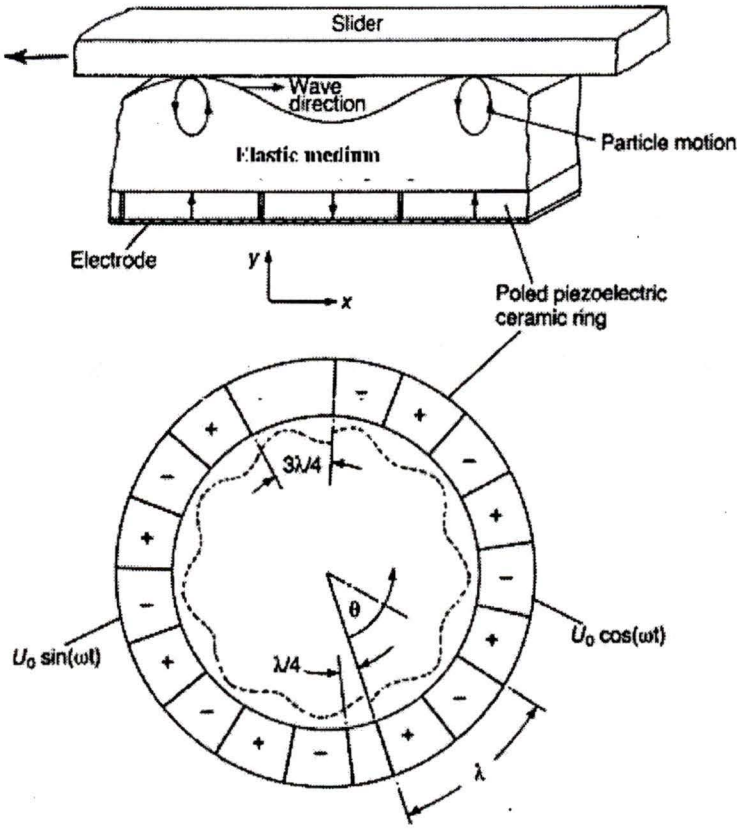

Figure 3.7: Operating principle of piezoelectric wave motor.

standing waves can be written as follows:

$$y_1(\omega, \theta) = y_0 \cos(n\theta) \cos(\omega t) \tag{3.6}$$

$$y_2(\omega, \theta) = y_0 \cos(n\theta - \pi/2) \cos(\omega t - \pi/2) \tag{3.7}$$

where y_1 and y_2 are the vertical displacements of the surface of the elastic medium, θ is the angular position on the ring, and n is the number of waves accommodated in the ring. The resultant travelling wave can be written by superimposing these two standing waves as follows:

$$y(\omega, \theta) = y_1(\omega, \theta) + y_2(\omega, \theta)$$

$$
\begin{aligned}
&= y_0 \left[\cos(n\theta)\cos(\omega t) + \sin(n\theta)\sin(\omega t)\right] \\
y(\omega, \theta) &= y_0 \cos(\omega t - n\theta) \qquad (3.8)
\end{aligned}
$$

which represents a surface wave travelling with a velocity of ω/n.

The vibrations induced by the oppositely polarized segments of the piezoelectric layer are propagated into the elastic ring. Due to the horizontal component of the motions of the surface particles, a slider (rotor) which is in contact with the surface of the elastic medium (usually with a constant preload applied by a compression spring) is forced to move in a direction which is opposite to that of the induced travelling wave. The slider moves in this direction because the elliptical motion of the surface particles is induced in the opposite direction to that of the induced travelling wave.

Piezoelectric wave motors have found many applications because of the advantages they offer [59]. Controllable low speeds makes them very suitable for direct drive applications. One main drawback, however, appears to be their relatively short life compared to conventional electromagnetic drives. The problem seems to be the high alternating tensile stresses induced in the piezoelectric ceramic. This is, in fact, one of the research topics on new piezoelectric ceramics. Also, piezoelectric wave motors are desirable for the applications where high speed but low torque are needed. For micropositioning applications, however, stepper piezoelectric rotary actuators become more desirable because of their high resolutions and high output torques at low speeds.

There are several patents issued on rotary and linear piezoelectric wave motors in Japan and in the US [59], [82]. The linear version of piezoelectric wave motors are essentially the same in principal, but they are different in that the mechanical design itself generates a linear motion [82], [83], [84], [85]. Detailed discussions and different design approaches regarding piezoelectric wave motors can be found in [82], [83], [84], [85], [86], [87], [88], and [89].

3.4.4 Stepper Piezoelectric Motors

Small displacements of piezoelectric actuation can be used to generate a step-wise linear or rotary continuous motion. Such actuators have many unique applications where high resolution and controllability, and high force/torque and low speed are needed. One of the commercialized products of this type, Inchworm Motor†, has already proven the viability of such a simple idea offering 4 nm resolution and a maximum travel distance up to 200 mm [14]. In this design, three simple piezoelectric tubes are used to create the step-wise motion. Basic structure of this linear piezoelectric actuator is shown in Figure 3.8 schematically.

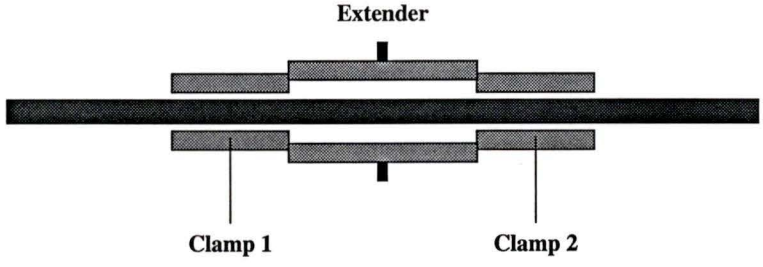

Figure 3.8: Operating principle of Inchworm motor.

Small steps are created by driving the piezoelectric tube actuators, shown in Figure 3.8, in a predefined sequence. In this design, the moving part is intended to be the shaft itself, but it can also be the housing accommodating the piezoelectric tubes depending on which one is fixed. Switching frequency determines the speed of the output shaft, and up to 2 mm/s shaft speed can be achieved at 500 KHz driving frequency. Smooth reduction of the shaft speed is also possible by reducing the frequency gradually. Since there is no mechanical amplification in this set-up, tight manufacturing tolerances between the moving shaft and the piezoelectric tubes should be realized for an efficient clamping between the tubes and the shaft. Special shaft

†Inchworm Motor is a trademark of Burleigh Instruments, Inc.

materials, ceramics in most cases, and manufacturing techniques are used to satisfy such requirements [90].

Based on the same simple idea, many other linear [91], [92] and rotary piezoelectric actuators with different design approaches have been developed. For the sake of brevity, however, only some of the significant rotary motors of the same type will be discussed in this subsection. This will make it possible to compare them with the actuator proposed in this thesis. Main advantages, drawbacks, and torque-speed characteristics of each particular approach are summarized briefly. Due to the diversity and different nature of the data provided by the authors for each rotary actuator covered in this section, characteristics of each actuator are plotted in separate figures. The characteristics included in these figures are considered to be sufficient to make a reasonable comparison. Related citations are also included.

3.4.4.1 Rotary Inchworm-type piezoelectric actuator by Ohnishi et al.

The proposed rotary actuator [93] is of stepper type and has been developed for precise positioning control. It consists of a torsional multilayer piezoelectric actuator and six longitudinal multilayer piezoelectric devices. Three of the longitudinal multilayer piezoelectric actuators are used to clamp the rotor while the other three are used to transmit the small angular displacements created by the torsional actuator to the rotor. Step-wise continuous rotary motion is generated by driving these actuators in a predefined sequence and at a high switching frequency. Basic structure of this rotary actuator is shown in Figure 3.9.

The actuator has a simple structure and a reasonably simple driving circuit, and it has a potential for further miniaturization. These are the main advantages of this actuator. There is no mechanical amplification mechanism used in this design, and small displacements of the multilayer piezoelectric units are utilized directly. There-

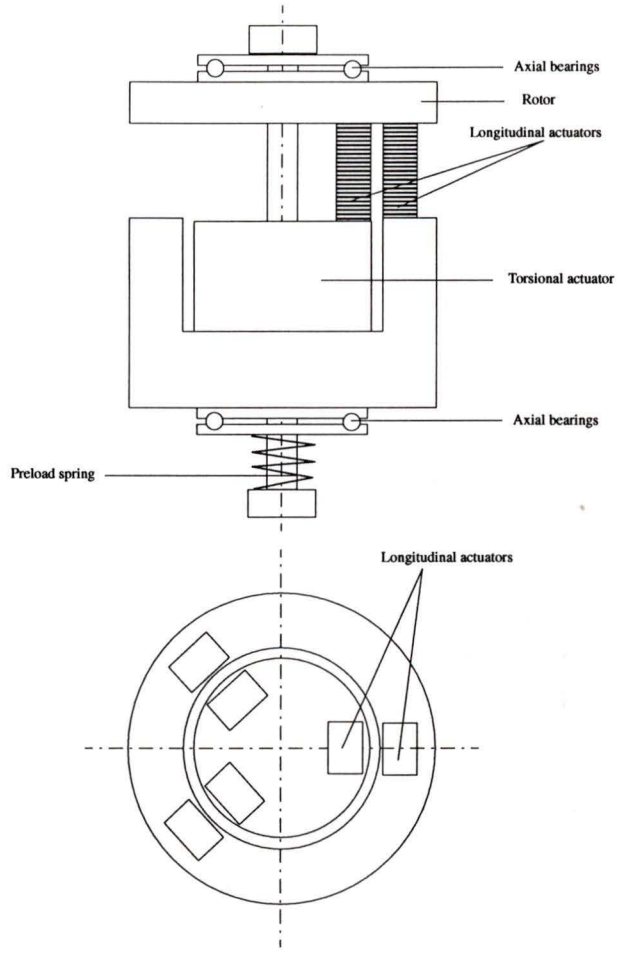

Figure 3.9: Schematic illustration of inchworm motor by Ohnishi et al.

fore, manufacturing tolerances are very crucial to realize the claimed torque-speed characteristics. Also, as known, piezoelectric ceramics cannot take shear forces well. Particularly for multilayered cases, this limitation becomes even more crucial since the shear force is transmitted through the bondings between the adjacent piezoelectric layers. In this design, torque transmission is done through the multilayer piezoelectric actuators, which is, in fact, a crucial limitation factor in terms of obtainable high torque-speed characteristic. Also, the proposed actuator is a high-voltage device requiring 800 V driving voltage to achieve the given characteristics. It can provide

maximum $\sim 9.5 \times 10^{-3}$ *rpm* output speed at 400 V applied voltage and 100 Hz driving frequency for zero applied load. Torque-speed characteristic of this rotary actuator is given in Figure 3.10.

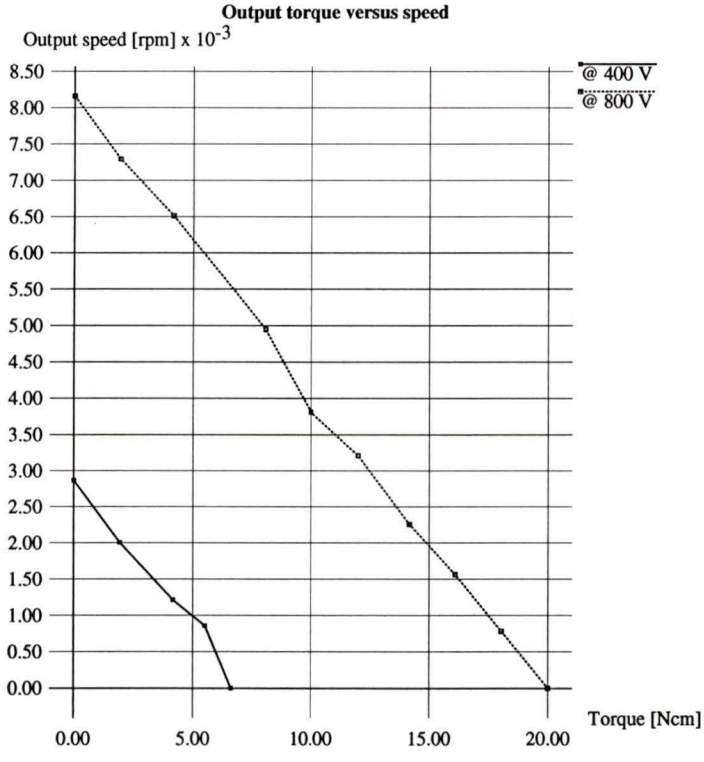

Figure 3.10: Torque versus output speed characteristic of rotary Inchworm-type piezoelectric actuator by Ohnishi et al.

3.4.4.2 Rotary inchworm piezoelectric motor by Duong et al.

The proposed rotary motor [94] consists of two clamp mechanisms and a swinger device. Step-wise continuous motion is generated by driving these three units in a predefined sequence. The rotary motor is shown in Figure 3.11 schematically.

In this particular design, each clamp mechanism has two and the swinger mechanism has one multilayer piezoelectric actuator. Specially designed flexure amplifica-

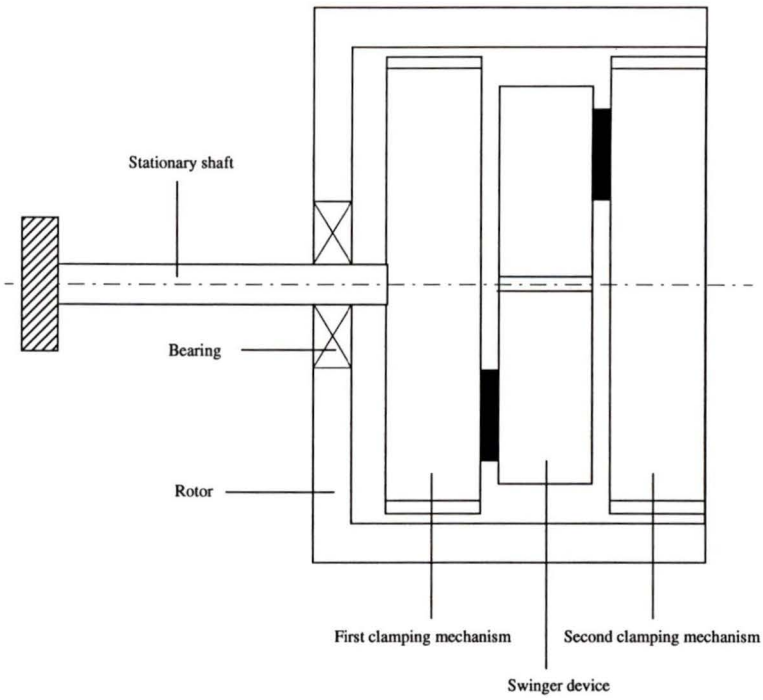

Figure 3.11: Schematic illustration of inchworm motor by Duong et al.

tion mechanisms are utilized in each unit. The swinger mechanism is able to rotate the second clamping unit with respect to the stationary shaft. During the rotation, the second clamping unit is activated, and it transmits the generated torque to the surrounding rotor. This unit is deactivated while the first clamping mechanism is active during the recovery of the swinger. These steps are repeated at a high switching frequency to generate the rotary motion. The proposed design is relatively complex due to the complex flexure mechanisms but relatively more reliable. A more reliable bearing support should be added if the actuator is to be used in industrial applications. Also, there is not a conventional output shaft on the actuator; some other auxiliary interface mechanisms may be needed to use the output torque. Excitation of the multilayer piezoelectric actuators can be achieved with a simple driving circuit.

Maximum static frictional torque is given as 212 Ncm for this actuator. The term

static frictional torque means the maximum holding torque right before the slipping occurs. The same term may be used hereafter for other actuators as well. Rotor speed versus switching frequency for varying loading conditions is given in Figure 3.12.

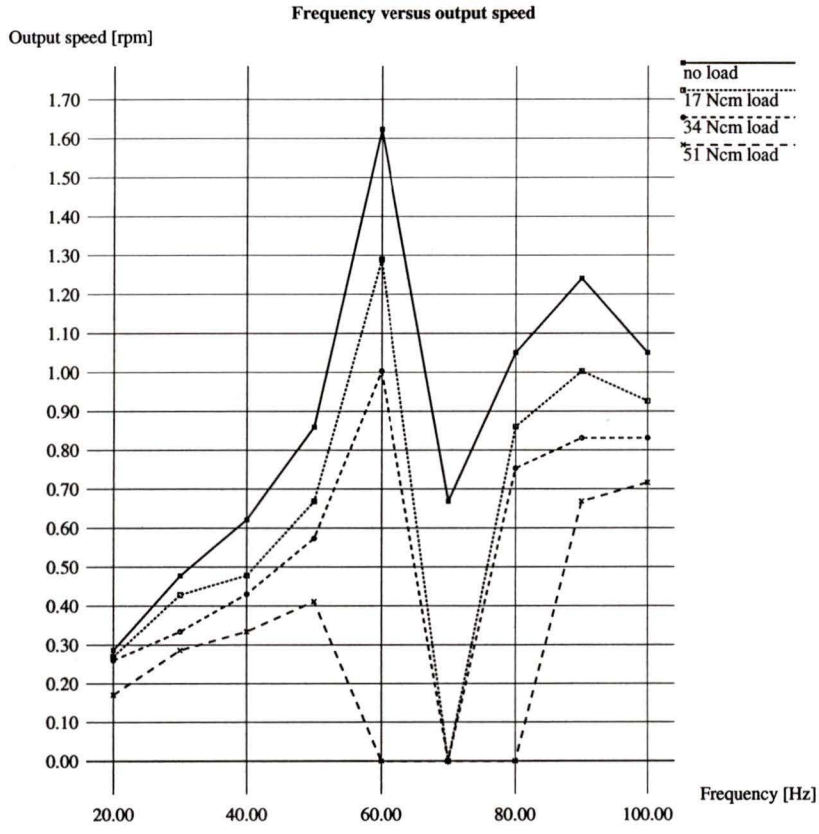

Figure 3.12: Frequency versus output speed characteristic of inchworm motor by Duong et al.

3.4.4.3 Piezoelectric cycloid motor by Hayashi et al.

The actuator has been proposed to overcome the limitations of piezoelectric ultrasonic motors [95]. Short operating life of such motors is being claimed to be the result of pure *friction-based* operating principle. Therefore, a cycloid gear mechanism is being

offered to overcome such limitation. The cycloid gear mechanism is employed to convert the small displacements of four multilayer piezoelectric actuators into continuous rotary motion. Torque transmission is realized via inner and outer gear teeth, and there is no slip between the rotor and stator in this design. Theoretically derived characteristics and experimental results are presented. Basic structure and operating principle of this rotary motor are shown schematically in Figure 3.13.

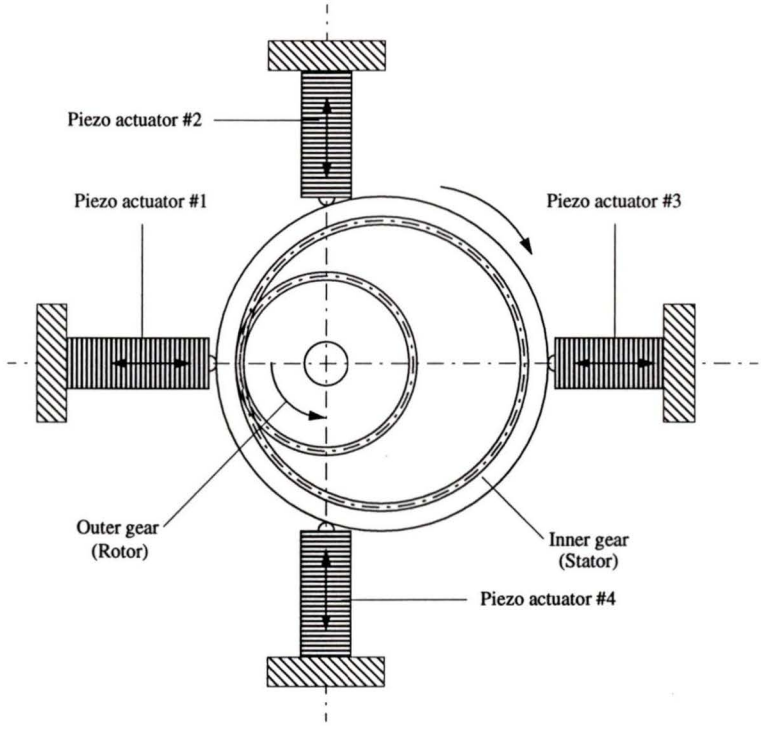

Figure 3.13: Operating principle of piezoelectric cycloid motor by Hayashi et al.

Rotation of the rotor is realized by applying an electric field to the piezo actuators #1, #2, #3 and #4 in the polarization directions and in the same order given. This allows the excited piezo actuator to expand along its longitudinal axis. Electric fields applied to two actuators located opposite to each other are also in opposite directions to let one of the piezo actuators expand while the other contracts along the same axis. This is done by applying sine wave voltages which are out of phase by 90 degrees to

these oppositely located piezo actuators. Cycloid motion is generated by moving the stator with respect to the rotor along the axes of the piezo actuators in a specified order. In other words, the stator oscillates without rotation. The difference between the number of teeth of the inner and outer gears causes the rotor to rotate. The rotational speed of the rotor is given as follows:

$$N = 60\frac{Z_i - Z_0}{Z_0}f \tag{3.9}$$

where N ,Z_i, Z_0 and f are the rotational speed of the rotor in rpm, the number of teeth of the inner gear, the number of teeth of the outer gear and the driving frequency in Hz, respectively.

In this approach, the gear mechanism introduces a mechanical shape constraint between the rotor and stator which, in turn, creates a tangential force between the tooth surfaces of the inner and outer gears. In fact, torque transmission between the stator and rotor is achieved through this force. The gear mechanism, on the other hand, requires macro displacements to engage and disengage the inner and outer gear teeth during the operation. In other words, sufficient amplification of small displacements is necessary.

Hayashi et al. used a two-stage flexure amplifier with a magnification ratio of 64 for each multilayer piezoelectric actuator. The resultant rotary actuator is a low voltage, 150 V, rotary actuator accommodating four piezo devices associated with four mechanical amplification mechanisms. It has a relatively complex driving circuit, and it is *not* suitable for further miniaturization because of the need for high mechanical amplification. Even though the experimental set-up proves the concept, the question of whether it can be built as a compact rotary actuator for industrial applications was left unanswered.

Motor output shaft rotational speed versus frequency (with no load) and torque

versus rotational speed characteristics for this actuator are given in Figure 3.14 and Figure 3.15, respectively.

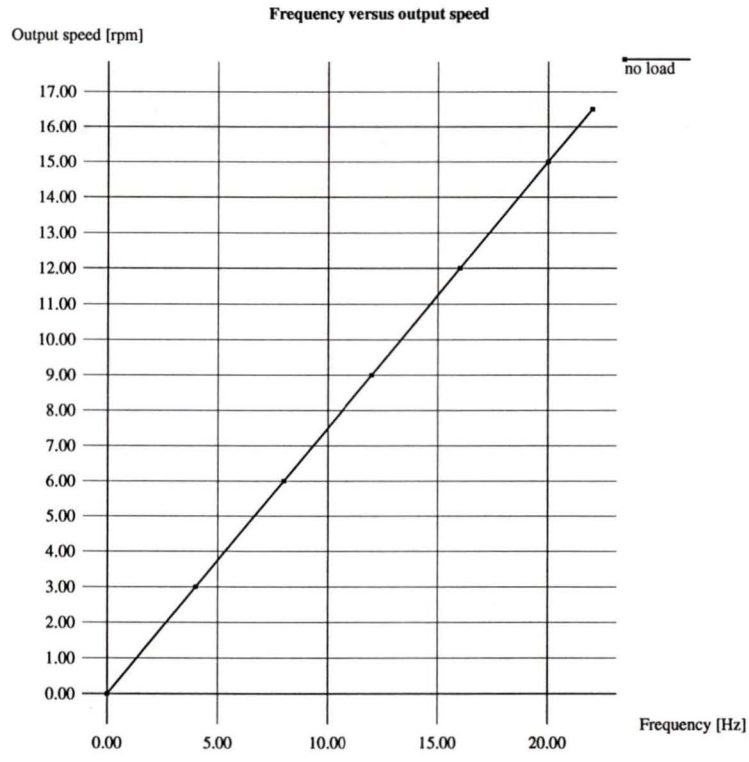

Figure 3.14: Frequency versus output speed characteristic of piezoelectric cycloid motor by Hayashi et al.

The torque speed characteristic is given for a driving frequency range of $1 - 20$ Hz. Above 20 Hz, the efficiency of the motor is stated to go down. Since there is no slip between the stator and the rotor due to the employed gear mechanism, the rotational speed does not decrease as the load increases. For the maximum generated torque of 1.4 Ncm, the cycloid motor operates steadily for all driving frequencies and, therefore, for all rotational speeds.

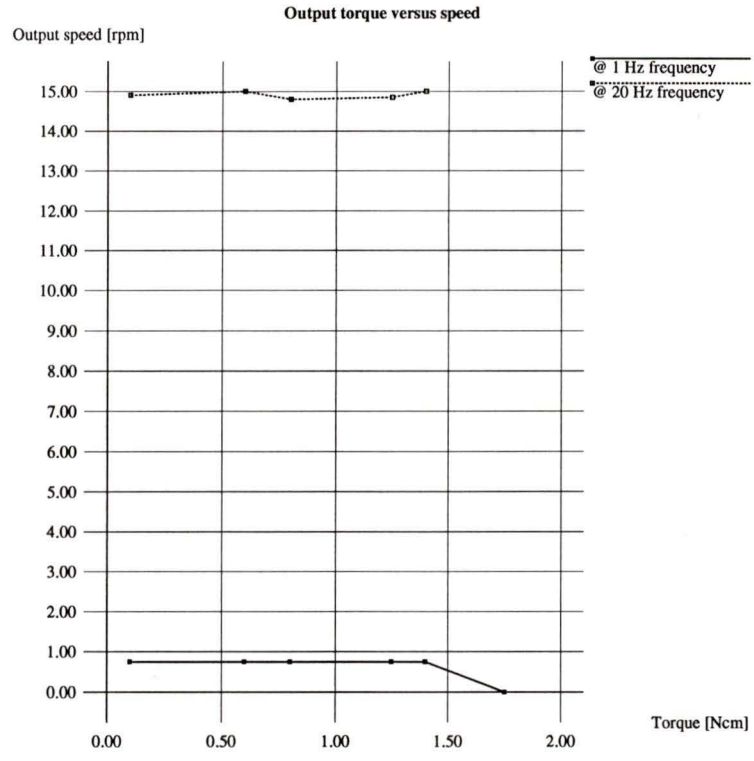

Figure 3.15: Torque versus output speed characteristic of piezoelectric cycloid motor by Hayashi et al.

3.4.4.4 Friction-type piezoelectric motor utilizing a strain wave gearing mechanism by Ishida et al.

The proposed motor [96] consists of a wave generator, a flexspline and a circular spline (rotor) as shown in Figure 3.16.

The flexspline is a very flexible hollow cylinder, and the circular spline is a solid cylinder inserted in the flexspline tightly. The wave generator consists of 16 piezoelectric devices distributed evenly around the circular spline. Both the piezo devices and the flexspline are preloaded with preload screws. When DC voltage is applied to some of the piezo devices which are 180 degrees apart, they push the flexspline onto the circular spline stronger than the other piezo devices. As a result, the flexspline is formed

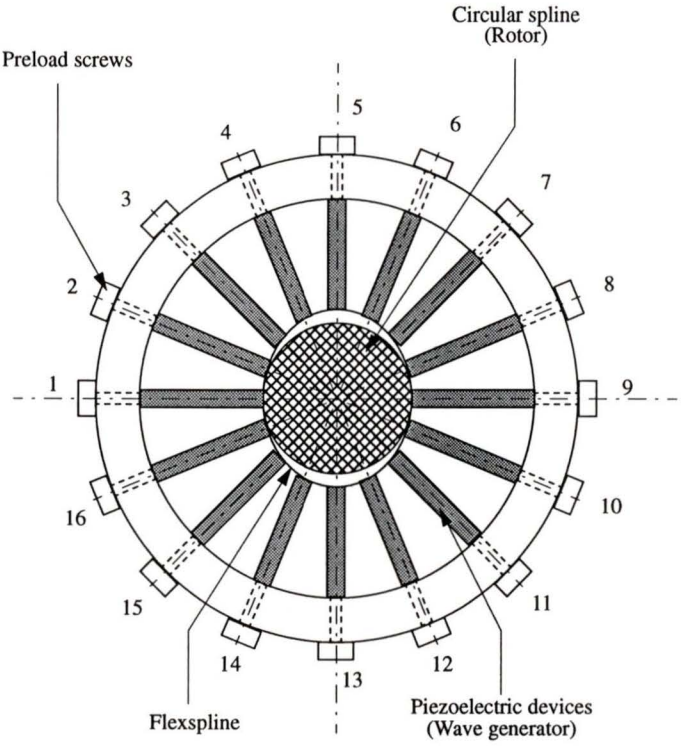

Figure 3.16: Schematic illustration of piezoelectric rotary motor by Ishida et al.

into an elliptical shape contacting the circular spline only at two locations which are, again, 180 degrees apart. This is shown in Figure 3.16 with a little exaggeration.

Operating principle of the strain wave gearing piezoelectric motor is shown in Figure 3.17. When biased multiphase AC voltage is applied to the piezo devices, the formed ellipsoid rotates around the circular spline. Therefore, the contact points C and C' also rotate as shown. Since the circumference of the flexspline is a little longer than that of the circular spline, initially coincident contact points of the flexspline and circular spline, shown as A and B, respectively, rotate with respect to each other as the ellipsoid rotates. In case the flexspline's motion is limited to elastic deformation only with no rotation, which is usually the case, the circular spline rotates in the opposite direction to that of the elliptic deformation [96].

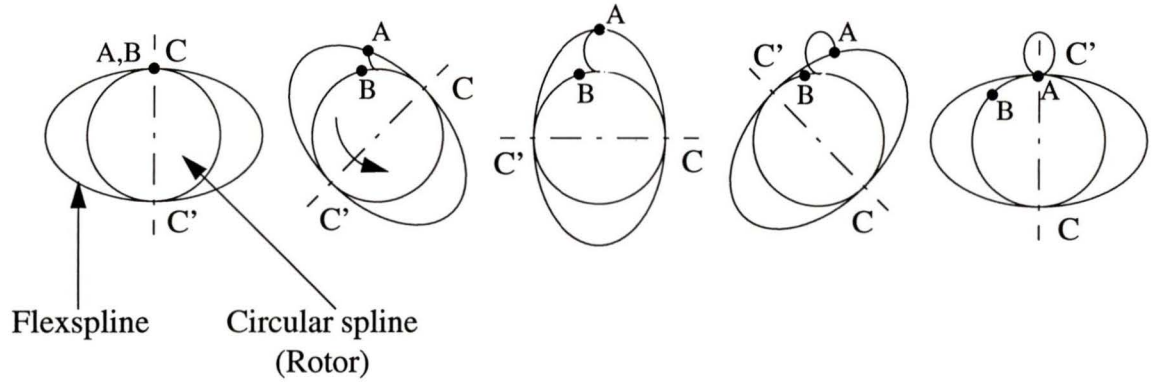

Figure 3.17: Operating principle of piezoelectric rotary motor developed by Ishida et al.

In robotics, this is, in fact, the operating principle of the well known backlash-free *harmonic drive mechanism.* The proposed rotary motor is slightly different from the harmonic drive mechanism in that in harmonic drive mechanism, torque transmission is achieved through the inner and outer teeth of the circular spline and flexspline, and the elliptical deformation is generated inside the circular spline via an elliptical ball bearing which is surrounded by the flexspline [97].

The actuator is a low voltage, 100 V, device; it is compact and relatively more suitable for further miniaturization. There are, however, 16 multilayer piezoelectric devices which increase the cost and make the driving circuit as well as the actuator relatively complex. Shaft rotational speed versus frequency (with no load) and torque versus rotational speed characteristics of this actuator are given in Figure 3.18 and Figure 3.19, respectively.

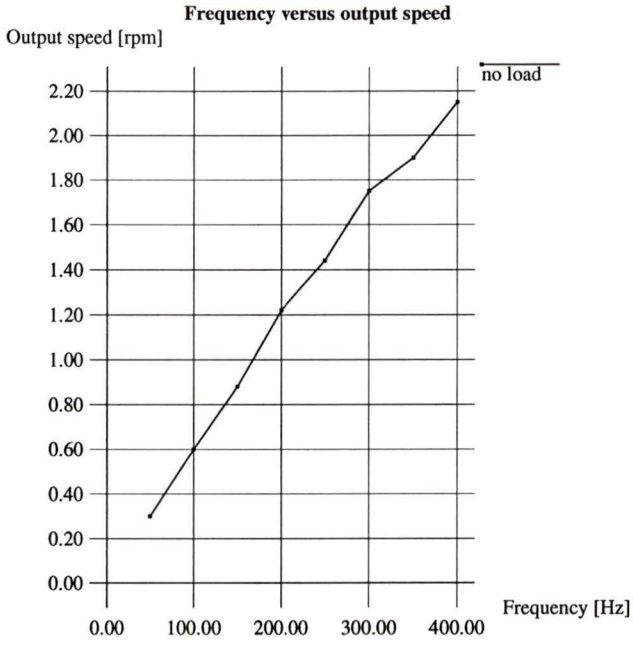

Figure 3.18: Frequency versus output speed characteristic of piezoelectric motor by Ishida et al.

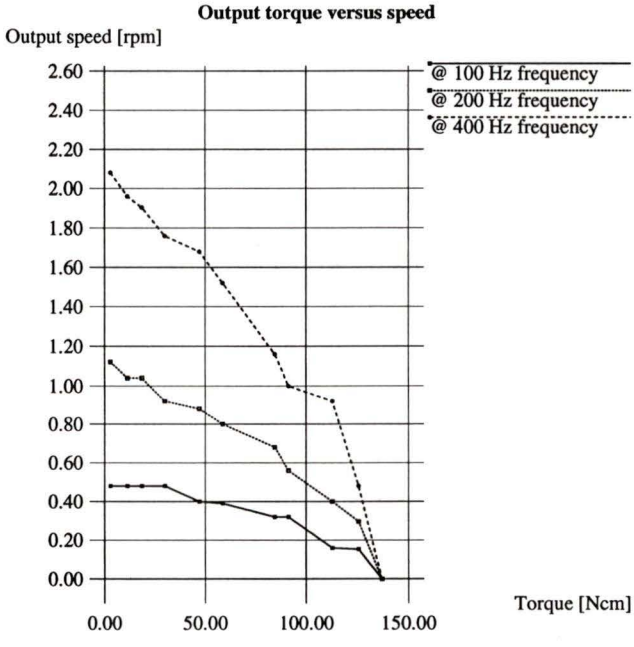

Figure 3.19: Torque versus output speed characteristic of piezoelectric motor by Ishida et al.

3.4.4.5 Miniature cybernetic piezoelectric rotary actuator by Ikuta et al.

The piezoelectric rotary actuator proposed by Ikuta et al. has a very simple structure and provide very low output torque at relatively high shaft speeds [92]. The actuator has been proposed for medical applications and claimed to meet the requirements of a cybernetic† actuator. Its simple structure is shown schematically in Figure 3.20.

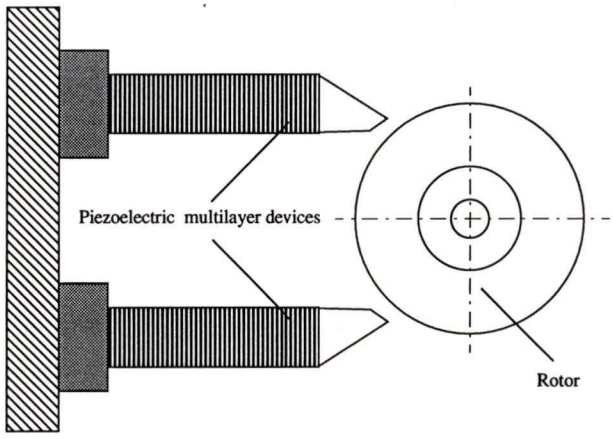

Figure 3.20: Schematic illustration of piezoelectric rotary motor developed by Ikuta et al.

Rotation of the rotor is achieved by driving the multilayer piezoelectric actuators at a certain frequency. *Locked* and *free* states are obtained by activating and releasing, respectively, both actuators simultaneously. The actuator is *not* reliable enough for industrial applications, and it is included here for the sake of completeness.

A similar work was also performed by King et al. [98]. Their design is different in that they utilize flexure hinge amplifiers to amplify the small displacements of piezo devices. For Ikuta's rotary motor, estimated maximum static frictional torque and maximum load-free rotational speed are claimed to be 12 Ncm and 180 rpm, respectively. There is, however, no sufficient experimental data provided by the authors.

† *Cybernetics* is a science in which control systems in electronic and mechanical devices are studied and compared to biological systems.

Characteristics of King's rotary motor are not included here since the actuator is not compatible with the proposed actuator in this thesis in terms of compactness and reliability.

3.4.4.6 Piezoelectric harmonic motor by King et al.

A piezoelectric harmonic rotary motor proposed by King et al. [99] is slightly different from the frictional strain wave gearing piezoelectric actuator in a sense that it is structurally identical to the harmonic drive mechanism. The wave generator is located within the circular spline, and torque transmission is achieved through the inner and outer gear teeth. The design itself, the flexure amplifiers used, and the stress analysis conducted for the gear teeth are presented by the authors in the cited article. Estimated output torque is claimed to be 6.4 Ncm, but no prototype and, therefore, no experimental data is available.

Chapter 4

A New Rotary Actuator

A rotary actuator should be able to provide reasonably high torque-speed characteristics so that it can be used in practical applications. It should also have a high resolution since most of the applications involve micropositioning tasks. It should be reliable enough so that it can operate for a long period of time without introducing any problems. A rotary actuator to be sent for a mission on a space vehicle, for instance, should definitely meet this criterion. It should not only be able to generate continuous motion by utilizing micron displacements but also be compact enough.

Less number of piezo devices is desirable to reduce the cost. Driving circuits also get more complex with any increase in the number of piezoelectric devices. An actuator providing the required torque-speed characteristic and having a relatively simpler driving circuit is definitely more preferable. The number of piezo devices also affects the compactness of the actuator.

High voltage piezoelectric devices are, in general, less compliant than that of low voltage ones. They also have relatively high electrical breakdown limits, and they can stand stronger electric fields without suffering electrical breakdown. This

makes it possible to obtain large displacements by applying high electric voltages. They provide better linearities and relatively lower hysteresis, which make them more attractive for open-loop micropositioning, as well. However, high voltage is usually not desirable since it introduces potential dangers in the workplace. High voltage devices are, also, relatively expensive. All these considerations should be taken into account during the development of such piezoelectric actuators.

In this chapter, the proposed piezoelectric rotary actuator will be introduced. The actuator is expected to provide better torque-speed characteristics in a more reliable and compact design than those of the previously proposed actuators [92], [93], [94], [95], and [96].

First, difficulties and challenges in generating continuous rotary motion by utilizing piezoelectric actuation will be discussed briefly. Then, the proposed rotary actuator will be introduced in detail. Its operating principle, actual design and the subunits, general design considerations, piezoelectric units and their properties will be discussed along with some recommendations to follow during the assembly. Flexure hinge amplification mechanisms implemented on the proposed actuator will be discussed in detail. Introduction of the driving circuit will follow. Finally, experiments conducted on a built prototype will be presented, and the results will be discussed.

4.1 Problems Associated with Continuous-Motion Piezoelectric Actuators

In piezoelectric actuation, displacements of a couple of microns are converted into linear or rotary continuous motion by utilizing specially designed mechanisms. Small displacements generated by the piezo devices should be amplified to certain usable

magnitudes. These amplification mechanisms should be able to respond to a mechanical input rapidly with minimum or no creep. They should be able to operate under required conditions for a long period of time without failure. They should, also, be able to stand high local stresses caused by high blocking forces under static or dynamic conditions. They should not exhibit any fatigue problems.

No structural clearance or backlash between the components of the actuator is tolerable in such devices. Every micron of the piezoelectric actuation should be utilized. Any unexpected compliance caused by a weak component can also fail the idea; this should be taken care of as well.

Not only dimensional but also geometric tolerancing is crucial in designing such devices. Machining techniques to manufacture the parts should be chosen carefully in order to accomplish the tolerancing required by the design. Assembly might require special attention as well; special techniques might be needed. Temperature changes during the operation may cause problems; therefore, excessive heat dissipation should be avoided or should be taken care of.

As mentioned earlier, piezoelectric ceramics cannot take tension or shear loadings. This is particularly important for multilayer or stack piezoelectric devices because of their multilayered structures and very high blocking forces that they generate. Thus, they should by no means be subjected to excessive tension or shear loadings during the operation. Some precautions might be necessary to protect the piezo devices. Some other concerns in addition to those mentioned above will also be discussed, and solutions will be given later in this chapter.

4.2 Proposed Rotary Actuator

The proposed rotary actuator is of stepper type combining small angular displacements created via piezoelectric actuation. It consists of three subunits:

1. Clamp flexure unit
2. Rotational flexure unit (Torque generator)
3. Clutch flexure unit

As the names imply, these three main units accommodate the flexure amplification mechanisms.

Continuous rotary motion is generated by rotating a mechanical unit, with only a rotational degree of freedom, back and forth. This mechanical unit can be considered as an oscillating unit with a certain frequency that can be controlled. The source of the oscillation is, on the other hand, a longitudinal multilayer piezoelectric device which is driven at a certain frequency.

The step-wise rotary continuous motion is generated by using only half period of this oscillatory motion (active stage) caused by the small angular displacement of the *rotational flexure* unit, which is, in turn, actuated by a multilayer piezo device. The other half period of the oscillation (passive stage) is used to recover the rotational flexure unit.

During the active stage of the oscillation, oscillating unit is mechanically connected to the actuator's shaft through a *clutch* mechanism. The clutching unit operates at the same frequency and is actuated by two other longitudinal multilayer piezo devices. At the end of the active stage, the clutching unit is released. This is when the passive stage of the oscillation begins, during which the rotational flexure unit is recovered.

The recovery is done mechanically by a compression spring in which certain amount of mechanical energy is stored during the active stage. The shaft is clamped during the passive stage to avoid the backward rotation, and this is done by a *clamping* unit. Clamping unit itself consists of two flexure units actuated by two other piezo devices of the same nature. The rotary motion is basically created by repeating these steps at a certain frequency.

4.2.1 Operating Principle of The Proposed Rotary Actuator

Simplified schematic illustration of the proposed actuator is given in Figure 4.1. The flexure mechanisms are not shown in the figure for simplicity. As seen, there are two longitudinal multilayer piezo devices which clamp the shaft to the inertial body when they are activated. When these two piezo devices are active, they exert a high blocking force on the shaft, and the shaft is *clamped.*

The clutch unit accommodates two other piezo devices. This is the oscillating unit mentioned in §4.2. The piezo devices are attached to this unit, and they all oscillate together as a single body. There are two other flexure mechanisms between the shaft and the piezo devices of this unit. The high blocking force generated in the piezo devices is utilized to attach the clutch unit to the shaft during the active stage of the oscillation. Clamping and clutching are achieved via high frictional torques.

One more longitudinal multilayer piezo device, shown on the lower right hand side in Figure 4.1, is used to rotate the clutch unit. This piezo device expands and rotate the clutch unit about its rotational axis while the clutching is active. The torque created by this single piezo device is transmitted to the shaft through clutching. During this half period of the oscillation, clamping unit is not active so that the

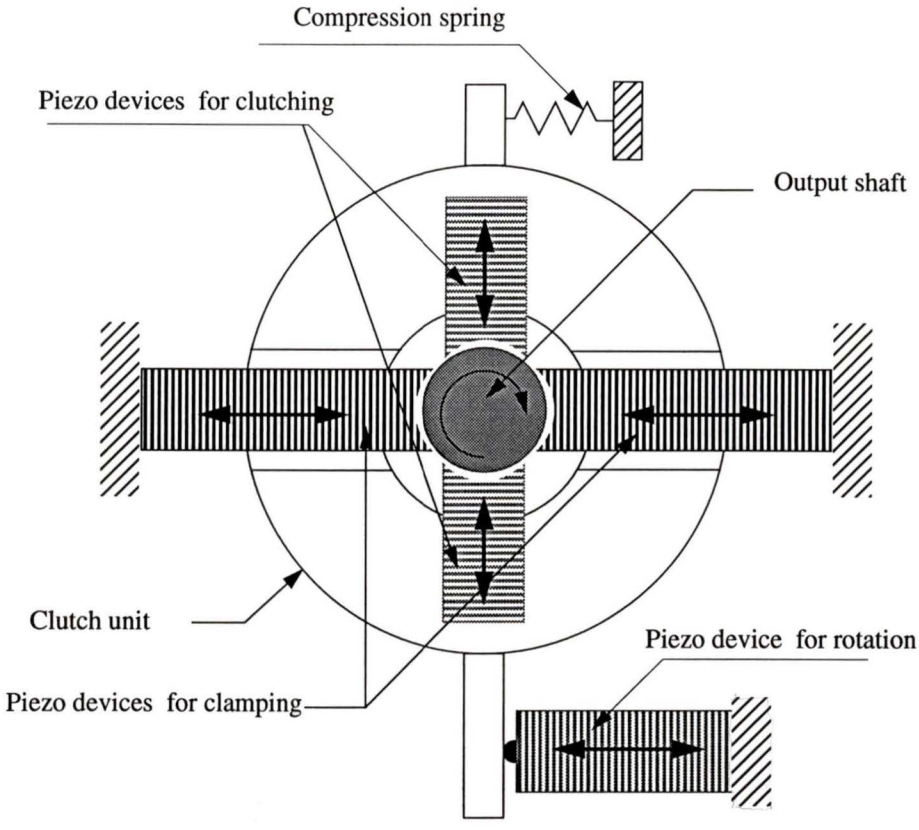

Figure 4.1: Schematic illustration of the proposed actuator.

shaft can rotate freely with respect to its housing. During the rotation of the clutch unit, certain amount of energy is stored in the compression spring placed between the clutch unit and the housing. This energy is used to rotate the clutch unit back to its initial position. During the passive stage, the rotational flexure unit also goes back to its initial position, and the clamping mechanism holds the shaft to prevent the backward rotation. At the end of each complete cycle, the shaft is rotated by a small angle. Step-wise continuous rotary motion of the shaft is created by repeating this cycle at a certain frequency.

The steps of one complete cycle are shown in Figure 4.2, and the associated activities are summarized in Table 4.1.

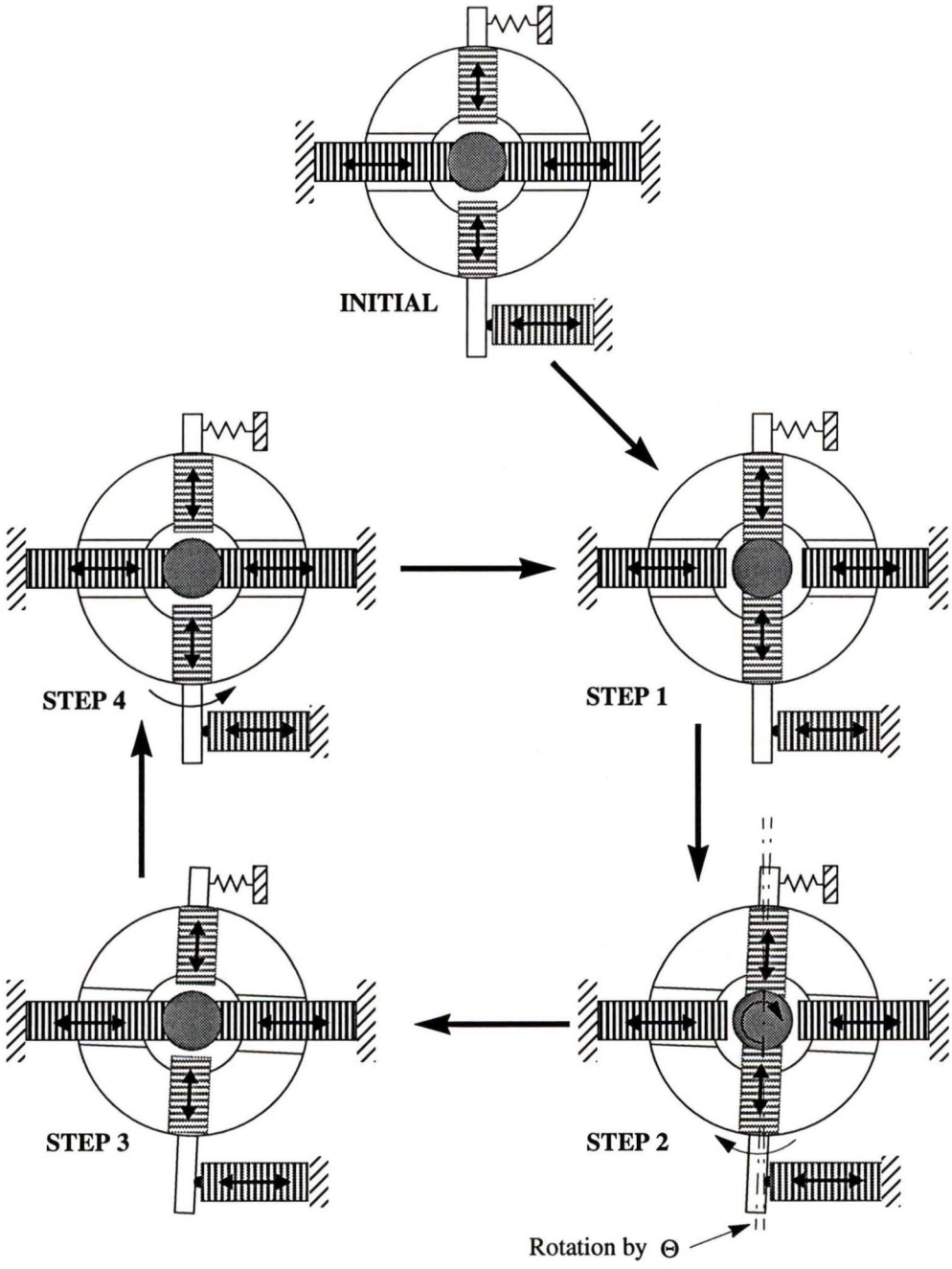

Figure 4.2: Basic operating principle of the proposed actuator.

STEP	ACTIVITY
Initial	Clamp unit is active; clutch unit is not active and at its initial position
Step 1	Clamping is released and clutching is activated
Step 2	Shaft is rotated by a small angle
Step 3	Clutching is released, and clamping is activated
Step 4	Clutch unit is rotated back to its initial position
	Go back to Step 1

Table 4.1: Summary of the steps of a complete operating cycle.

Table 4.2 shows the states of the piezoelectric devices at each step. In the table, state "0" and state "1" denote the states corresponding to zero and 250 V operating voltages, respectively.

Steps	State of piezoelectric devices		
	Clamp unit	Clutch unit	Rotation unit
Initial	1	0	0
Step 1	0	1	0
Step 2	0	1	1
Step 3	1	0	1
Step 4	1	0	0
	Go back to Step 1		

Table 4.2: States of the piezoelectric devices at each step.

It should be mentioned that the switching shown in Table 4.2 takes place at a high frequency. There are short overlap regions where the piezo devices of more than one unit are all active to avoid the slippage of the shaft under a certain load torque. This is not shown in Table 4.2 for simplicity but will be discussed later in this chapter.

4.2.2 The Actual Design

The proposed rotary actuator was designed by utilizing 3-D solid modelling techniques. *I-DEAS VI*[†] 3-D solid modelling software was used throughout the design process. The solid models were used to create the rotary actuator itself and the detailed part drawings of each component. The same models were also used in the finite element simulations of the flexure mechanisms.

Utilization of solid modelling techniques provides advantages in designing such complex mechanisms. The modelling makes it possible to see the components and their relations with each other in the assembly before manufacturing. Physical properties may also be included in the models for static or dynamic simulations. In short, the rotary actuator to be designed can be simulated completely without manufacturing one single component. Any modifications and corrections in the design can also be easily incorporated.

Figure 4.3, together with Table 4.3, shows the surface boundary representation of the actuator and its major units. Shaded image and surface boundary representations are given in Figure D.1 and Figure D.2, respectively, in Appendix D for a clear illustration.

[†]I-DEAS is a trademark of SDRC (Structural Dynamics Research Corporation)

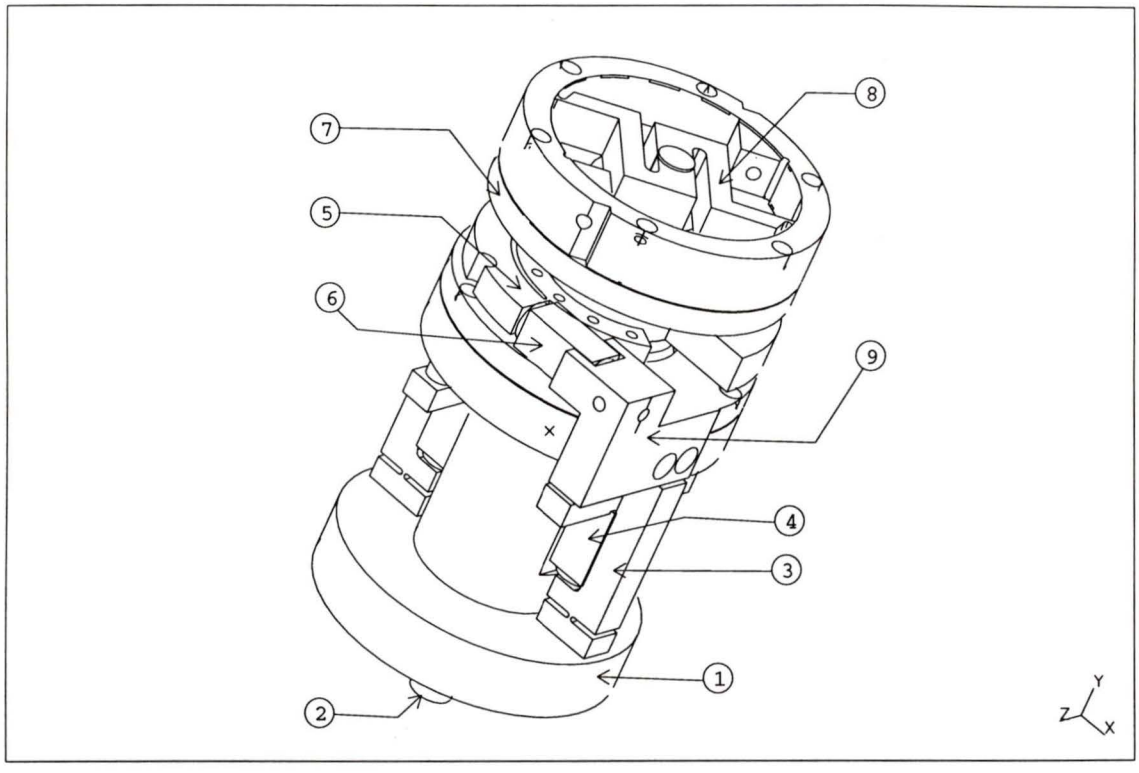

Figure 4.3: Surface boundary representation, with labelled major units, of the proposed actuator.

As seen in Figure 4.3, two clamp flexures and associated piezo devices, being 180 degrees apart from each other, make up the clamp unit. Components 7 and 8 constitute the oscillatory unit mentioned earlier. Component 5 is the flexure that creates the rotational motion. Other important components will be discussed in detail in the following subsections.

Number	Description
1	Housing
2	Output shaft
3	Clamp flexure
4	Clamp flexure piezo device
5	Rotational flexure
6	Rotational flexure piezo device
7	Clutch unit bearing housing
8	Clutch flexure
9	Piezo device holder

Table 4.3: Major components of the assembly.

4.2.3 Subunits of The Proposed Actuator

As mentioned earlier in §4.2, there are three main subunits comprising the rotary actuator. These units are all mounted on a housing. Output shaft of the actuator is supported by specially chosen ball bearings. Structures of these units and their physical relations with the other components of the actuator will be discussed in this section.

4.2.3.1 Clamp flexure unit

The clamp flexure unit is shown in Figure 4.4, and its main components are listed in Table 4.4. Detailed technical drawings of each part (except the standard ones) are given in Appendix C.

As briefly introduced in §3.3 in Chapter 3, flexure hinge mechanisms are the most commonly used mechanical amplification techniques to amplify the small displacements of piezoelectric actuation. Flexure hinges introduce compliance in bending about one axis while they are rigid about the other axes. Under an external load, the flexure hinge acts like a pivot point and allows the relatively more rigid part of the

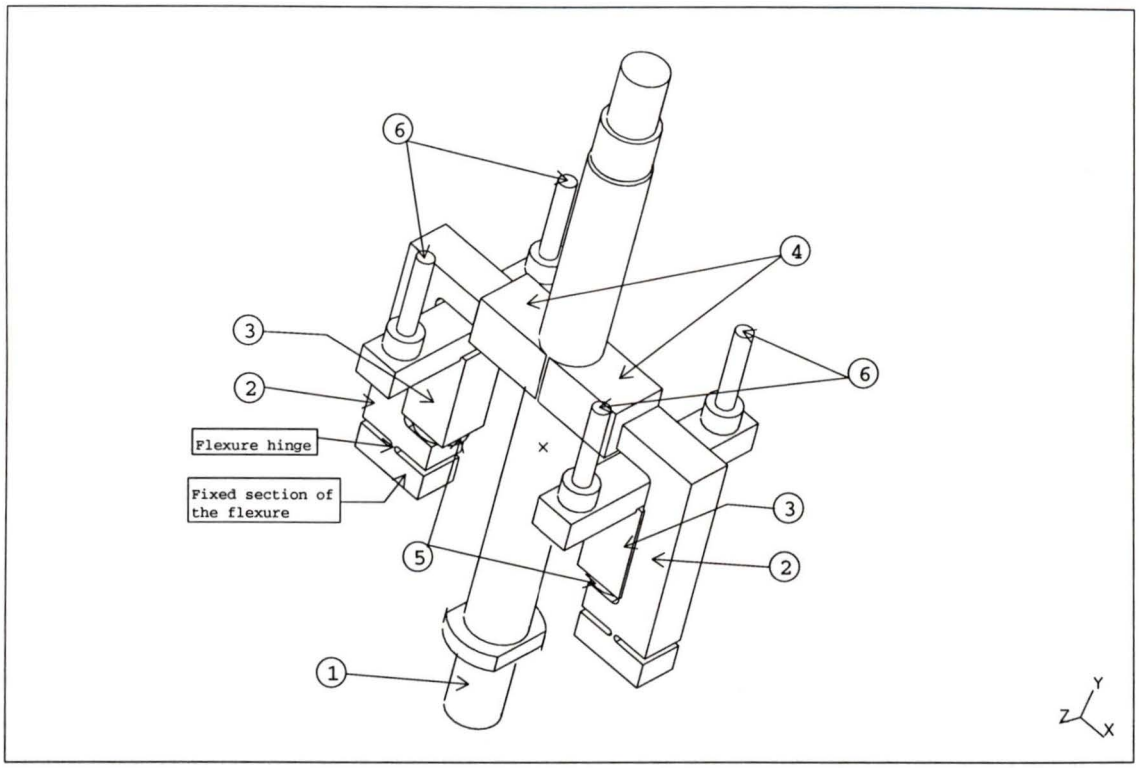

Figure 4.4: Clamp flexure unit and its components.

body to rotate about this point. The geometry of the flexure mechanism determines the amplification ratio. The point where the force is applied is displaced by a certain amount from its initial position during the actuation. This small displacement is amplified by the amplification ratio at the tip, and the tip force is reduced by the same ratio as well.

Even though geometric and dimensional tolerancing is specified very carefully on the part drawings as seen in Appendix C, there are always manufacturing errors resulting from a variety of sources such as the precision of the machine tool itself, human errors, temperature variations during the machining, and even the mechanical

Number	Description
1	Output shaft
2	Clamp flexure
3	Clamp flexure piezo device
4	Clamping shoes
5	Piezo device shear plates
6	Piezo device assembly and preloading bolts

Table 4.4: Main components of the clamp flexure unit.

compliance of the components which constitute such actuators. There is, however, not much tolerance for such errors in the design of piezoelectric actuators since the displacements obtained from piezoelectric actuation are in the order of microns.

There are two identical clamping flexures, shown in Figure 4.4, accommodated in the proposed actuator. Mechanical inputs to these flexures are provided by the longitudinal multilayer piezoelectric devices. The multilayer piezoelectric devices expand in the $-Y$ direction since the other ends are mechanically constrained as shown in the figure. Displacements of the piezoelectric devices are amplified at the tip by the amplification ratio of the flexure units. Thus, the tips are displaced by larger magnitudes in the $\pm X$ directions.

Displaced tips of the flexure units push the clamping shoes against the shaft wall and exert a normal force on the shaft through the surrounding clamping shoes. This force secures the static frictional torque between the rotating shaft and the inertial housing. At this state, the clamping unit and the shaft are said to be *active* and *clamped*, respectively. The reaction force, which determines the generated frictional torque, between the clamping shoes and the tip of the flexures is mainly determined by the total expansion of the piezo device itself, the amplification ratio of the flexure, and the blocking force-expansion characteristic of the piezoelectric device.

4.2.3.2 Rotational flexure unit

The rotational flexure unit and its components are shown in Figure 4.5. Main components of the rotational flexure unit are also listed in Table 4.5. Detailed technical drawings of each part can be found in Appendix C.

As seen in Figure 4.5, small angular displacements about the Y axis is generated by the expansion of a multilayer piezoelectric device accommodated in the subunit. The piezo device expands in the $-X$ direction, as shown in the figure, since, again, one end of the piezo device is mechanically constrained. This small expansion is amplified by the flexure leading to a larger displacement at the tip of the flexure arm in the $+X$ direction.

The tip of the flexure pushes the clutch unit's wall (see Figure 4.6) and rotates the clutch unit about its rotational axis by a small angle each time the piezo device is activated. During this torque transmission, clutching is active, and the generated torque is transmitted to the shaft. When the piezo device is deactivated, the rotational flexure is returned to its initial position by a compression spring placed between the housing and the other side of the circular push wall. The compression spring can be seen clearly in Figure D.7 given in Appendix D. During the passive stage, the clutching is not active whereas the clamp unit is active to clamp the output shaft.

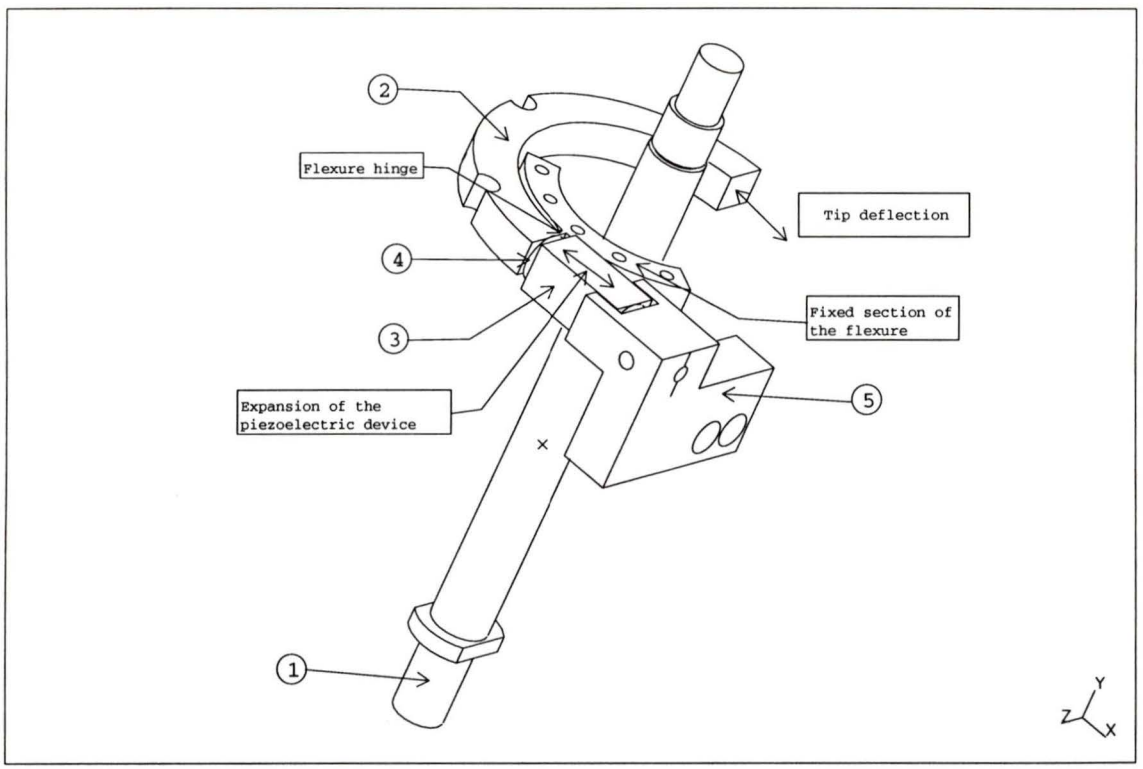

Figure 4.5: Rotational flexure unit and its components.

Number	Description
1	Output shaft
2	Rotational flexure
3	Rotational flexure piezo device
4	Piezo device shear plate
5	Piezo device holder

Table 4.5: Main components of the rotational flexure unit.

4.2.3.3 Clutch flexure unit

The clutch flexure unit and its components are shown in Figure 4.6. Detailed technical drawings of this unit are given in in Appendix C.

As mentioned in §4.2, step-wise continuous motion is generated by using only one half period of the oscillatory motion created by the piezoelectric actuation. Component 2 together with 4 form the oscillating unit. This complete subassembly is mounted on the shaft with special ball bearings and has one rotational degree of freedom. It can rotate with respect to the shaft about the Y axis. Clutching flexure itself is a monolithic flexure unit having two flexure arms (the flexure arms can be seen clearly in Figure 4.15). These flexure arms are actuated by two piezoelectric devices, only one of which is shown in Figure 4.6.

Flexure arms clamp the whole clutching subassembly to the shaft when the two piezo devices are activated. At this state, the clutch unit is said to be *active*. When the clutching is active, any torque applied to the push wall of the clutch flexure unit is transmitted to the shaft through the friction generated by the high blocking forces of the piezoelectric devices.

Component 4 has several functions (see Appendix C for details). This component carries the bearings which support the whole subassembly on the shaft, and it gives the clutch flexure unit the rotational degree of freedom about the Y axis. The torque generated by the rotational flexure unit is also transmitted to the shaft through this component. Monolithic circular section of this component is pushed by the rotational flexure in one direction during the first half of the oscillation, and it is pushed back by the compression spring in reverse direction during the second half. This mechanical relation can be seen in D.7.

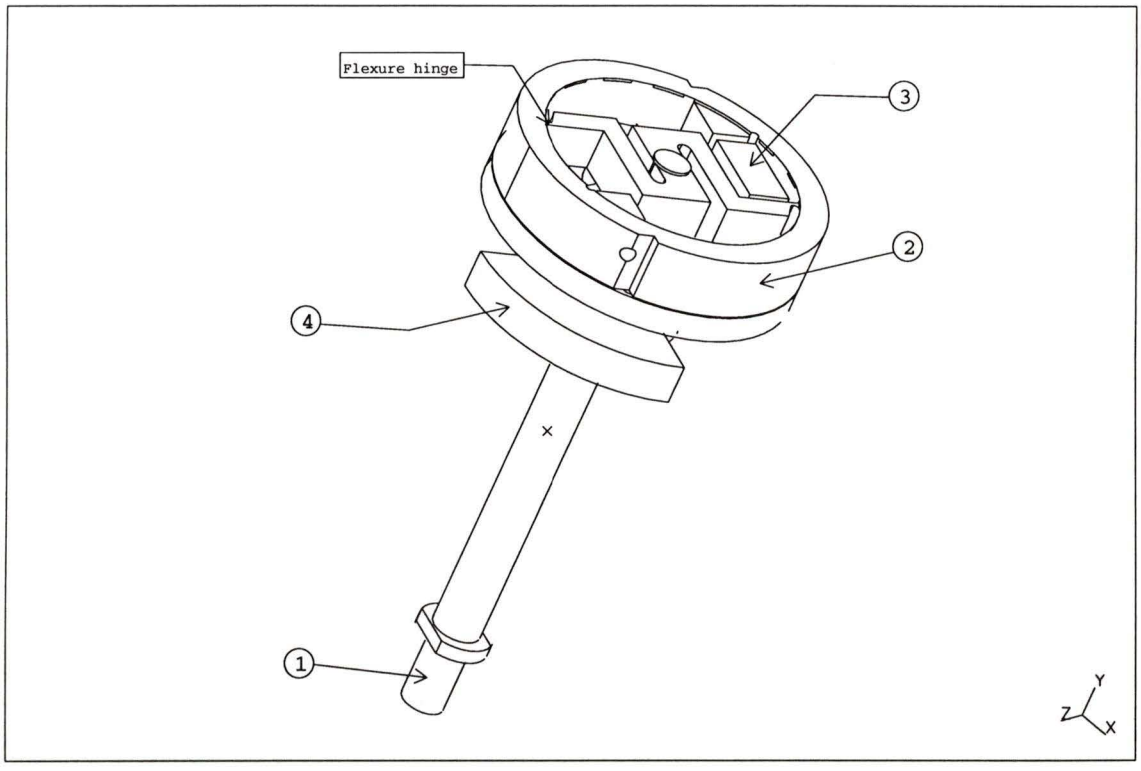

Figure 4.6: Clutch flexure unit and its components.

Main components of the clutch flexure unit are listed in Table 4.6

Number	Description
1	Output shaft
2	Clutch flexure
3	Clutch flexure piezo device
4	Clutch flexure unit push wall

Table 4.6: Main components of the clutch flexure unit.

4.2.4 Design Considerations

As mentioned earlier, there are certain additional considerations that have to be taken into account in the process of generating continuous motion by utilizing piezoelectric actuation. Failing to do so, even for a perfect design, may lead to an unsuccessful development. Some of these considerations are discussed below.

4.2.4.1 Backlash problem

Clearance or backlash between the components of a piezoelectric actuator may create problems. Since the mechanical displacements obtained from the piezoelectric actuation are very small, any backlash in the system can cause the displacements to die out before they are transmitted to the very end component in the mechanical loop. Even if the mechanism does not fail completely, the performance may be affected drastically. For a rotary actuator case, for instance, poor torque-speed characteristic and micropositioning accuracy might be the undesired consequences.

Not only the dimensional but also the geometric tolerancing has been found to be very crucial to the success of the device. Tolerances assigned, however, should not be tighter than what is actually needed since tight tolerancing is one of the factors which affect the final cost of the device. Unnecessary tolerancing should also be avoided.

A careful tolerance analysis has been performed during the design process of the proposed actuator. *Locational transition* and *locational interference* fits have been assigned to the mechanically adjacent components. Geometric tolerancing such as *flatness, roundness, cylindricity, perpendicularity*, and *parallelism* have also been assigned when needed. Such a careful tolerancing has, definitely, been one of the keys leading to a successful implementation of the conceptual design. Assigned tolerances can be examined on the part drawings given in Appendix C.

Preloading is another resorted solution to deal with the backlash problem. Mechanical chain between the piezo devices and the flexure mechanisms, for example, are all established through preloading. The flexures accommodated in the actuator have certain structural stiffness, and they behave like compression springs when they are loaded. Preload is mainly generated by pushing the piezo devices against the flexure walls, and this is realized by set screws or preloading bolts in each subunit. Preloading mechanisms for each subunit are shown in Figures 4.4–4.6.

It should also be mentioned that even a thin layer of industrial glue or adhesive of very high quality and stiffness may introduce undesired compliance. The use of such adhesives while building the prototype was deliberately avoided at the expense of more complex preloading mechanisms.

4.2.4.2 Mechanical amplifiers

As discussed earlier, utilization of *monolithic flexure hinges* is one of the most common techniques for displacement amplification. Flexure mechanisms used in the proposed rotary actuator have been already introduced in detail earlier in this chapter.

Due to the complexity of the flexure design, the finite element analysis technique was utilized to simulate the developed flexures prior to manufacturing. Some earlier works [25], [63], [64], [91], [98] were also used as starting points in determining the material type, the flexure heights and thicknesses. Then, the experimental data taken on the built mechanisms were compared with the finite element simulation results.

Two important criteria to be considered in selecting the flexure hinge material are the material's maximum ultimate tensile stress and maximum Young's modulus (modulus of elasticity) [25].

Titanium appears to be one of the most appropriate material options since it

meets both criteria mentioned above. In addition, it has other desirable mechanical properties such as high fatigue resistance and high speed of response, which is due to its high modulus of elasticity and relatively low density, and high hardness, which is essential for the flexure material when it is also used as a frictional element. Titanium was also the choice for a long-stroke piezo actuator developed for vibration isolation and suppression, and steering of precision subsystems on a spacecraft [100].

King et al. [98] discussed not only the effect of the material but also the geometry of the flexure hinge on the behaviour of such amplification mechanisms. Behaviour of *right-angle, elliptical, circular* and *corner-filleted* hinges are all elaborated and the finite element results for various geometries are documented by the same authors.

Scire et al. [63] elaborated on various material options in an early work proposing a piezo-driven micropositioning stage developed for optical and electron microscopes. Negligible backlash, lubricant-free operation, negligible stick-slip friction, noise-free and smooth operation, and high resolution displacement characteristic of flexure hinge amplification were underlined as advantages over bearings and sliding components. An iron-nickel alloy and the aluminum alloy *6061-T6* were suggested and tested as candidate materials since they closely match the thermal expansion coefficient of the piezo ceramic used. It was stated that the aluminum alloy may be the choice unless thermal stability is a major concern. An aluminum alloy was also the choice for a high precision translation mechanism developed for scanning tunneling microscopes in [64], where the importance of mechanical tolerances and the use of finite element technique were also emphasized. *AISI 1040* standard carbon steel was used for the flexure mechanism built for a linear piezoelectric actuator [91].

Considering its overall advantages, titanium was selected as the flexure material for the prototype rotary actuator of this thesis.

4.2.4.3 Machining techniques

Conventional machine tools such as milling machine and lathe were used to manufacture the prototype. Designing the components for lathe, whenever it is possible, may reduce the total manufacturing cost drastically. This fact has been taken into account during the design process of the actuator; this can be seen in the complete assembly and part drawings given in Appendix D and Appendix C, respectively.

Wire EDM (*Electro Discharge Machining*), a relatively expensive machining process, is one of the unavoidable machining techniques to manufacture the flexure hinges. Hinge profiles can be machined without introducing significant stresses by using wire EDM.

4.2.4.4 Bearing selection

The output shaft is the final component through which the generated high torque is transmitted to the load. Therefore, a proper support for the shaft is very crucial to the success and reliability of the actuator. The bearings should not introduce any backlash for the reasons discussed earlier. Furthermore, high blocking forces generated in the piezo devices are also transmitted to the inertial housing through the bearings; therefore, bearings should not introduce any additional compliance.

The use of *precision angular contact ball bearings* [101] to support the shaft is suggested in this thesis. Such bearings are also used in most machine tools to ensure the desired precision. They are supplied with substantial preloads and high tolerance classes. Using these bearings in pair or applying appropriate preload can provide zero backlash or even interference clearance. Precision angular contact ball bearings with the smallest possible contact angle should be used where high radial stiffness is needed [101].

Since the precision bearings are relatively expensive, angular contact ball bearings with standard tolerance class were used for the prototype. Output shaft itself and the clutch unit are both supported by such bearings. The axial preload is applied to the bearing pairs by specially designed self-locking nuts. Proper tolerancing is included on the part drawings of the related components (see Appendix C).

4.2.4.5 Shear loads acting on multilayer piezoelectric devices

As mentioned earlier in §4.1, piezoelectric ceramics cannot sustain high shear loads even though they can stand very high compressive forces. This limitation requires even more attention for multilayered piezo devices. In some cases, shear loads may be developed by the amplification mechanism. Such loading should be minimized to protect the multilayer devices.

One of the common solutions to suppress the shear loading is to accommodate a secondary flexure hinge being compliant in the generated shear stress direction. This method has been utilized in [63] and [98], and it is considered to be a relatively complex solution since it introduces an additional flexure hinge in the amplification mechanism.

Another simpler method is to transmit the generated blocking force through a stiff rolling element, a steel ball in most cases, which is free to move in the direction of generated shear force. By limiting the contact area to a single point on the ball, one can reduce the shear force to a small rolling friction force which can be tolerated by the multilayer devices. This method has been acknowledged by others [91], and it has been used for the proposed rotary actuator as well. The *shear plates*, given in Appendix C, are the contacting surfaces between the rolling elements, piezo devices and flexure walls. Continuous contacts between the adjacent components are all established by preloading mechanisms as explained earlier in §4.2.4.1. Shear plates

and the rolling elements are also included in the finite element simulations of the flexure mechanisms.

4.2.4.6 Assembly

The tolerances required by the design may not be completely realized because of the limitations of the machining facilities. Some of the manufacturing errors can be compensated during the assembly. Also, appropriate assembly techniques should be employed for the assembly process particularly for the interference fits required by the design.

Interference fits have been achieved by heating or cooling the components when it was possible to do so. For example, the angular contact ball bearings were inserted into their housing, shown in Figure C.6, by heating the housing. Inserting the shaft, shown in Figure C.3, was, on the other hand, performed by cooling the shaft. An ordinary cooler was used to achieve the required inserting temperature; liquid nitrogen might also be an option. The same technique was also used for the assembly of some other components such as the bearing housing unit shown in Figure C.21.

Appropriate preloads were applied to the flexure amplification mechanisms as mentioned in §4.2.4.1 previously. The use of any sort of adhesives during the assembly was avoided not to introduce any additional compliance in the adhesive layers.

Some parts whose function is crucial to the success of the rotary actuator may be *pinned* to each other during the assembly. Pinning can be done by drilling a precision hole through the adjacent parts while they are positioned and bolted already. Interference fit between the pins and corresponding parts ensures a backlash-free assembly. Monolithic rotational flexure, shown in Figure C.18, is pinned to its flange, shown in Figure C.14, for example, at two locations to avoid any small rotation

between these two components with respect to each other. Although pinning between some other components was planned at the design stage of the prototype, they were not performed since the required tolerances had already been achieved.

It should be reminded that pinning these components does not necessarily enforce a permanent fastening; it is also possible to disassemble them when needed.

4.2.5 Multilayer Piezoelectric Devices of The Proposed Rotary Actuator

Five multilayer piezoelectric devices are used in the proposed rotary actuator. The main reason behind this selection is the fact that such devices are capable of providing large displacements and high blocking forces.

The piezo devices were manufactured by Morgan Matroc Inc. [102], and the related data provided by the manufacturer are given in Table 4.7.

Material	$PZT\text{-}5H$
Dimensions	$15 \times 15 \times 30$ $[mm]$
Layer thickness	~ 0.14 mm
Operating voltage	250 V DC or ± 125 V AC
Maximum displacement	~ 30 μm @ 250 V DC
Maximum blocking force	$\sim 10,000$ N @ 250 V DC
Capacitance	~ 7.0 μF tested with 1 V @ 1 kHz
Dielectric coating	Provided against moisture and contamination

Table 4.7: Specifications of the multilayer piezoelectric devices used in the proposed rotary actuator.

Properties of $PZT\text{-}5H$ piezoelectric ceramic are presented in Table 4.8.

The piezo devices have been tested for their free displacements by using non-contact measuring techniques. The *interferometry* set-up designed and built at IRIS

Property	Value
Relative dielectric constant K_{33}^T	3400
Piezoelectric coefficient d_{33}	550×10^{-12} $[m/V]$
Young's modulus Y_{33}^E	4.8×10^{10} N/m^2
Maximum allowable applied field	20 kV/cm
Curie temperature	200 $°C$
Response time (max)	100 μsec

Table 4.8: Properties of PZT-5H piezoelectric ceramic.

Laboratory of the University of Victoria has been used to test the piezo devices. The interferometry set-up is capable of measuring the piezoelectric displacements with the accuracy of 0.1 μm. Measured data were taken by applying electric voltage to the multilayer piezoelectric devices while they are preloaded in a specially designed case. The expansion characteristic of the piezo devices versus applied voltage for increasing and decreasing voltages is shown in Figure 4.7. Such data also convey information about the nonlinearity and hysteresis characteristic of the multilayer piezo devices. Hysteresis characteristic, however, has been disregarded throughout this work since the piezo devices are driven only between "*on*" and "*off*" states during the operation of the rotary actuator.

Empirical formulae provided by the manufacturer are also included here. Substitution of the known values gives the specifications provided in Table 4.7.

$$\Delta h = nVd_{33} \tag{4.1}$$

Equation (4.1) was already discussed in §3.2.3. The number of layers, n, was provided as ~ 200 by the manufacturer for the piezo devices.

The capacitance for the square cross-section is given by:

$$C = \frac{nK_{33}^T \epsilon_0 A}{t} \tag{4.2}$$

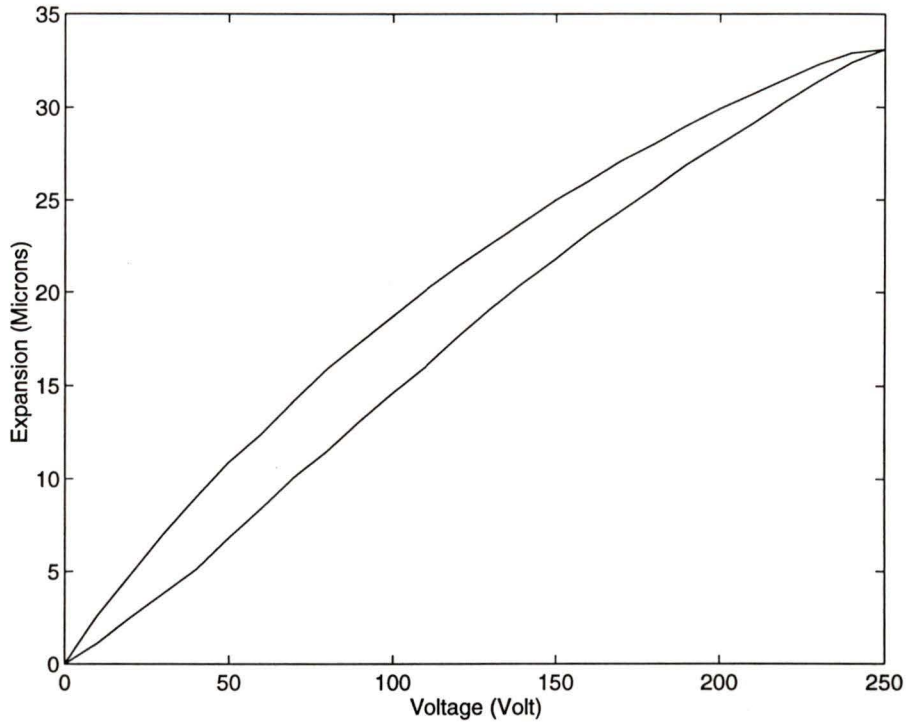

Figure 4.7: The expansion characteristic of the piezo devices versus applied voltage.

where C, n, K_{33}^T, A, t and ϵ_0 are the capacitance, number of layers, relative dielectric constant of the piezoelectric material, cross-sectional area of the multilayer device, layer thickness and permittivity of free space, which is 8.864×10^{-12} F/m, respectively.

The maximum blocking force generated by the multilayer devices can be calculated as follows:

$$F_b = \frac{nVd_{33}Y_{33}^E A}{h} \tag{4.3}$$

where F_b, n, V, d_{33}, Y_{33}^E, A and h are the generated blocking force, number of layers, applied voltage, piezoelectric coefficient, Young's modulus of the piezoelectric ceramic, cross-sectional area and length of the multilayer piezoelectric device, respectively. Equations (4.1), (4.2) and (4.3) are all given in MKS units.

The generated blocking force is approximately $10,000$ N as given in Table 4.7 and

calculated by Equation (4.3). However, the blocking force is the force generated in *zero* expansion case, and it is inversely proportional to the expansion as shown in Figure 4.8. It should be reminded that the relation shown in Figure 4.8 is idealized and may not be necessarily linear for actual devices.

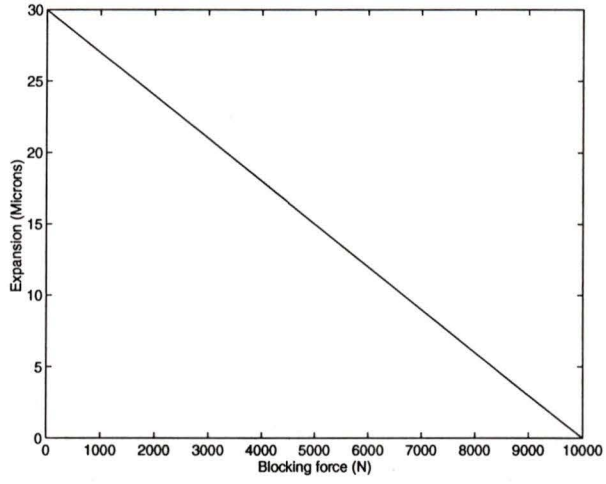

Figure 4.8: The expansion characteristic versus blocking force, @ 250 V DC operating voltage, of the piezo devices used for the proposed rotary actuator.

The piezo devices are able to provide very large expansion and blocking force at the expense of relatively high capacitance as given in Table 4.7. They also have relatively high dissipation factors. These characteristics reduce the bandwidth drastically. Also, high heat dissipation may result in excessive heating at high driving frequencies. This means that the driving frequency should be relatively low for the built prototype. This, consequently, affects the output speed-driving frequency characteristic of the prototype. The fact that using high-capacitance multilayer devices would reduce the output speed has been deliberately disregarded since the objective of the prototype design was to prove *the concept* with a high output torque.

4.3 Finite Element Simulations of The Flexure Hinge Mechanisms

The rotary actuator was solid modelled prior to the actual manufacturing. Solid modelling also made it possible to simulate the flexure amplification mechanisms. Although there are many assumptions involved in the finite element approach itself along with the assumptions made throughout the modelling process in this work, it is, still, a good approach to estimate the behaviour of the flexures before they are actually manufactured.

ANSYS5.2† was used throughout the finite element simulations. The linear equations of piezoelectricity used in ANSYS5.2 are [103]:

$$\mathbf{T} = \mathbf{c}^{\mathbf{E}}\mathbf{S} - \mathbf{e}\mathbf{E} \tag{4.4}$$

$$\mathbf{D} = \mathbf{e}^{T}\mathbf{S} + \epsilon^{\mathbf{S}}\mathbf{E} \tag{4.5}$$

where $\mathbf{e}^T$ represents the transpose matrix of the piezoelectric coefficient matrix $\mathbf{e}$. There is no need, of course, to mention that the use of linear equations of piezoelectricity in the simulations is an assumption itself.

SOLID5 and *SOLID98* are the two available built-in *coupled-field* solid elements of ANSYS5.2. SOLID5 is a brick element having three-dimensional magnetic, thermal, electric, piezoelectric and mechanical field capability with limited coupling between the fields. The element has eight nodes with up to six degrees of freedom (U_x, U_y, U_z, $Temp$, $Volt$, Mag) at each node. SOLID98, on the other hand, is a *10-node tetrahedral* version of the 8-node SOLID5 element. The element has the same degrees of freedoms at its each node as those of the brick element. It has a quadratic displacement

†ANSYS is a trademark of SAS IP.

behaviour, and it is well suited to mesh irregular shapes such as the geometries produced from various *CAD/CAM* systems [104].

Even though using the brick element might have reduced the solution time a little bit since it is a relatively simpler element, it would not be practical to use this element type because of drastic cross-sectional changes through the flexure hinges. Minimization of the computation time was not the main concern of this work; therefore, the 10-node tetrahedral solid element was used for the mesh generation throughout the simulations.

As mentioned earlier, due to the complex nature of the problem, a number of assumptions are involved in the modelling process in addition to the potential assumptions of the finite element approach itself; the assumptions are mainly due to the multilayer piezoelectric devices. As mentioned in §3.2.3, it is difficult to estimate the mechanical behavior of the multilayer piezoelectric devices analytically; therefore, such properties are usually determined experimentally. However, there is not even enough experimental data available in most cases. In fact, there were no available experimental data for the piezo devices used in this thesis work. Since modelling the multilayer piezo actuators was not the main objective of this work, the following assumptions were made throughout the finite element simulations:

e matrix: The total expansion of a multilayer device is proportional to the number of layers (see Equation (4.1)). The main contribution to the expansion value in the polarization direction comes from the e_{33} element of the **e** matrix given in Equations (4.4) and (4.5). Therefore, in modelling, the multilayer piezo devices were treated as single ceramic blocks having the piezoelectric properties of PZT-5 piezoelectric ceramic. However, the e_{33} element of the **e** matrix was modified so that it can provide the total displacement of the actual multilayer device. The modification was made by simply multiplying this matrix element

by the number of layers.

Stiffness matrix: Stiffness matrix for *PZT-5* material is available. However, such data is not available for the multilayer piezo devices. Therefore, the stiffness matrix of PZT-5 piezoelectric ceramic was used in the simulations. Here, again, the multilayer piezo devices were treated as single ceramic blocks with the mechanical properties of PZT-5 piezoelectric ceramic. To support this approach in the modelling, a 250 V operating voltage was applied to the piezo model itself in the direction of polarization. Both ends of the piezo device were constrained in the expansion direction to obtain the maximum blocking force. A $9,504$ N blocking force was observed. This value is very close to the manufacturer data given in Table 4.7.

Corner fillets: Finally, it was assumed that the flexure hinges have no filleted corners even though Wire EDM machining process creates approximately $0.007''$ corner radius at the flexure hinges because of the radius of the wire itself and a small amount of *overburn*. Corner radii make the flexure stiffer and decrease the amplification ratio. Corner-filleted flexures, however, have relatively longer life because of lower stress concentrations at the hinges. More about the effects of corner radius on flexure behaviour can be found in [98]. The reason behind this assumption is that meshing the models with no corner fillets is much easier and takes less computation time. Since the actual induced maximum stresses are less than those of the model, this can be considered as an additional safety factor in the design. Corner fillets are shown (with exaggeration) in Figures 4.9, 4.12, and 4.15 given later in this chapter.

Having made the assumptions discussed above, the dielectric, piezoelectric and mechanical properties of PZT-5 piezoelectric ceramic can be given as follows [105]:

$$\epsilon^{\mathbf{S}}\ [F/m] = \begin{bmatrix} 1.505 \times 10^{-8} & 0 & 0 \\ 0 & 1.505 \times 10^{-8} & 0 \\ 0 & 0 & 1.302 \times 10^{-8} \end{bmatrix}$$

$$\mathbf{e}\ [C/m^2] = \begin{bmatrix} 0 & 0 & 0 & 0 & 17 & 0 \\ 0 & 0 & 0 & 17 & 0 & 0 \\ -6.55 & -6.55 & 23.3 & 0 & 0 & 0 \end{bmatrix}$$

$$\mathbf{C}^{\mathbf{E}}\ [N/m^2] = \begin{bmatrix} 12.6 & 7.95 & 8.41 & 0 & 0 & 0 \\ & 12.6 & 8.41 & 0 & 0 & 0 \\ & & 11.7 & 0 & 0 & 0 \\ & & & 2.3 & 0 & 0 \\ & & & & 2.3 & 0 \\ & & & & & 2.35 \end{bmatrix} \times 10^{10}$$

Mechanical properties of *Titanium Grade-2*, of which the flexures are made, are given in Table 4.9.

Property	Value
Density $[gr/cm^3]$	4.506
Yield Strength(Tensile) $[N/m^2]$	280.86×10^6
Ultimate Strength(Tensile) $[N/m^2]$	351.076×10^6
Modulus of Elasticity(Tensile) $[N/m^2]$	45640×10^6

Table 4.9: Properties of Titanium Grade-2.

Based on the assumptions made and the available data, two different simulations were carried out:

1. Free deflection of the flexures

2. Induced maximum stresses at the flexure hinges for constrained deflection case

The simulations and their results for each flexure are discussed in the following subsections.

4.3.1 Finite Element Simulations of Clamp Flexure

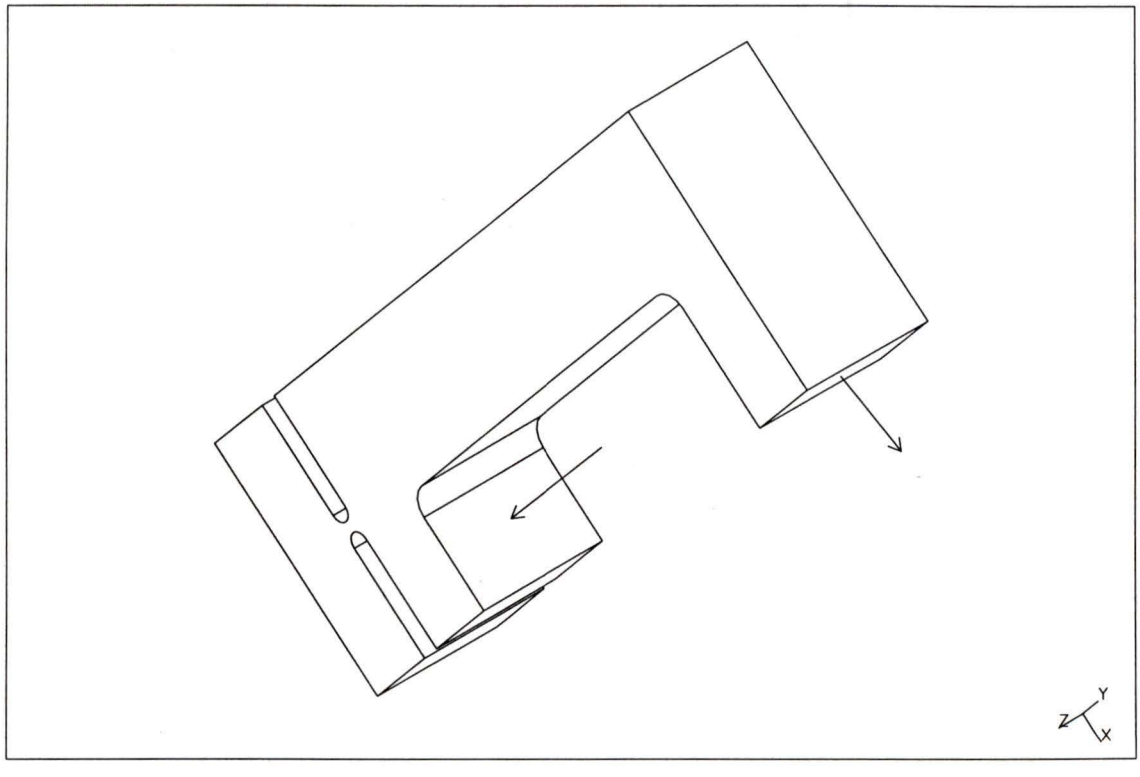

Figure 4.9: Surface boundary representation of the clamp flexure.

A surface boundary representation of the clamp flexure is given in Figure 4.9. The input applied by the multilayer piezoelectric device and tip deflection directions are

shown in the figure. The flexure hinge can also be seen clearly in the figure. Detailed technical drawings of this flexure can be found in Figure C.37.

The finite element simulation was carried out for the free deflection case. The body of the flexure was constrained completely, in all three directions, and a 250 V DC voltage was applied to the multilayer device in the direction of polarization. One end of the multilayer piezo device was also constrained in the direction of expansion. The simulated free deflection of the clamp flexure is given in Figure 4.10. A colour-coded

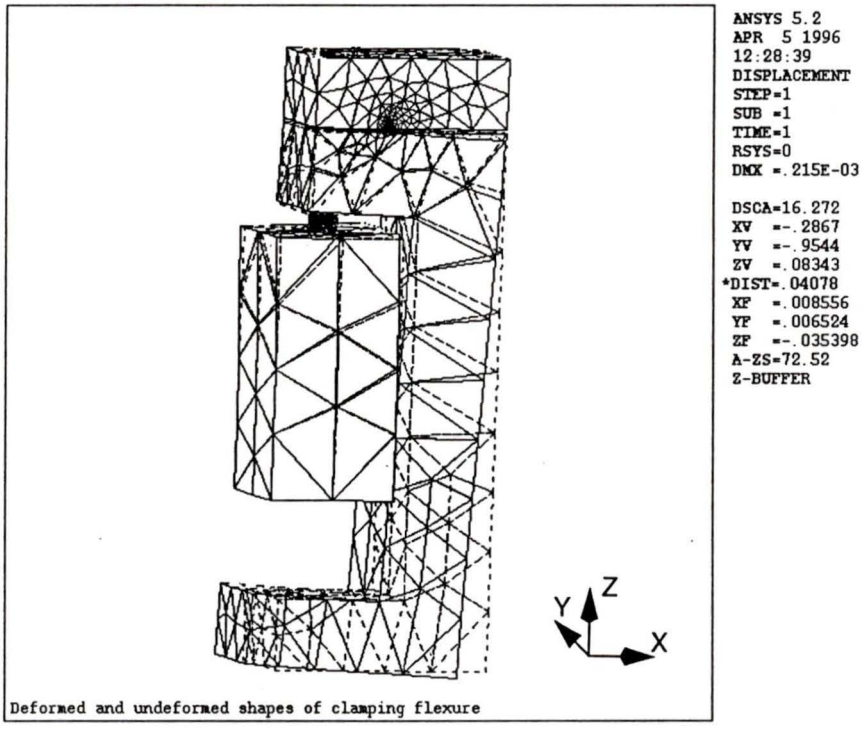

Figure 4.10: Free deflection of the clamp flexure.

plot of the deflection in the X direction is also given in Figure D.3 in Appendix D.

Free displacement simulation results of the clamp flexure are summarized in Table 4.10.

FE Simulation result	Value
Tip deflection in X direction $[\mu m]$	-195
Piezo expansion in Z direction $[\mu m]$	25
Approximate flexure amplification ratio	7.8

Table 4.10: Free displacement simulation results of the clamp flexure.

A similar simulation was conducted for the constrained case as well. Translation of the clamp flexure tip was constrained in the $-X$ direction *only*. Although the tip is actually allowed to translate in the $-X$ direction by the amount of the clearance between the shaft and the clamping shoes, such a clearance between these elements was not included in the model since it is not essential. Deformation of the clamp flexure for the constrained case is shown in Figure 4.11. Induced maximum stresses at the hinge are summarized in Table 4.11.

FE Simulation result	Value
Maximum σ_x at the hinge $[N/m^2]$	23.23×10^6
Maximum σ_y at the hinge $[N/m^2]$	27.60×10^6
Maximum σ_z at the hinge $[N/m^2]$	34.73×10^6
Maximum σ_{xy} at the hinge $[N/m^2]$	12.48×10^6
Maximum σ_{yz} at the hinge $[N/m^2]$	15.92×10^6
Maximum σ_{xz} at the hinge $[N/m^2]$	28.81×10^6

Table 4.11: Induced stresses for the clamp flexure.

It should be pointed out that maximum induced stresses at the flexure hinge are well below the allowable stress limits of titanium. Also, the maximum driving frequency for this prototype is as low as 40 Hz. Fatigue analysis for the flexure hinges was not conducted for this prototype. Such analysis, however, is important and should be performed if such devices are to be produced commercially.

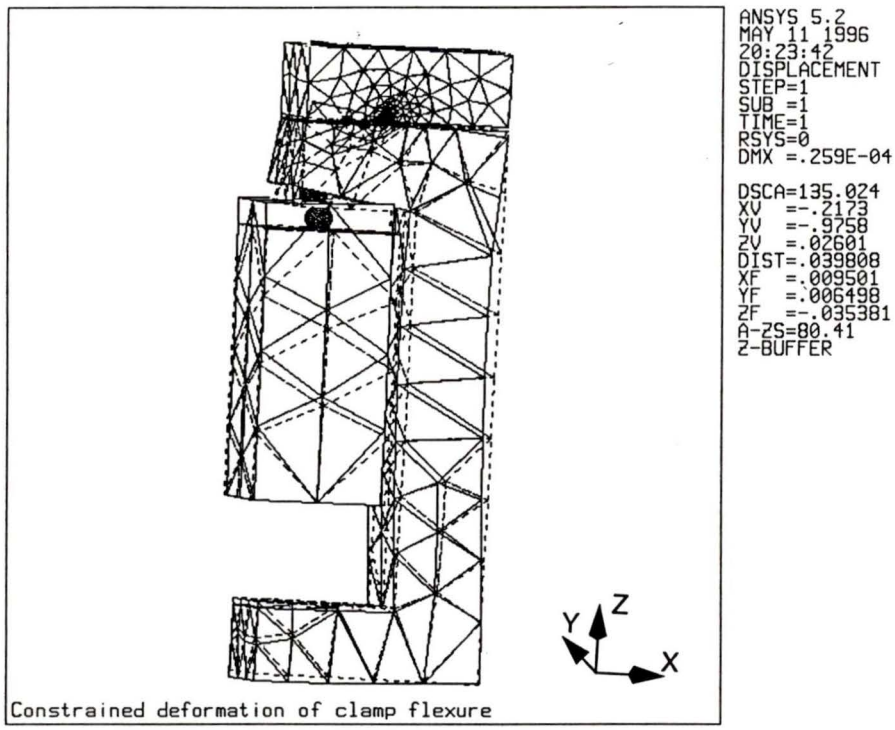

Figure 4.11: Deformation of the clamp flexure constrained in the $-X$ direction.

4.3.2 Finite Element Simulations of Rotational Flexure

A surface boundary representation of the rotational flexure including the input and tip deflection directions is given in Figure 4.12. A detailed technical drawing of the rotational flexure is given in Figure C.19.

In the free deflection finite element simulation of the rotational flexure, the body of the flexure was fixed, and a 250 V DC voltage was applied to the multilayer device. One end of the multilayer piezo device was also constrained in the direction of expansion. The simulated free deflection is presented in Figure 4.13.

A colour-coded illustration for this flexure is also included in Appendix D, Figure D.4, for a better visualization of the tip deflection in the $-Z$ direction. Free

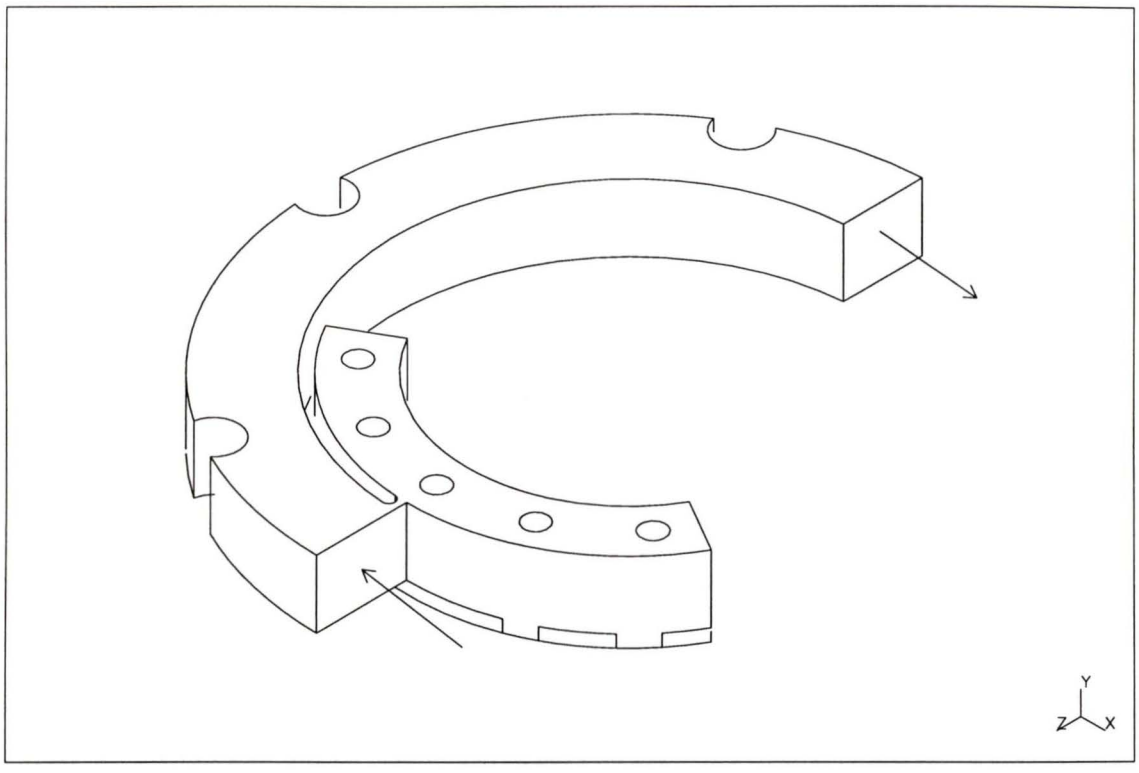

Figure 4.12: Surface boundary representation of the rotational flexure.

displacement simulation results are summarized in Table 4.12.

The simulation was carried out for the constrained case as well. It was assumed that the translation of the rotational flexure tip was completely constrained in the $-Z$ direction. However, the flexure tip is constrained by a compression spring and the payload itself in the actual case. Since it is relatively simpler to simulate and the induced maximum stresses at the hinge are even higher than those of the actual case, the simulation was performed for the rigidly constrained case. Maximum induced stresses at the hinge are summarized in Table 4.13.

Since there is no constraint in the X direction at the tip, the tip deflects in this direction during the actuation. A vector representation of this translation is shown in

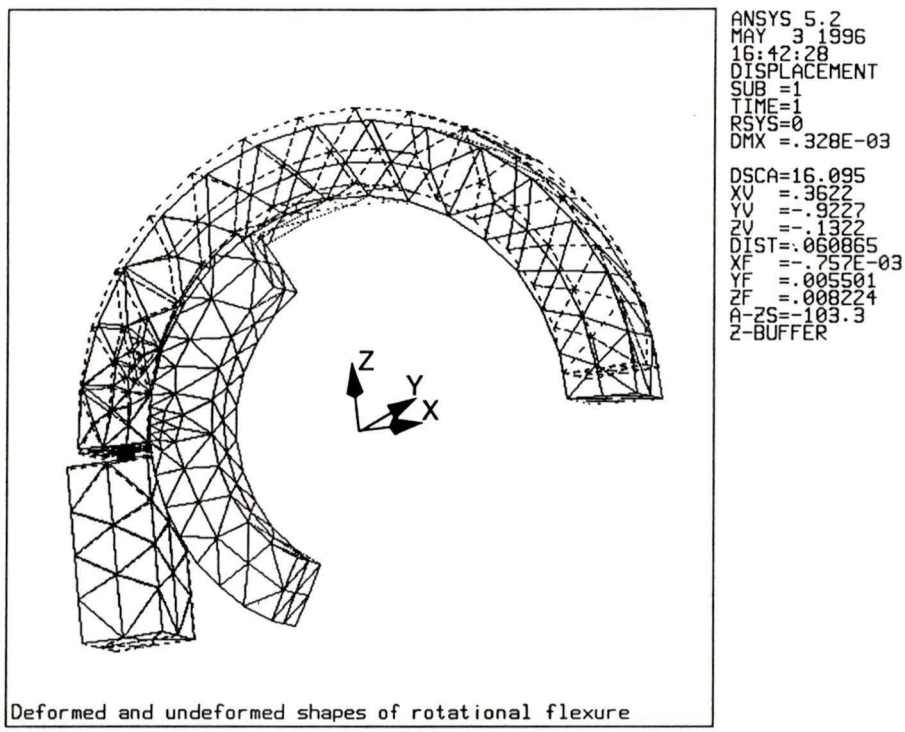

Figure 4.13: Free deflection of the rotational flexure.

Figure 4.14. In fact, this translation and deformation of the hinge are what reduces the generated blocking force. It is difficult to restrain the tip in the X direction in reality; therefore, this case was not simulated at all.

FE Simulation result	Value
Tip deflection in Z direction $[\mu m]$	-304
Piezo expansion in Z direction $[\mu m]$	25
Approximate flexure amplification ratio	12.2

Table 4.12: Free displacement simulation results of the rotational flexure.

FE Simulation result	Value
Maximum σ_x at the hinge $[N/m^2]$	55.07×10^6
Maximum σ_y at the hinge $[N/m^2]$	39.23×10^6
Maximum σ_z at the hinge $[N/m^2]$	122.68×10^6
Maximum σ_{xy} at the hinge $[N/m^2]$	10.85×10^6
Maximum σ_{yz} at the hinge $[N/m^2]$	12.19×10^6
Maximum σ_{xz} at the hinge $[N/m^2]$	38.26×10^6

Table 4.13: Induced stresses for the rotational flexure.

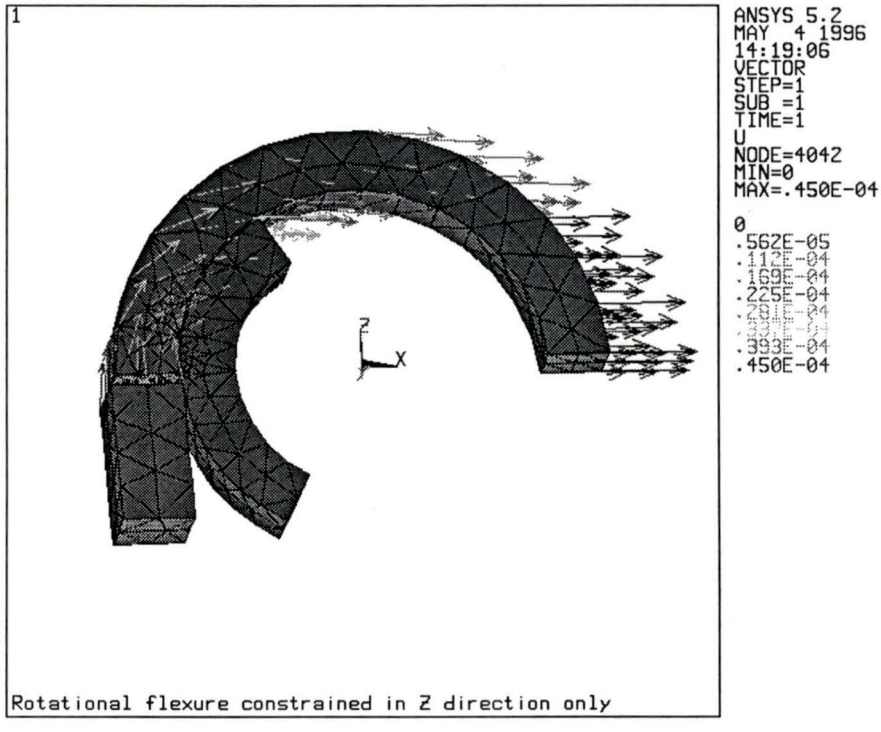

Figure 4.14: Deflection of the rotational flexure constrained in the $-Z$ direction.

4.3.3 Finite Element Simulations of Clutch Flexure

A surface boundary representation of the clutch flexure including the input and tip deflection directions is given in Figure 4.15. The flexure arms can be seen clearly in this representation. A detailed technical drawing of this flexure unit is given in Figure C.26.

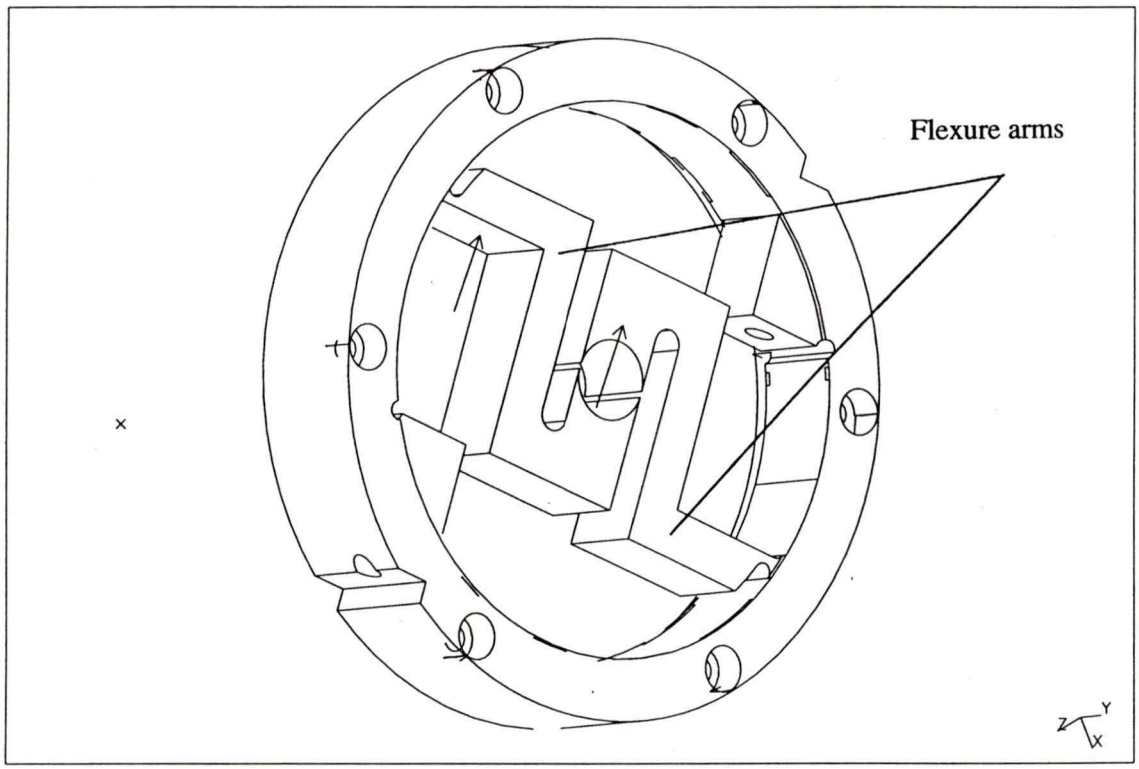

Figure 4.15: Surface boundary representation of the clutch flexure.

Only one of the two flexure arms was simulated. The body of the clutch flexure was fixed in all three directions in the model. With the same assumptions, material properties, applied voltage and boundary conditions as explained for the clamp and

rotational flexures, the finite element simulation was carried out for the free deflection of the flexure tip. The simulated free deflection of the clutch flexure is shown in Figure 4.16. A colour-coded illustration is also included in Appendix D, Figure D.5. Free displacement simulation results of the clutch flexure are summarized in Table 4.14.

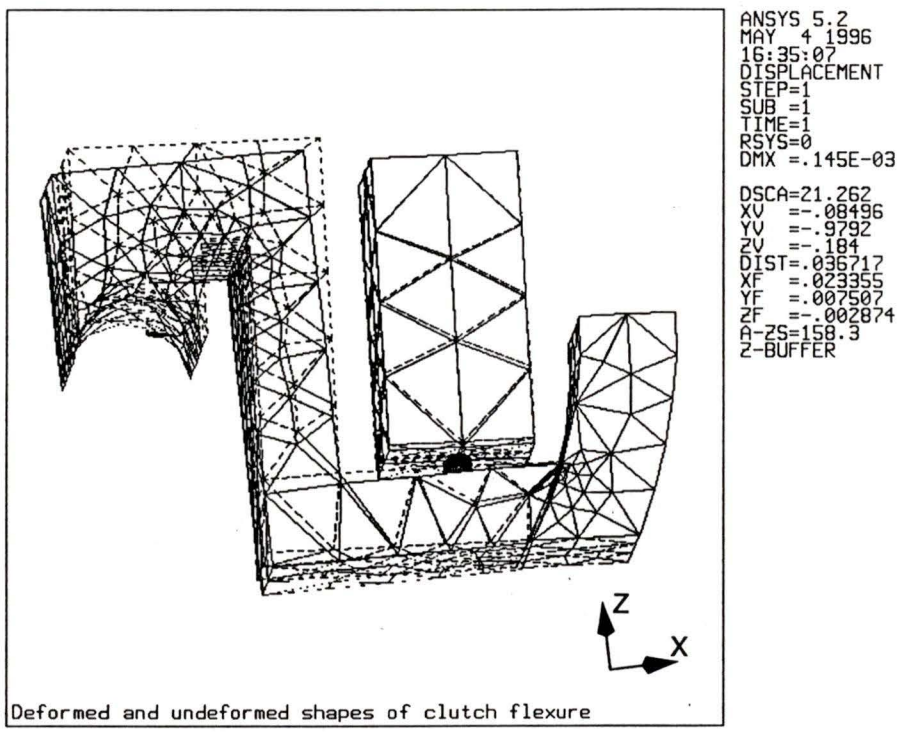

Figure 4.16: Free deflection of the clutch flexure.

FE Simulation result	Value
Tip deflection in Z direction $[\mu m]$	-107
Piezo expansion in Z direction $[\mu m]$	-25
Approximate flexure amplification ratio	4.3

Table 4.14: Free displacement simulation results of the clutch flexure.

A simulation for the constrained case was run for the clutch flexure arm as well. In

this case, translation of the clutch flexure tip was constrained in both the $-Z$ and $-X$ directions. These boundary conditions are imposed by the contacting shaft surface in the actual case. Although the tip is actually allowed to translate in both directions before the contact begins, it was, again, assumed that there was no clearance between the clutch flexure tip and the shaft boundary. Deformation of the clutch flexure arm is shown in Figure 4.17.

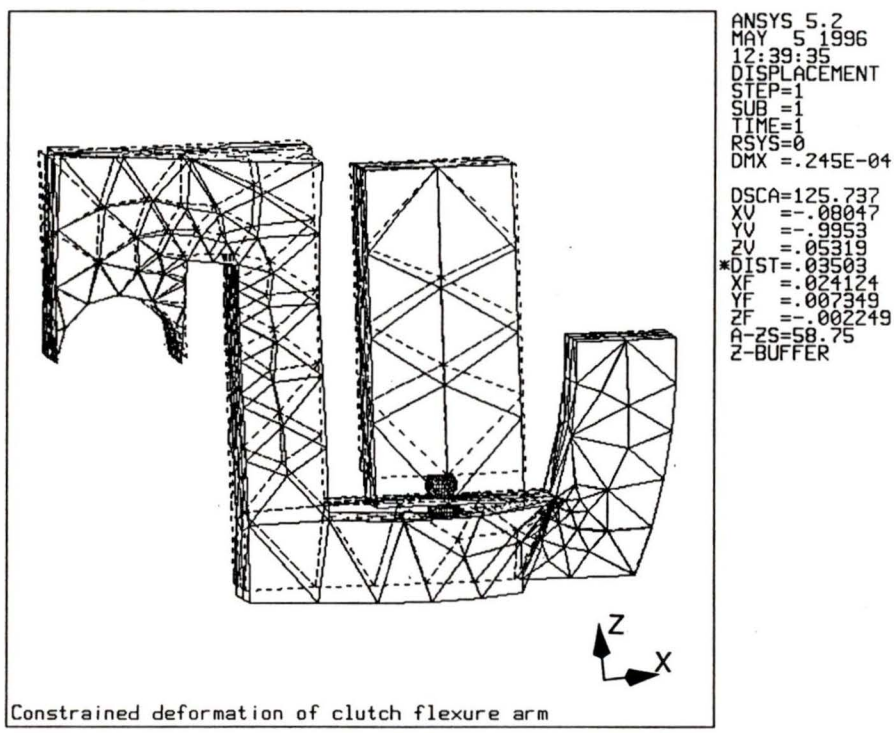

Figure 4.17: Constrained deformation of the clutch flexure.

Induced maximum stresses at the hinge, on the other hand, are summarized in Table 4.15.

FE Simulation result	Value
Maximum σ_x at the hinge $[N/m^2]$	32.33×10^6
Maximum σ_y at the hinge $[N/m^2]$	21.42×10^6
Maximum σ_z at the hinge $[N/m^2]$	33.21×10^6
Maximum σ_{xy} at the hinge $[N/m^2]$	8.94×10^6
Maximum σ_{yz} at the hinge $[N/m^2]$	13.14×10^6
Maximum σ_{xz} at the hinge $[N/m^2]$	34.12×10^6

Table 4.15: Induced stresses for the clutch flexure.

4.4 Experiments

There are four different experimental phases involved, and they will be discussed in this section. The following experiments were performed:

1. Free expansion tests of the multilayer piezoelectric devices
2. Free tip deflection test of each flexure
3. Switching frequency-speed characteristic of the proposed rotary actuator
4. Torque-speed characteristic of the proposed rotary actuator

Detailed elaboration of each experimental phase along with the results will be presented in the following subsections.

4.4.1 Free Expansion Test of The Multilayer Piezoelectric Devices

The multilayer devices were tested for their free expansion characteristics prior to their use. A 250 V operating voltage was applied to the piezo devices while they were preloaded in a specially-designed case. Experimental data were taken for increasing

and decreasing applied voltages by using non-contact measurement techniques as explained in §4.2.5 previously. Applied voltage-free expansion characteristic of one of the piezo devices is presented in the same section in Figure 4.7. All of the piezo devices exhibit similar characteristics; detailed discussions on the piezo units of the rotary actuator is given in §4.2.5.

4.4.2 Free Displacement Test of The Flexures

Testing the flexures for their free deflection characteristics was the second experimental phase. Free deflection tests of the flexures were conducted while they are in their subassembly state as previously shown in Figure 4.4, Figure 4.5 and Figure 4.6.

The flexures were preloaded appropriately, and the deflections at the tips were recorded by reading the mechanical dial indicators while increasing the applied voltage manually. The interferometer was not suitable for the measurement of the tip deflections because of the small angular motions of the flexure tips. Dial indicators, however, were able to provide satisfactory data to validate the finite element simulations.

Free deflection tests of the flexures were performed both increasing and decreasing applied voltages. Figures 4.18, 4.19, and 4.20 show the deflections for increasing voltages. The data taken for decreasing voltages were not accurate enough, and they are not presented here. The indicators were not able to respond to small voltage changes accurately and linearly in reverse direction.

Test for each flexure mechanism was performed in the same fashion, and the results are presented in the following plots. The experimental set-up is shown in Figure D.6 in Appendix D.

The plots provided in Figure 4.18, Figure 4.19 and Figure 4.20 can be compared to

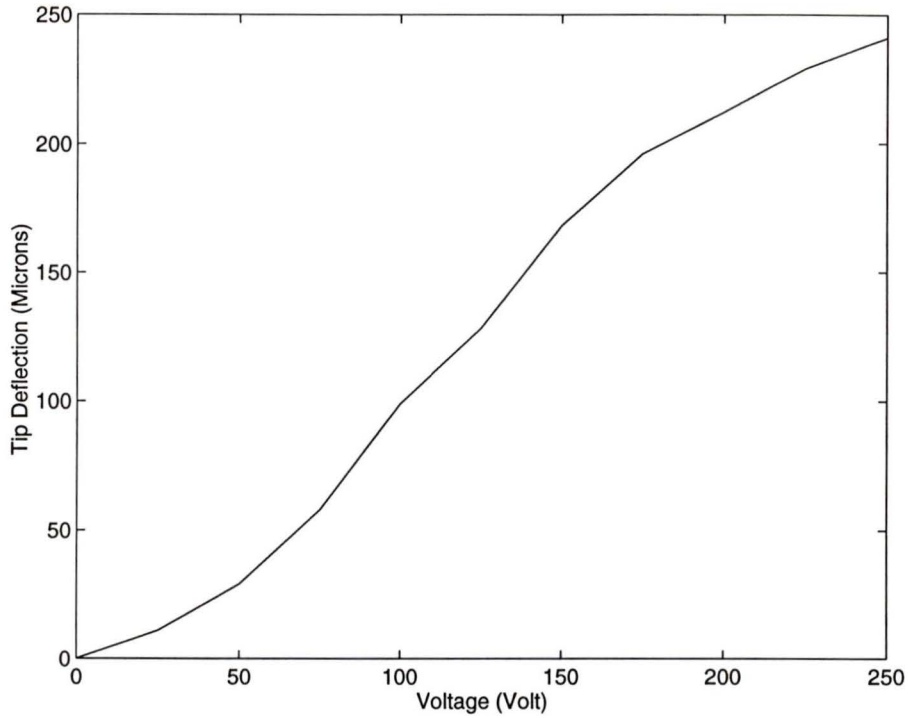

Figure 4.18: Free deflection of the clamp flexure for increasing voltages.

the increasing voltage portion of the voltage-expansion characteristic of the multilayer devices, which was given in Figure 4.7 previously. The observed difference is more likely due to the insufficient accuracy of the dial indicators used for the measurements. It should also be mentioned that the data presented in these plots had to be taken several times since each time the data appeared slightly different from the previously taken data for the same flexure. This is, again, due to the poor respond of the dial indicators to the small voltage changes. The plots presented here are based on the average values of these measurements. The maximum tip deflections measured each time, however, seemed to be in agreement, and these values are used to validate the simulation results.

Table 4.16 compares the experimental and simulation results of each flexure mechanism. Actual maximum tip deflection for each flexure is slightly different from the

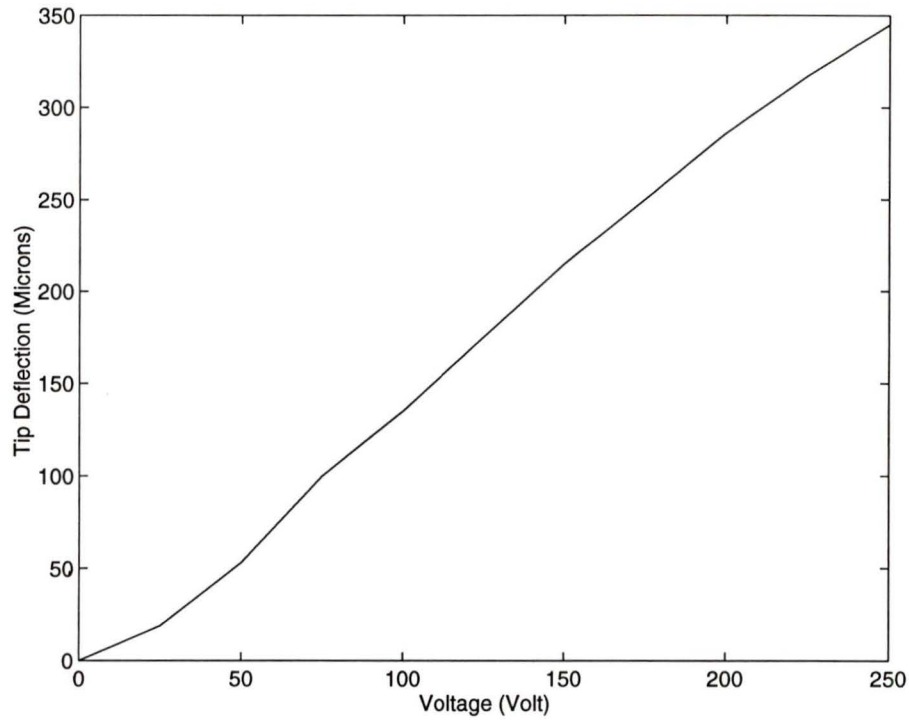

Figure 4.19: Free deflection of the rotational flexure for increasing voltages.

associated simulation result. Such discrepancy is mainly due to the assumptions explained earlier in §4.3. The difference in measured and simulated piezo expansions is also due to the same assumptions. Even the actual piezo expansions at 250 V are slightly greater than the manufacturer value provided in Table 4.7 earlier in §4.2.5.

Table 4.16 implies that the amplification ratio of each flexure is slightly smaller (except the clutch flexure) than that of the associated simulation result. This is, again, because of the assumption made for the corner fillets. In general, the experimental results appear to be in agreement with the discussions given along with the assumptions which are explained in §4.3. The differences between the simulated and experimental values are small from practical point of view justifying the assumptions made. Overall approach and the results are considered to be satisfactory for the design of flexure amplification mechanisms.

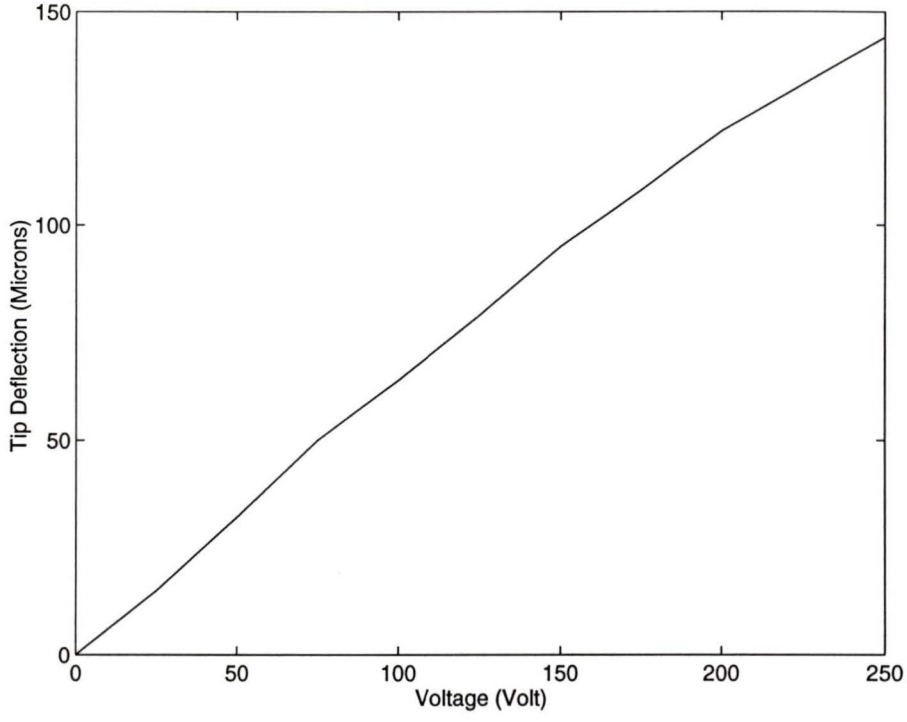

Figure 4.20: Free deflection of the clutch flexure for increasing voltages.

	Clamp		Rotational		Clutch	
	FE	Exp	FE	Exp	FE	Exp
Piezo expansion @ 250 V [μm]	25	33	25	33	25	33
Maximum free tip deflection [μm]	195	241	304	345	107	144
Approximate flexure amplification ratio	7.8	7.3	12.2	10.5	4.3	4.4

Table 4.16: Comparison of the simulation and experimental results for free deflection of the flexure tips.

4.4.3 Switching Frequency-Output Shaft Speed Characteristic of The Proposed Actuator

The prototype was tested for its driving frequency-shaft speed characteristic at zero load. The test was carried out by timing the output shaft of the actuator for increasing driving frequencies. 240 V operating voltage was applied to the piezoelectric devices during the test. Driving frequency was changed by changing the time parameters in the program. Frequency versus output shaft rotational speed (with no load) characteristic of the proposed actuator is given in Figure 4.21. As expected,

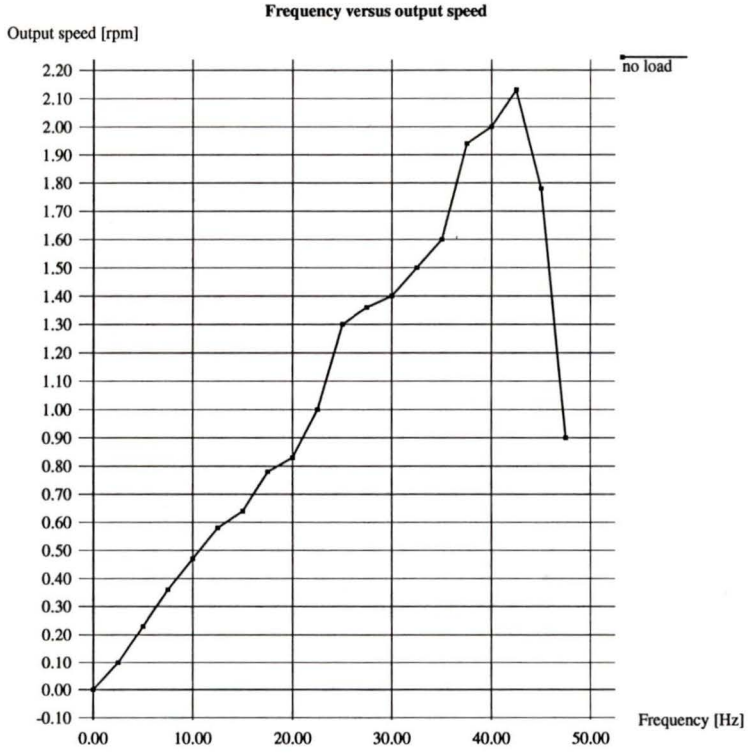

Figure 4.21: Frequency versus output speed characteristic of the proposed actuator.

the shaft speed increases as the driving frequency is increased. The actuator reaches its maximum speed, $\sim$ 2.0 rpm, at about 42 Hz driving frequency. The maximum

shaft speed is believed to be the result of operating at a frequency near the resonant frequency of the rotational flexure. Above this frequency, the shaft speed declines, and the shaft eventually stops at higher frequencies. There are two basic explanations for declining shaft speed. First, the voltage amplifiers of the driving circuit are not able switch the piezo devices at the same speed as those of the generated driving signals, and this has a minor effect on declining shaft speed at higher frequencies. The main reason, on the other hand, is that the rotational flexure operates out of phase in a frequency range above its resonant frequency, and synchronization with the other subunits is distorted. As a result, the shaft speed drops. This effect was also noted in other publications [91], [93], [94], [96].

The actuator is able to provide a resolution of 1500 and 1300 of a revolution ($\sim 0.24°$ and $\sim 0.28°$) at low and moderate speeds, respectively. The resolution was calculated by timing the shaft and dividing the travelled rotation angle by the number of excitation in this interval. These values were obtained at 240 V operating voltage, and the resolution can be further increased by simply decreasing the applied voltage at the expense of lower torque values. The proposed actuator has even potential for higher resolutions without decreasing the obtained torque. It is possible to reduce the step size even further by simply changing the amplification ratio of the rotational flexure.

In addition to its potential advantages such as its compactness and reliability, the proposed actuator exhibits better speed characteristic than those of previously proposed actuators of the same type [93], [94], [96] (see §3.4.4). The rotary actuator proposed by Hayashi et al. [95], §3.4.4.3, seems to provide higher shaft speeds at low driving frequencies. However, it should be mentioned that such high speed is achieved by utilizing very high mechanical amplification. Such amplification mechanisms introduce potential drawbacks such as poor resolution, lack of compactness and

not being suitable for miniaturization. The rotary actuator proposed by Ishida et al. [96], §3.4.4.4, exhibits similar speed characteristic at high frequencies at the expense of more multilayer piezoelectric devices used and a more complex driving circuit.

4.4.4 Toque-Speed Characteristic of The Proposed Actuator

The prototype was also tested for its static frictional torques and torque-speed characteristic. Torque measurement was performed by mounting a pulley of a known diameter and loading the shaft by hanging varying weights through a metal string fixed at the pulley. 240 V operating voltage was, again, used for the torque measurements.

First, the static frictional torque of each subunit was measured by activating the piezoelectric devices of that particular unit only. The clamp and clutch units were able to provide ~ 36 Ncm and ~ 39 Ncm static frictional torques, respectively. The torque generator itself, on the other hand, was able to generate a very high torque of over 250 Ncm. Although excessive loading of the torque generator was avoided for safety reasons, the maximum obtainable torque is believed to be even higher. Then, the torques for varying shaft speeds were measured. Measured torque-speed characteristic of the proposed actuator is given in Figure 4.22.

The maximum torque is better than those of previously proposed actuators of the same type [93], [94], [95] (see §3.4.4) considering the obtainable shaft speed for similar payloads. The rotary actuator proposed by Ishida et al. [96], §3.4.4.4, offers very high shaft speeds at high driving frequencies at the expense of more multilayer piezoelectric devices used and a more complex driving circuit. The overall approach is also completely different than those reviewed in §3.4.4.

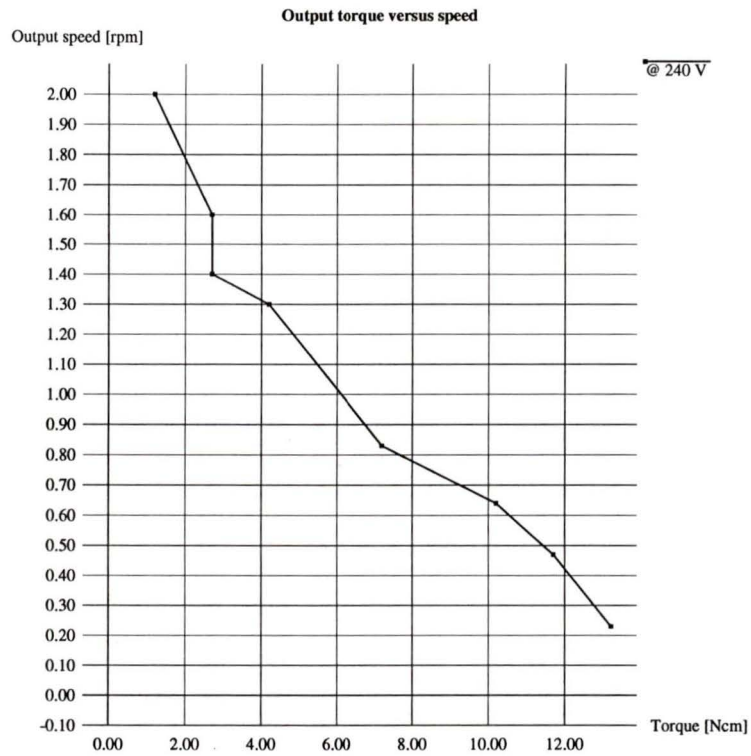

Figure 4.22: Torque versus output speed characteristic of the proposed actuator.

Although the actuator proposed in this thesis is able to generate very high torque, such high torque is not transmitted to the shaft completely because of relatively lower frictional clutching and clamping torques. No special attention has been paid to the quality of the friction surfaces during the development process. It is, however, possible to increase the frictional torques of these subunits by increasing the friction surfaces slightly and by paying more attention to the quality of these surfaces. The proposed actuator is expected to provide even better torque values with such technical improvements.

4.5 Driving Circuit

Simplicity of the driving circuit is one of the advantages of the proposed actuator. The driving circuit is, mainly, a high voltage and high speed switching circuit for the multilayer piezo devices. It consists of a controller which generates the required signals with the appropriate timing, a main power supply which provides 250 V operating voltage, a five-channel amplifier, and finally, 5-V and 12-V low voltage power supplies.

An 8-line I/O *Basic Stamp I Module (BS1-IC)*† [106] is used as a controller. Basic Stamp module is a miniature single-board computer which runs a BASIC-like programming language. It is designed for data acquisition, interfacing, and industrial control where low cost and simplicity of the components are important considerations. The module has a BASIC interpreter, an EEPROM, a resonator, and a 5-$Volt$ regulator in it. The program is stored in the EEPROM and maintained there with no power requirement. When the module is turned on, its BASIC interpreter reads and executes the BASIC instructions stored in its EEPROM. The programming language is a special language called *PBASIC* having familiar BASIC instructions and additional instructions for I/O functions. The programs can be edited by using an ordinary PC, and they can be converted into PBASIC tokens by using a simple company-provided software. Finally, the instructions can be downloaded through a three-pin cable over the parallel port of the PC. Some important specifications of the controller are given in Table 4.17 [106].

Schematic layout of the driving circuit is given in Figure 4.23. It should be reminded that the PC shown in Figure 4.23 does not have to be in the loop once the final program is written and downloaded to the controller.

Amplifier circuit for each piezo channel is shown in Figure 4.24. The box labelled

†Basic Stamp I Module (BS1-IC) is a trademark of PARALLAX, Inc.

Controller	
I/O Lines	8
EEPROM (programs & data)	256 bytes
RAM (variables)	14 bytes
Maximum Program Length	80 instructions
Clock Speed	4 MHz
Program Execution Speed	2000 instructions/sec.
Maximum Serial I/O Speed	2400 baud
Package	14-pin module
PC Programming Interface	Parallel

Table 4.17: Specifications of the controller used for the driving circuit.

as "5-channel amplifier" in Figure 4.23 contains one of these switching circuits for each multilayer piezo device.

Typical signal configuration, which can be achieved with the presented driving circuit, to drive the rotary actuator is given in Figure 4.25. In Figure 4.25, time delay between the signals which are applied to the clamp, clutch and rotational flexure unit's piezoelectric devices are shown. In the figure, T represents the total signal interval while τ represents the overlapping intervals between the consecutive signals. Overlapping between the clamp and clutch flexure's piezoelectric devices is given to make sure that clamping is not released before clutching is completed. This prevents the payload from rotating the shaft in reverse direction during the transition. Overlap region between the rotational and clutch flexure piezoelectric devices ensures that clutching is active when the rotational flexure's piezoelectric device is activated. Overlapping between the clamp and rotational flexure units, on the other hand, prevents the shaft rotation in reverse direction by the payload and the small frictional torque between the shaft surface and the flexure arms during the recovery of the rotational flexure.

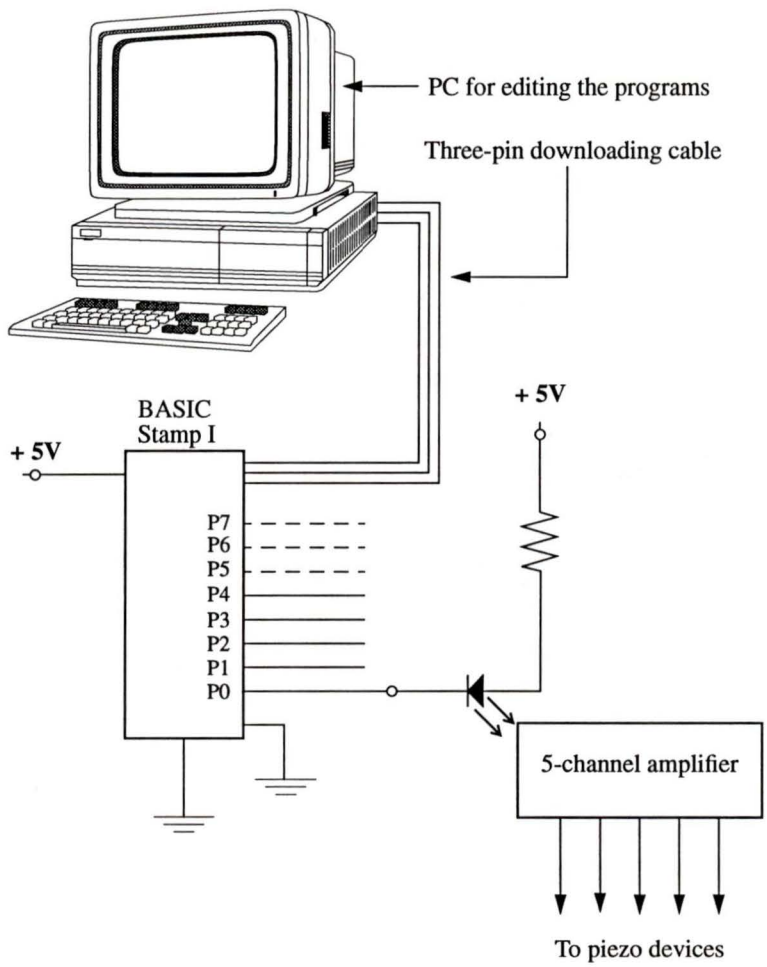

Figure 4.23: Schematic layout of the driving circuit.

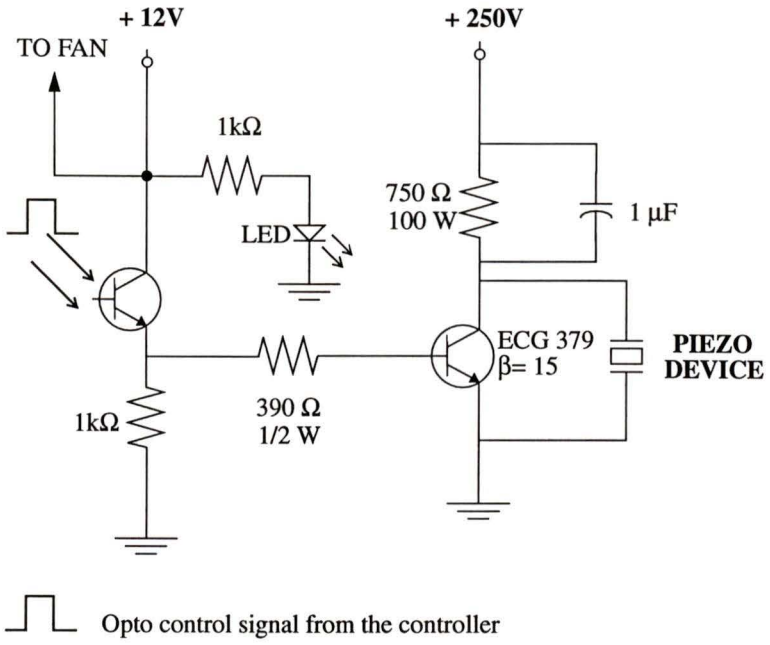

Figure 4.24: Amplifier circuit for the multilayer piezo devices.

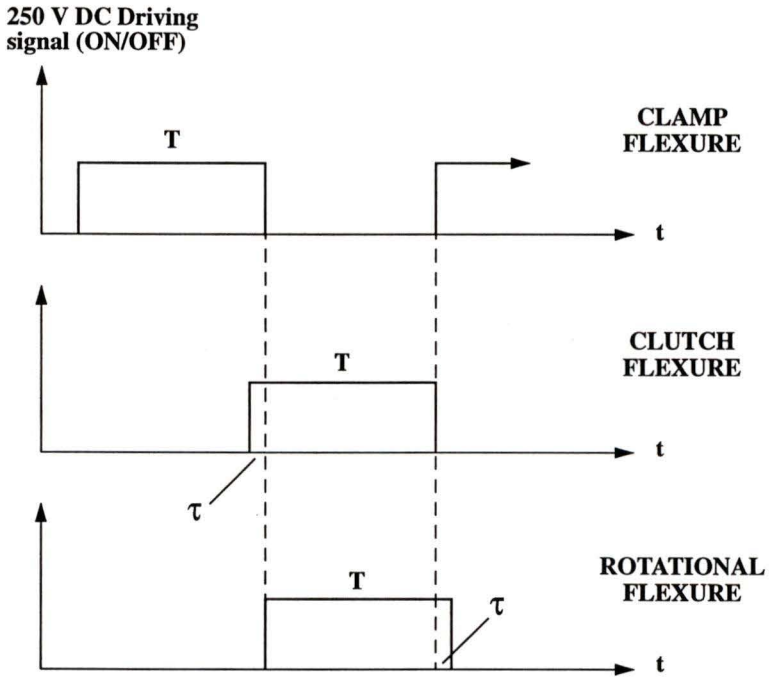

Figure 4.25: Driving signals for the proposed rotary actuator.

Chapter 5

Conclusions and Recommendations for Future Developments

This work confirms the potential of piezoelectric actuation for high-precision positioning devices. Micropositioning devices of this sort are required by a wide range of industrial and medical applications. The utilization of the converse piezoelectric effect in such challenging applications, however, requires special attention and expertise. The most important technological aspects of utilizing the converse piezoelectric effect such as the design approach, material selection, manufacturing, assembly, and final adjustments are addressed and associated solutions are suggested in this thesis.

Conversion of the micron displacements into continuous rotary motion with the desired characteristics requires preliminary physical and numerical modelling. The proposed mechanisms should be evaluated numerically prior to their actual fabrication. A systematic design approach based on solid modelling and numerical simula-

tions has been developed. Successful operation of the proposed rotary actuator proves the importance of the modelling approach.

A new piezoelectric rotary actuator has been developed. The developed actuator converts the small expansions (in the order of microns) of piezoelectric actuation into the step-wise continuous rotary motion. The entire approach of this thesis work including the proposed actuator itself is unique and offers a number of potential advantages.

The developed actuator includes three different and unique flexure amplification mechanisms. The design of these mechanisms was the most challenging aspect of this work. The proposed flexure mechanisms have been built following the solid and numerical modellings. The assumptions made throughout the numerical modelling allow to develop a relatively simple modelling procedure for actuators with multi-layer piezoelectric devices. The suggested approach also reduces the computation time within an acceptable range of computational errors. The results of the physical experiments which were conducted on the built flexures are in agreement with those of the simulations. This confirms the validity of the modelling assumptions. Such an agreement and failure-free operation of the developed flexure hinge amplification mechanisms verify the reliability of the suggested approach.

A prototype of the proposed actuator and associated driving circuit have been built for experimental validation. A smooth transition from the solid model to the built prototype has been achieved. Disappointment-free operation of the built prototype is the *proof of concept* for not only the operating principle proposed in this thesis but also the suggested methodology for the entire development process.

The main subunits of the prototype actuator were tested for their *static frictional torques.* The maximum static torques, at a 240 V operating voltage, were measured as $\sim 36\ Ncm$ and $\sim 39\ Ncm$ for the clamp and clutch flexure units, respectively. The

maximum torque which can be generated by the developed rotational flexure unit (or the torque generator) was measured as 250 Ncm. The proposed flexure design for torque generation is unique offering highly compact, reliable and high torque with the advantage of its simple structure. The actuator exhibits potential for higher torque values.

The prototype actuator has been tested for its driving frequency-shaft speed characteristic for zero load as well as for its torque-speed characteristic for various loading conditions. The actuator shows remarkable characteristics and presents a number of advantages over the existing actuators of the same nature. Experimental results are presented and compared with those of previously proposed actuators to show the potential superiority of the developed actuator. Overall results have been found to be highly promising.

The prototype is able to provide a resolution of 1500 of a revolution ($\sim 0.24°$) at low speeds and 1300 of a revolution ($\sim 0.28°$) at moderate speeds. The actuator itself, however, has also potential for higher resolutions with no decrease in the maximum obtainable torque. It is possible to reduce the step size further by simply changing the amplification ratio of the rotational flexure, which can be done by modifying either the overall geometry of the flexure mechanism or the hinge itself. The first prototype aimed at proving the concept rather than providing the highest possible resolution of microseconds. However, one can foresee that such resolutions can easily be achieved based on the promising results of the first prototype.

The proposed piezoelectric rotary actuator can be used in micropositioning and mechatronics applications where high torque-speed characteristics, compactness and reliability and electromagnetic disturbance-free operation are required. It would not be too overly stated if it is claimed that the proposed actuator has a commercial potential even at its first prototype stage.

Future work to improve the characteristics of the proposed actuator can be summarized as follows:

- The proposed actuator shows good potential for further miniaturization, and this should be included in the objectives of future designs.
- Fatigue analysis for the flexure hinges should be performed to optimize their geometries and amplification ratios.
- With increased friction surfaces and improved surface qualities (special coatings, for instance) higher torques can be achieved; such additions should also be taken into consideration.
- Optimal selection of the piezoelectric devices with the lowest possible capacitance and highest possible blocking force has a profound effect on the torque-speed characteristics of the actuator, and this should be performed as well.
- The moving components of the actuator should be made as light as possible to reduce the inertia. This can be done by optimizing the geometries and using alternative materials such as special ceramics. Such an improvement will increase the frequency-speed and torque-speed characteristics of the actuator.
- The actuator has potential for extremely high resolutions, and this feature should be shown in future designs as well.

Patent application for the developed actuator is currently in progress.

References

[1] *Micropositioning Systems.* Burleigh Instruments, Inc., New York.

[2] RAYMOND B. SEYMOUR & GEORGE B. KAUFFMAN (1990). Piezoelectric Polymers. *Journal of Chemical Education*, 67B(9):763-765.

[3] WALTER GUYTON CADY (1964). *Piezoelectricty: An Introduction to the Theory and Applications of Electromechanical Phenomena in Crystals*, Vol. 1. Dover Publications, New York.

[4] TAKURO IKEDA (1990). *Fundamentals of Piezoeectricity.* Oxford University Press, New York.

[5] BERNARD JAFFE, WILLIAM R. COOK & HANS JAFFE (1971). *Piezoelectric Ceramics.* Academic Press, New York.

[6] SIDNEY B. LANG (1974). *Sourcebook of Pyroelectricity.* Gordon and Breach Science Publishers, New York.

[7] CAROL ZWICK ROSEN, BASAVARAJ V. HIREMATH & ROBERT NEWNHAM (1992). *Key papers in Physics —Piezoelectricity.—* American Institute of Physics, New York.

[8] J. GRINDLAY (1970). *An Introduction to the Phenomenological Theory of Ferroelectricity.* Pergamon Press, Oxford.

[9] JACK C. BURFOOT (1967). *Ferroelectrics.* D. Van Nostrand Company Ltd., London.

[10] R. E. NEWNHAM (1984). Structure-Property Relations in Electronic Ceramics. *Journal of Material Education*, 6(5):813-839.

[11] WAI-FAH CHEN & ATEF F. SALEEB (1994). *Constitutive Equations for Engineering Materials, Volume 1.* Elsevier Science B.V., New York.

[12] E. FATUZZO & W. J. MERZ (1967). *Ferroelectricity.* John Wiley & Sons, Inc., New York.

[13] T. G. KING, M. E. PRESTON, B. J. M. MURPHY & D. S. CANNELL (1990). Piezoelectric Ceramic Actuators: A Review of Machinery Applications. *Precision Engineering*, 12(3):131-136.

[14] *The Piezo Book.* Burleigh Instruments, Inc., New York.

[15] KENJI UCHINO & SHOICHIRO NOMURA (1981). New Electromechanical Materials and Their Applications. *Japanese Journal of Applied Physics*, 20(Supplement 20-4):225-228.

[16] A. YA. DANTSIGER, O. N. RAZUMOVSKAYA, L. A. REZNICHHENKO, L. D. GRINEVA, R. U. DEVLIKANOVA, S. I. DUDKINA, S. V. GAVRILYACHENKO & N. V. DERGUNOVA (1993). New, Highly Effective Piezoceramic Materials. *Inorganic Materials*, 29(9):1145-1147.

[17] N. V. DERGUNOVA, A. YA. DANTSIGER, S. I. DUDKINA, O. N. RAZUMOVSKAYA & L. A. REZNICHENKO (1993). Piezoceramic Material for Effectors in Robotics. *Inorganic Materials*, 29(9):1153-1154.

[18] DON BERLINCOURT (1981). Piezoelectric Ceramics: Characteristics and Applications. *Journal of The Acoustical Society of America*, 70(6):1586-1595.

[19] WANG YONGLING (1990). Recent Developments on The Applications of Ferroelectrics in China. *IEEE 7th International Symposium on Appplications of Ferroelectrics*, pp. 9-10.

[20] SHINJIRO TASHIRO, HIDEJI IGARASHI & KIYOSHI OKAZAKI (1981). Mechanical Strength of Several Kinds of Piezolelectric Ceramics. *Japanese Journal of Applied Physics*, 20(Supplement 20-4):197-200.

[21] SHOICHIRO NOMURA, KUMIKO KANETA, JUN KUWATA & KENJI UCHINO (1981). Electromechanical Properties of Piezoelectric Ceramics in the PLZT-PZN System. *Japanese Journal of Applied Physics*, 20(Supplement 20-4):179-182.

[22] TOSHIO TANIMOTO AND TAKASHI YAMAMOTO & KIYOSHI OKAZAKI (1990). Mechanical and Electrical Properties of Piezoelectric Ceramics Under Repeated Compression Fatigue Tests. *IEEE 7th International Symposium on Applications of Ferroelectrics*, pp. 202-205.

[23] LESLIE J. BOWEN & KENNETH W. FRENCH (1992). Fabrication of Piezoelectric Ceramic/Polymer Composites by Injection Molding. *IEEE International Symposium on Applications of Ferroelectrics*, pp. 160-163.

[24] *Piezoelectric Ceramics: Product Catalogue, Application Notes.* B.M. Hi-Tech Inc., Collingwood, Ontario.

[25] J. K. THORNLEY (1993). *Methods of Application of Piezoelectric Multilayer Actuators to High-Speed Clutching, Using Displacement Amplification.* PhD Thesis, Loughborough University of Technology, UK.

[26] YUTAKA ICHINOSE & MIZUHIRO TOBITA (1985). Piezoelectric Ceramic Transducers for Electronic Telephone Sets. *Japanese Journal of Applied Physics*, 24(Supplement 24-2):28-30.

[27] TOSHIYUKI MATSUOKA, MOTOMU ASANO, HIROSHI FUKUSHIMA, HIROMU OKAMOTO, MASAYOSHI UCHIDA & TERUYUKI MATSUI (1993). Mechanical Analysis for Micro Mobile Machine with Piezoelectric Element. *Proceedings of the IEEE/RSJ International Conference on Intelligent Robots and Systems*, pp. 1685-1690.

[28] TORSTEN GERLACH & HELMUT WURMUS (1995). The Dynamic Micropump: A Piezoelectric Actuator for Liquids & Gases. *International Conference on Recent Advances in Mechatronics*, pp. 373-380.

[29] C. TURNER, R. M. PARKIN & J. A. G. KNIGHT (1995). The Use of Piezomechanics in High Speed Pneumatic Actuators. *International Conference on Recent Advances in Mechatronics*, pp. 388-395.

[30] P. K. WATLER & M. V. SEFTON (1990). A Piezoelectric Driven Controlled Release Micropump for Insulin Delivery. *Transactions on American Society for Artificial Internal Organs*, 36:70-77.

[31] H. P. TRAH, H. BAUMANN, C. DORING, H. GOEBEL, T. GRAUER & M. METTNER (1993). Micromachined Valve with Hydraulically Actuated Membrane Subsequent to a Thermoelectrically Controlled Bimorph Cantilever. *Sensors and Actuators A*, 39:169-176.

[32] DIANN E. BREI & JAMES BLECHSCMIDT (1992). Design and Static Modeling of a Semicircular Polymeric Piezoelectric Microactuator. *Journal of Microelectromechanical Systems*, 1(3):106-115.

[33] H. S. Tzou (1989). Development of a Light-Weight Robot End-Effector Using Polymeric Piezoelectric Bimorph. *IEEE International Conference on Robotics and Automation*, pp. 1704-1709.

[34] Jan G. Smits & Arthur Ballato (1994). Dynamic Admittence Matrix of Piezoelectric Cantilever Bimorphs. *Journal of Microelectromechanical Systems*, 3(3):105-111.

[35] Yoshiaki Fuda, Minoru Murata & Yashuyuki Matsuo (1985). Multilayer Piezoelectric Ceramic Bimorph Actuator. *Japanese Journal of Applied Physics*, 24(Supplement 24-2):485-487.

[36] Toshio Fukuda, Shinobu Hattori, Fumihito Arai, Hideo Matsuura, Tsutomu Hiramatsu, Yoichi Ikeda & Akinari Maekawa (1993). Characteristics of Optical Actuator-Servomechanisms Using Bimorph Optical Piezoelectric Actuator. *IEEE International Conference on Robotics and Automation*, pp. 618-623.

[37] Hiroya Seki (1992). Modeling and Impedance Control of a Piezoelectric Bimorph Microgripper. *Proceedings of the IEEE/RSJ International Conference on Intelligent Robots and Systems*, pp. 958-965.

[38] Muneo Yorinaga, Daisuke Makino, Kiyoshi Kawaguchi & Masataka Naito (1985). A Piezoelectric Fan Using PZT Ceramics. *Japanese Journal of Applied Physics*, 24(Supplement 24-3):203-205.

[39] C. Julian Chen (1992). Electromechanical Deflections of Piezoelectric Tubes with Quartered Electrodes. *Applied Physics Letters*, 60(1):132-134.

[40] G. Binnig & D. P. E. Smith (1986). Single-tube Three-dimensional Scanner for Scanning Tunneling Microscopy . *Review of Scientific Instruments*, 57(8):1688-1689.

[41] C. Julian Chen (1992). In Situ Testing and Calibration of Tube Piezoelectric Scanners. *Ultramicroscopy*, 42(44):1653-1658.

[42] R. G. Carr (1988). Finite Element Analysis of PZT Tube Scanner Motion for Scanning Tunelling Microscopy. *Journal of Microscopy*, 152(2):379-385.

[43] M. Locatelli & G. Lamboley (1988). Easy Method To Characterize A Piezoelectric Ceramic Tube As A Displacer. *Review of Scientific Instruments*, 59(4):661-663.

[44] RYUICHI MATSUDA & REIZO KANEKO (1991). Micro-step XY-Stage Using Piezoelectric Tube Actuator. *IEEE Micro Electro Mechanical Systems*, pp. 137-141.

[45] W. WERSING AND M. SCHNOLLER & H. WAHL (1986). Multilayer Piezoelectric Ceramic Actuators. *IEEE International Symposium on Applications of Ferroelectrics*, pp. 652-655.

[46] W. B. HARRISON, K. D. MCHENRY & B. G. KOEPKE (1986). Monolithic Multilayer Piezoelectric Ceramic Transducers. *IEEE International Symposium on Applications of Ferroelectrics*, pp. 265-272.

[47] YUZO SHIMADA, KAZUAKI UTSUMI, MASATOMO YONEZAWA & HIDEO TAKAMIZAWA (1981). Properties of the Large-capacitance Multilayer Ceramic Capacitor. *Japanese Journal of Applied Physics*, 20(Supplement 20-4):143-146.

[48] SADAYUKI TAKAHASHI, ATSUSHI OCHI, MASATOMO YONEZAWA, TAKESHI YANO, TAKESHIGE HAMATSUKI & IZUMU FUKUI (1983). Internal Electrode Piezoelectric Ceramic Actuator. *Japanese Journal of Applied Physics*, 22(Supplement 22-2):157-159.

[49] L. J. BOWEN, T. SHROUT, W. A. SCHULZE & J. V. BIGGERS (1980). Piezoelectric Properties of Internally Electroded PZT Multilayers. *Ferroelectrics*, 27:59-62.

[50] W. WERSING, H. WAHL & M. SCHNOLLER (1988). PZT-based Multilayer Piezoelectric Ceramics with AgPd Internal Electrodes. *Ferroelectrics*, 87:271-294.

[51] K. LUBITZ & H. HELLEBRAND (1990). Properties of PZT Multilayer Actuators. *IEEE International Symposium on Applications of Ferroelectrics*, pp. 509-512.

[52] SYUJI YAMASHITA (1981). Piezoelectric Pile. *Japanese Journal of Applied Physics*, 20(Supplement 20-4):93-95.

[53] M. KONDO, K. OHYA & S. SHIMIZU (1990). Effects of One-dimensional Compressive Stress on the Properties of Multilayer Piezoelectric Ceramic Actuator. *IEEE International Symposium on Applications of Ferroelectrics*, pp. 530-534.

[54] ATUSHI OCHI, SADAYUKI TAKAHASHI & SATORU TAGAMI (1985). Temperature Characteristics for Multilayer Piezoelectric Ceramic Actuator. *Japanese Journal of Applied Physics*, 24(Supplement 24-3):209-212.

[55] W. B. CARLSON, S. E. TROLIER, A. SAFARI, R. E. NEWNHAM & L. E. CROSS (1986). Multilayer Actuator Design. *IEEE International Symposium on Applications of Ferroelectrics*, pp. 641-644.

[56] SADAYUKI TAKAHASHI (1985). Multilayer Piezoelectric Ceramic Actuators and Their Applications. *Japanese Journal of Applied Physics*, 24(Supplement 24-2):41-45.

[57] HORACIO SOSA & FOROUZA POURKI (1993). Modelling of Piezoelectric Multilayer Structures. *SPIE*, 1916:222-230.

[58] X. GONG & Z. SUO (1995). Reliabiltiy of Ceramic Multilayer Actuators: A Nonlinear Finite Element Simulation. *Journal of Mechanics and Physics of Solids*(submitted).

[59] H. P. SCHONER (1992). Piezoelectric Motors and Their Applications. *European Transactions on Electrical Power Engineering*, 2(6):367-371.

[60] J. K. THORNLEY, M. E. PRESTON & T. G. KING (1991). A Fast Electromechanical Clutch Element Using A Piezoelectric Multilayer Actuator. *Colloquium on Robot Actuators*, pp. 1-4.

[61] J. M. PAROS & L. WEISBORD (1965). How To Design Flexure Hinges. *Machine Design*, 37:151-156.

[62] *Products for Micropositioning.* Physik Instrumente GmbH&Co, Waldbronn, Germany.

[63] FREDRIC E. SCIRE & E. CLAYTON TEAGUE (1978). Piezodriven 50-μm Range Stage with Subnanometer Resolution. *Review of Scientific Instruments*, 49(12):1735-1740.

[64] S. T. SMITH, D. G. CHETWYND & D. K. BOWEN (1987). Design and Assessment of Monolithic High Precision Translation Mechanisms. *Journal of Physics E: Scientific Instruments*, 20(1987):977-983.

[65] J. K. THORNLEY, T. G. KING & M. E. PRESTON (1992). A Piezoelectrically-Controlled Rotary Micropositioner for Applications in Surface Finish Metrology. *International Symposium on Theory of Machine and Mechanisms.*

[66] M. ALEMANNI, G. MANA, G. PEDROTTI, P. P. STRONA & G. ZOSI (1986). On the Construction of a Zerodur Translation Device for X-Ray Interferometric Scanning. *Metrologia*, 22:55-63.

[67] LOWELL JONES, EPHRAHIM GARCIA & HENRY WAITES (1994). Self-sensing Control As Applied To A PZT Stack Actuator Used As a Micropositioner. *Smart Materials and Structures*, 3(1994):147-156.

[68] KNANH DUONG & EPHRAHIM GARCIA (1995). Open Loop Compensation in a Stack-Mass Positioning System. *Journal of Intelligent Material Systems And Structures*, 6(2):292-296.

[69] H. S. TZOU (1991). Design of a Piezoelectric Exciter/Actuator for Micro-Displacement Control: Theory and Experiment. *Precision Engineering*, 13(2):104-110.

[70] A. BERGAMIN, G. CAVAGNERO & G. MANA (1993). Servoposotioning with Picometer Resolution. *Review of Scientific Instruments*, 64(1):168-173.

[71] K. MORI, T. MUNEMOTO, H. OTSUKI, Y. YAMAGUCHI & K. AKAGI (1991). A Dual Stage Magnetic Disk Drive Actuator Using A Piezoelectric Device for A High Track Density. *IEEE Transactions on Magnetics*, 27(6):5298-5300.

[72] KOJI IKUTA, SATOSHI ARITOMI & TAKEFUMI KABASHIMA (1992). Tiny Silent Linear Cybernetic Actuator Driven by Piezoelectric Device with Electromagnetic Clamp. *IEEE Micro Electro Mechanical Systems*, pp. 232-237.

[73] D. J. PETERS & B. L. BLACKFORD (1989). Piezoelectric Bimorph-Based Translation Device for Two-Dimensional Remote Micropositioning. *Review of Scientific Instruments*, 60(1):138-140.

[74] KAZUYOSHI SUGIHARA, ICHIRO MORI, TORU TOJO, CHIKARA ITO, MITSUI TABATA & TOSHIAKI SHINOZAKI (1989). Piezoelectrically Driven $XY\theta$ Table for Submicron Lithography Systems. *Review of Scientific Instruments*, 60(9):3024-3028.

[75] KAZUMASA OHNISHI (1990). A Novel Ultrasonic Linear Actuator. *IEEE International Symposium on Applications of Ferroelectrics*, pp. 206-212.

[76] Z. X. WANG, M. K. JOUANEH & D. DORNFELD (1989). Design and Characterization of A Linear Motion Piezoelectric Microactuator. *IEEE International Conference on Robotics and Automation*, (3):1710-1715.

[77] JACK W. JUDY, DENNIS L. POLLA & WILLIAM P. ROBBINS (1990). A Linear Piezoelectric Stepper Motor With Submicrometer Step Size and Centimeter Travel Range. *IEEE Transactions on Ultrasonics, Ferroelectrics, and Frequency Control*, 37(5):428-436.

[78] D. W. POHL (1987). Dynamic Piezoelectric Translation Devices. *Review of Scientific Instruments*, 58(1):54-56.

[79] SIJIA WU & K. W. NG (1991). A Piezoelectric-Driven Micropositioner with Magnetic Locking Mechanism. *Review of Scientific Instruments*, 62(1):93-95.

[80] TOSHIRO HIGUCHI, YUSOF HOJJAT & MASAHIRO WATANABE (1987). Micro Actuators Using Recoil of An Ejected Mass. *IEEE Micro Robots and Teleoperators Workshop.*

[81] CH. RENNER, PH. NIEDERMANN, A. D. KENT & O. FISCHER (1990). A Vertical Piezoelectric Inertial Slider. *Review of Scientific Instruments*, 61(3):965-967.

[82] SHINSEI KOGYO CO., LTD. (1985). Ultrasonic Wave Motor, The First Actuator Incorporating Ceramic Technologhy.

[83] TAKEHIRO TAKANO, YOSHIRO TOMIKAWA, MASATOSHI YAGINUMA & TOSHIHARU OGASAWARA (1990). A Linearly Moving Ultrasonic Motor Using A Longitudinal and Bending Multi-Mode Vibrator. *IEEE International Symposium on Applications of Ferroelectrics*, pp. 521-524.

[84] YOSHIRO TOMIKAWA, MANABU AOYAGI & CHIHARU KUSAKABE (1990). Piezoelectric Actuators in Rotary or Linear Motions by Excitation of Assymmetric Displacement. *IEEE International Symposium on Applications of Ferroelectrics*, pp. 537-540.

[85] ATSUO KAWAMURA & NORIHIKO TAKEDA (1991). *IEEE Transactions on Industry Applications*, 27(1):23-26.

[86] MAXIMILIAN FLEISCHER, DIETER STEIN & HANS MEIXNER (1989). New Type of Piezoelectric Ultrasonic Motor. *IEEE Transactions on Ultrasonics, Ferroelectrics, and Frequency Control*, 36(6):614-619.

[87] AKIO KUMADA (1985). A Piezoelectric Ultrasonic Motor. *Japanese Journal of Applied Physics*, 24(Supplement 24-2):739-741.

[88] KOHJI TODA & AKIHIKO KAMO (1990). Ultrasonic Motor Operation Using The Unidirectional Surface Displacement of A Cylindrical Piezoelectric Vibrator. *Journal of Applied Physics*, 67(6):3148-3151.

[89] K. RAGULSKIS, R. BANSEVICIUS, R. BARAUSKAS & G. KULVIETIS (1988). *Vibromotors for Precision Microrobots.* Hemisphere Publishing Corporation, New York.

[90] C. JULIAN CHEN (1993). *Introduction to Scanning Tunneling Microscopy.* Oxford University Press, New York.

[91] DAVID V. NEWTON (1994). *Development of A Linear Piezoelectric Motor.* M.Sc. Thesis, Vanderbilt University, Department of Mechanical Engineering, Nashville, Tennessee, USA.

[92] KOJI IKUTA, ATSUSHI KAWAHARA & SHUJI YAMAZUMI (1991). Miniature Cybernetic Actuators Using Piezoelectric Device. *IEEE Micro Electro Mechanical Systems*, pp. 131-136.

[93] KAZUMASA OHNISHI, MIKIO UMEDA, MINORU KUROSAWA & SADAYUKI UHEA (1990). Rotary Inchworm-Type Piezoelectric Actuator. *Electrical Engineering in Japan*, 110(3):107-114.

[94] KHANH DUONG & EPHRAHIM GARCIA (1995). Development of A Rotary Inchworm Piezoelectric Motor. *Technichal Report* obtained through personal communication.

[95] IWAO HAYASHI, NOBUYUKI IWATSUKI, MOTOYOSHI KAWAI, JYUNJI SHIBATA & TAKIJI KITAGAWA (1992). Development of A Piezoelectric Cycloid Motor. *Mechatronics*, 2(5):433-444.

[96] MUNEAKI ISHIDA, JUNICHI HAMAGUCHI, KEIICHI SHIRASUKA & TAKAMASA HORI (1992). A New Friction-Type Piezoelectric Motor Utilizing Mechanism of the Strain Wave Gearing. *IEEE Transactions on Industrial Electronics*, 39(1):30-35.

[97] HAMILTON H. MABIE & CHARLES F. REINHOLTZ (1987). *Mechanisms and Dynamics of Machinery.* John Wiley & Sons Publishing, New York.

[98] TIM KING & WEI XU (1995). The Design and Characteristics of Piezomotors Using Flexure Hinged Displacement Amplifiers. *International Conference on Recent Advances in Mechatronics*, pp. 381-387.

[99] TIM KING, WEI XU & JOHN THORNLEY (1994). A Piezoelectric Harmonic Motor. *Mechatronics-The Basis for New Industrial Development*, pp. 411-417.

[100] ROBERT BAMFORD, C. P. KUO, ROBERT GLASER & BEN K. WADA (1995). Long Stroke Precision PZT Actuator. *California Institute of Technology, Jet Propulsion Laboratory*, Draft obtained through personal communication.

[101] *Precision Bearings.* Catalogue 3700 E, SKF.

[102] *Product Catalogue.* Morgan Matroc Inc., Electro Ceramics Division, Bedford, OH.

[103] *ANSYS5.2 Theory Manual.* ANSYS, Inc., Houston, PA.

[104] *ANSYS5.2 Elements Manual.* ANSYS, Inc., Houston, PA.

[105] D. BERLINCOURT & H. H. A. KRUEGER. Properties of Vernitron Ceramics. Company report obtained through personal communication.

[106] *Parallax, Inc.*, 3805 Atherton Road #102, Rocklin, CA 95765. http://www.parallaxinc.com

Appendix A

Tensor Index Abbreviations

Tensor symmetries allow us to reduce the number of independent constants and write them in matrix forms. In matrix rotation, the indices ij and kl are replaced by p or q, where i, j, k, l take the values $1, 2, 3$, and p, q take values $1, 2, 3, 4, 5, 6$. the replacement is done according to the Table A.1.

ij or kl	p or q
11	1
22	2
33	3
23 or 32	4
31 or 13	5
12 or 21	6

Table A.1: Index abbreviations

The identifications for abbreviations are as follows:

$$c^E_{ijkl} \equiv c^E_{pq} \qquad e_{ikl} \equiv e_{ip} \qquad T_{ij} \equiv T_p \tag{A.1}$$

$$S_{ij} = S_p \qquad \text{when } i = j, p = 1, 2, 3 \tag{A.2}$$

$$2S_{ij} = S_p \qquad \text{when } i \neq j, p = 4, 5, 6 \tag{A.3}$$

By using index abbreviations, the tensorial quantities seen in piezoelectric constitutive equations can be easily written in matrix forms as follows:

$$\mathbf{T} = \begin{bmatrix} T_1 \\ T_2 \\ T_3 \\ T_4 \\ T_5 \\ T_6 \end{bmatrix} \qquad \mathbf{S} = \begin{bmatrix} S_1 \\ S_2 \\ S_3 \\ S_4 \\ S_5 \\ S_6 \end{bmatrix} \qquad \mathbf{s} = \begin{bmatrix} s_{11} & s_{12} & s_{13} & s_{14} & s_{15} & s_{16} \\ s_{21} & s_{22} & s_{23} & s_{24} & s_{25} & s_{26} \\ s_{31} & s_{32} & s_{33} & s_{34} & s_{35} & s_{36} \\ s_{41} & s_{42} & s_{43} & s_{44} & s_{45} & s_{46} \\ s_{51} & s_{52} & s_{53} & s_{54} & s_{55} & s_{56} \\ s_{61} & s_{62} & s_{63} & s_{64} & s_{65} & s_{66} \end{bmatrix} \tag{A.4}$$

$$\mathbf{E} = \begin{bmatrix} E_1 \\ E_2 \\ E_3 \end{bmatrix} \qquad \mathbf{D} = \begin{bmatrix} D_1 \\ D_2 \\ D_3 \end{bmatrix} \qquad \mathbf{P} = \begin{bmatrix} P_1 \\ P_2 \\ P_3 \end{bmatrix} \tag{A.5}$$

$$\mathbf{d} = \begin{bmatrix} d_{11} & d_{12} & d_{13} & d_{14} & d_{15} & d_{16} \\ d_{21} & d_{22} & d_{23} & d_{24} & d_{25} & d_{26} \\ d_{31} & d_{32} & d_{33} & d_{34} & d_{35} & d_{36} \end{bmatrix} \qquad \epsilon = \begin{bmatrix} \epsilon_{11} & \epsilon_{12} & \epsilon_{13} \\ \epsilon_{21} & \epsilon_{22} & \epsilon_{23} \\ \epsilon_{31} & \epsilon_{32} & \epsilon_{33} \end{bmatrix} \tag{A.6}$$

Appendix B

Relations Between the Coefficients Appeared in Piezoelectric Constitutive Equations

$$
\begin{aligned}
c^E_{pr} s^E_{qr} &= \delta_{pq} & \qquad c^D_{pr} s^D_{qr} &= \delta_{pq} \\
\beta^S_{ik} \epsilon^S_{jk} &= \delta_{ij} & \qquad \beta^T_{ik} \epsilon^T_{jk} &= \delta_{ij} \\
c^D_{pq} &= c^E_{pq} + e_{kp} h_{kq} & \qquad s^D_{pq} &= s^E_{pq} - d_{kp} g_{kq} \\
\epsilon^T_{ij} &= \epsilon^S_{ij} + D_{iq} e_{jq} & \qquad \beta^T_{ij} &= \beta^S_{ij} - g_{iq} h_{jq} \\
e_{ip} &= d_{iq} c^E_{qp} & \qquad d_{ip} &= \epsilon^T_{iq} g_{kp} \\
g_{ip} &= \beta^T_{ik} d_{kp} & \qquad h_{ip} &= g_{iq} c^D_{qp}
\end{aligned}
$$

Also,

$$\mathbf{c} = \mathbf{s}^{-1}, \qquad \text{that is,} \qquad c_{pq} = (-1)^{p+q} \Delta^{\mathbf{s}}_{qp} / \Delta^{\mathbf{s}}$$

where, $\Delta^{\mathbf{s}}$ is the determinant $\mathbf{s}$ and $\Delta^{\mathbf{s}}_{qp}$ is the minor determinant for qpth element of $\mathbf{s}$. In the equations given above, δ_{ij} and δ_{pq} are 3x3 and 6x6 unit matrices, respectively.

Also, as a result of index abbreviations given in Appendix A, the following relations can also be written:

$$
\begin{aligned}
s^E_{pq} &= s^E_{ijkl}, \quad i = j \quad \text{and} \quad k = l, \quad p,q = 1,2,3 \\
s^E_{pq} &= 2 s^E_{ijkl}, \quad i = j \quad \text{and} \quad k \neq l, \quad p = 1,2,3, \quad q = 4,5,6 \\
s^E_{pq} &= 4 s^E_{ijkl}, \quad i \neq j \quad \text{and} \quad k \neq l, \quad p,q = 4,5,6
\end{aligned}
$$

Similar relations are also valid for s^D_{pq}.

For piezoelectric coefficient d, the following relations can also be written:

$$
\begin{aligned}
d_{iq} &= d_{ikl}, \quad k = l, \quad q = 1,2,3 \\
d_{iq} &= 2 d_{ikl}, \quad k \neq l, \quad q = 4,5,6
\end{aligned}
$$

Similar relations are also true for g_{iq}.

The relations between piezoelectric constants h_{iq} and h_{ijl} can be written in the same fashion as those of e_{iq} and e_{ikl}. The relations between c^D_{pq} and c^D_{ijkl}, on the other hand, are the same as those of c^E_{pq} and c^E_{ijkl} which is given in Appendix A.

Appendix C

Technical Drawings of the Piezoelectric Rotary Actuator

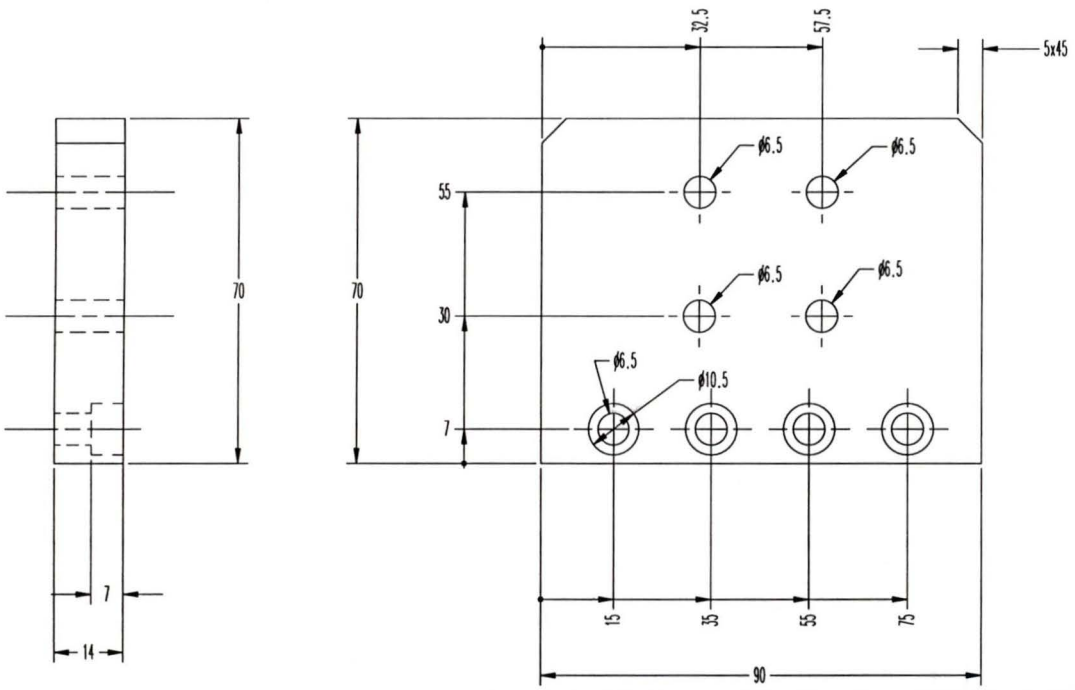

IRIS - Materials & Mechatronics Laboratory	
PROJECT CODE	IRIS-AMD4 - Actuator
PROJECT NAME	Piezoelectric Rotary Actuator
PART NAME / NUMBER	Mounting Plate(Horizontal) / PZT-ACT:1
SCALE	1:1
MATERIAL	6061 - T6
QUANTITY	1
DESIGNED BY	Selcuk Gursan
DRAWN BY	Selcuk Gursan

Figure C.1: Mounting plate (Horizontal).

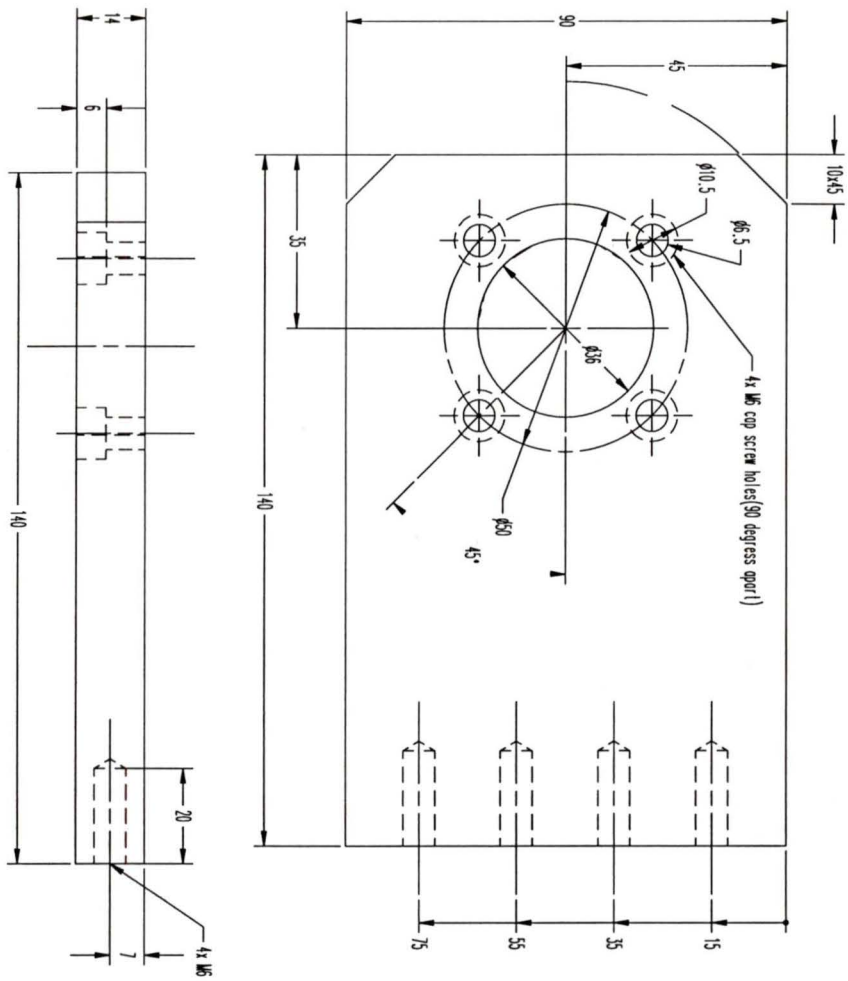

IRIS - Materials & Mechatronics Laboratory	
PROJECT CODE	IRIS-AMD4 - Actuator
PROJECT NAME	Piezoelectric Rotary Actuator
PART NAME / NUMBER	Mounting Plate(Vertical) / PZT-ACT:2
SCALE	1:1
MATERIAL	6061-T6
QUANTITY	1
DESIGNED BY	Selcuk Gursan
DRAWN BY	Selcuk Gursan

Figure C.2: Mounting plate (Vertical).

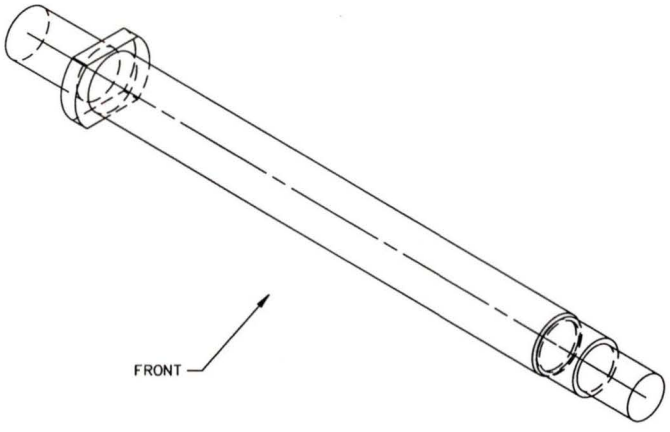

SHAFT(ISOMETRIC VIEW) / SCALE: 0.82

IRIS - Materials & Mechatronics Laboratory	
PROJECT CODE	IRIS-AMD4 - Actuator
PROJECT NAME	Piezoelectric Rotary Actuator
PART NAME / NUMBER	Shaft / PZT-ACT:3
SCALE	
MATERIAL	304 Stainless
QUANTITY	1
DESIGNED BY	Selcuk Gursan
DRAWN BY	Selcuk Gursan

Figure C.3: Shaft (Isometric view).

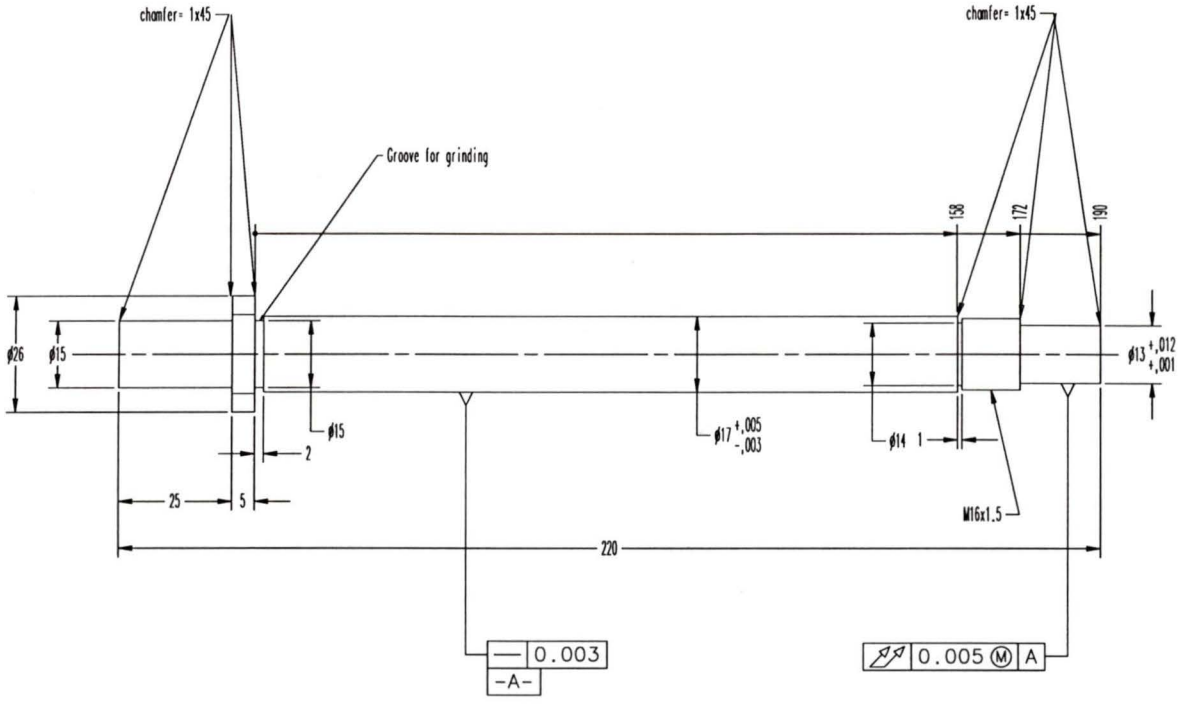

SHAFT(FRONT VIEW) / SCALE: 1:1

Figure C.4: Shaft (Front view).

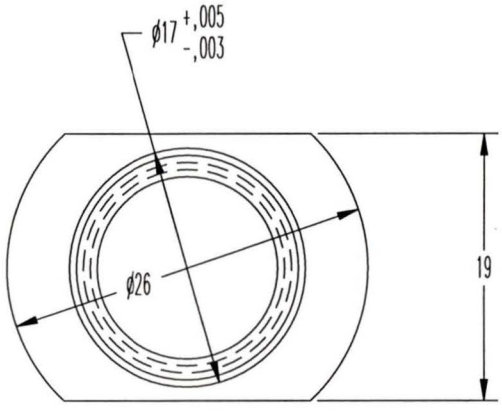

SHAFT(RIGHT VIEW) / SCALE: 2:1

Figure C.5: Shaft (Right view).

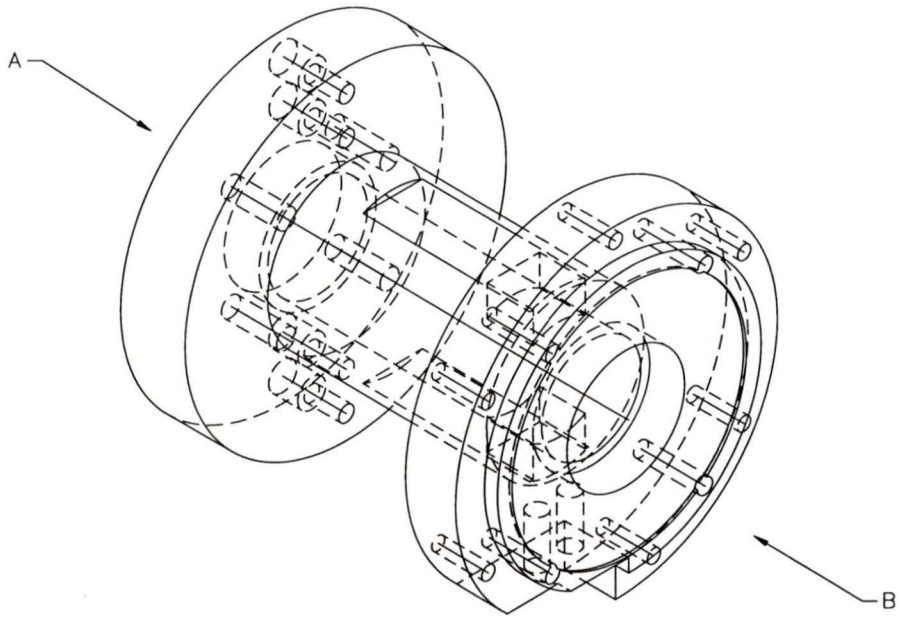

HOUSING(ISOMETRIC VIEW) / SCALE: 0.85

IRIS - Materials & Mechatronics Laboratory	
PROJECT CODE	IRIS-AMD4 - Actuator
PROJECT NAME	Piezoelectric Rotary Actuator
PART NAME / NUMBER	Housing / PZT-ACT:4
SCALE	1:1
MATERIAL	6061 - T6
QUANTITY	1
DESIGNED BY	Selcuk Gursan
DRAWN BY	Selcuk Gursan

Figure C.6: Housing (Isometric view).

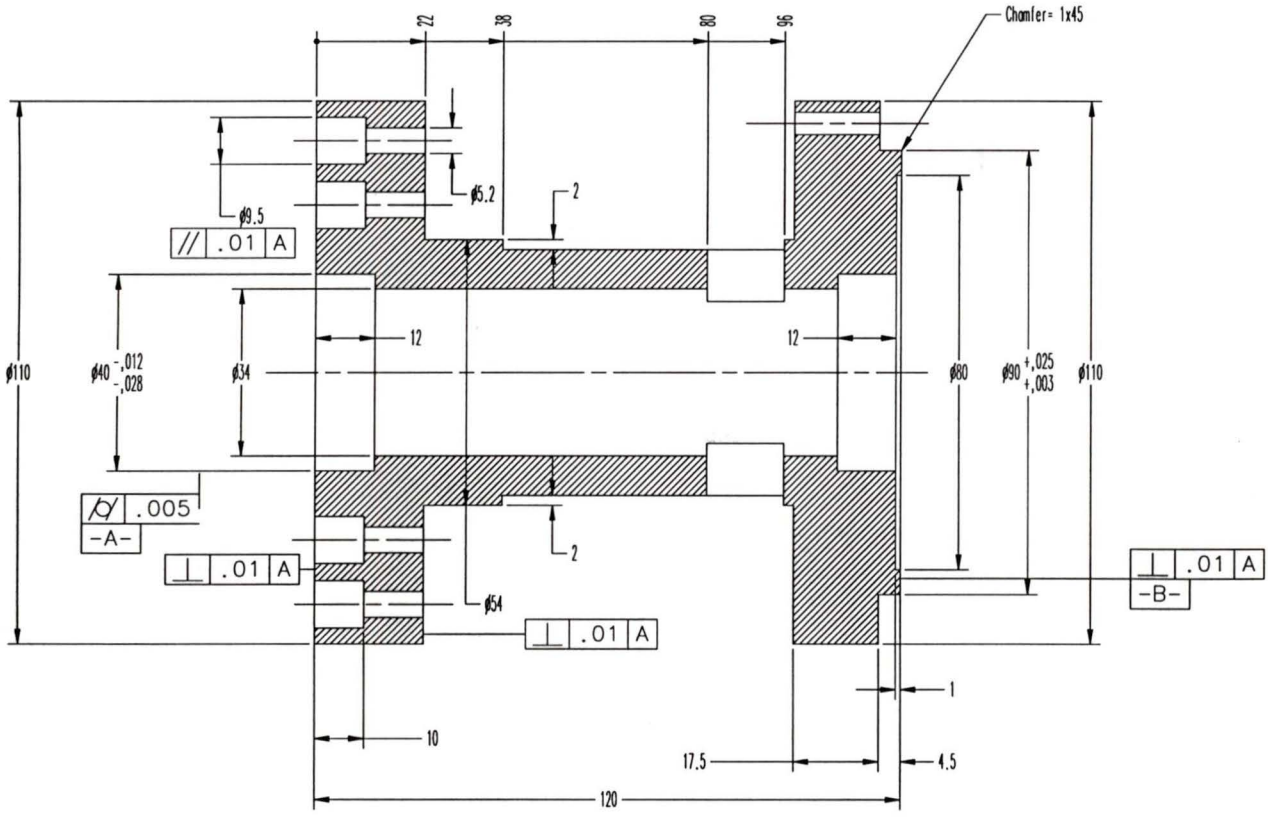

HOUSING(FRONT CROSS SECTIONAL VIEW)

Figure C.7: Housing (Cross-sectional view).

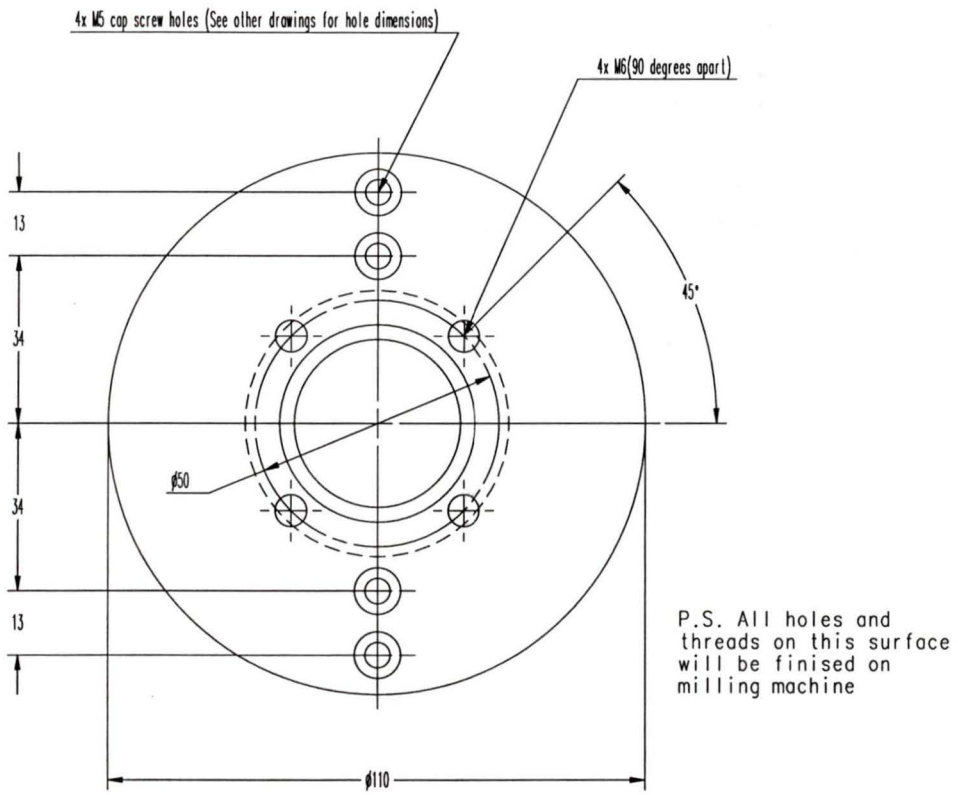

HOUSING(VIEW A -No hidden line is shown-)

Figure C.8: Housing (View A).

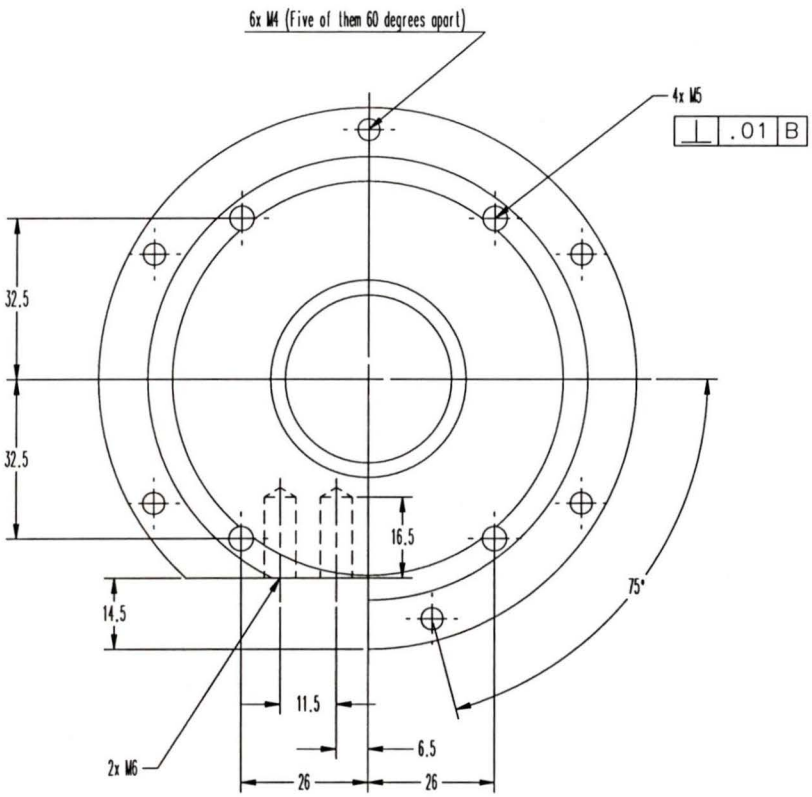

Figure C.9: Housing (View B).

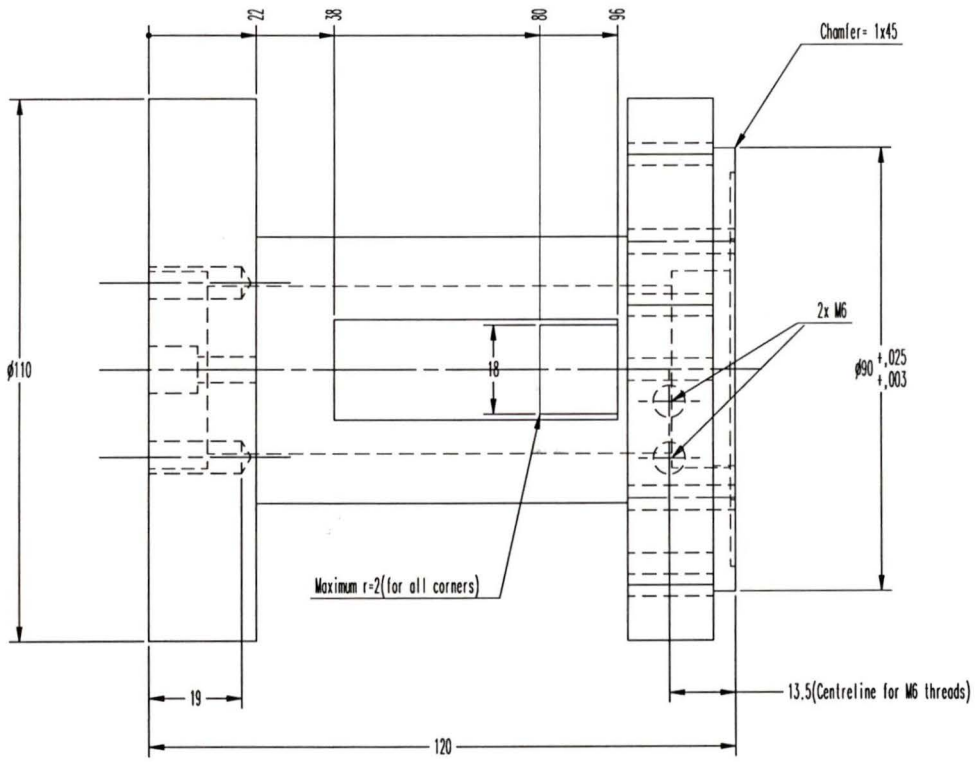

HOUSING(TOP VIEW)

Figure C.10: Housing (Top view).

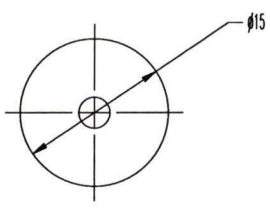

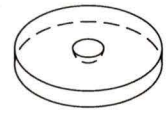

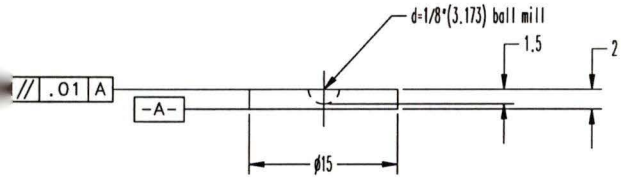

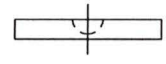

.S. Only six of these plates
ill have d=1/8" semi-sphere
machining.

IRIS - Materials & Mechatronics Laboratory	
PROJECT CODE	IRIS-AMD4 - Actuator
PROJECT NAME	Piezoelectric Rotary Actuator
PART NAME / NUMBER	Shear Plates for PZT Actuators/ PZT-ACT:5
SCALE	2:1
MATERIAL	304 Stainless
QUANTITY	9
DESIGNED BY	Selcuk Gursan
DRAWN BY	Selcuk Gursan

Figure C.11: Shear plates for PZT actuators.

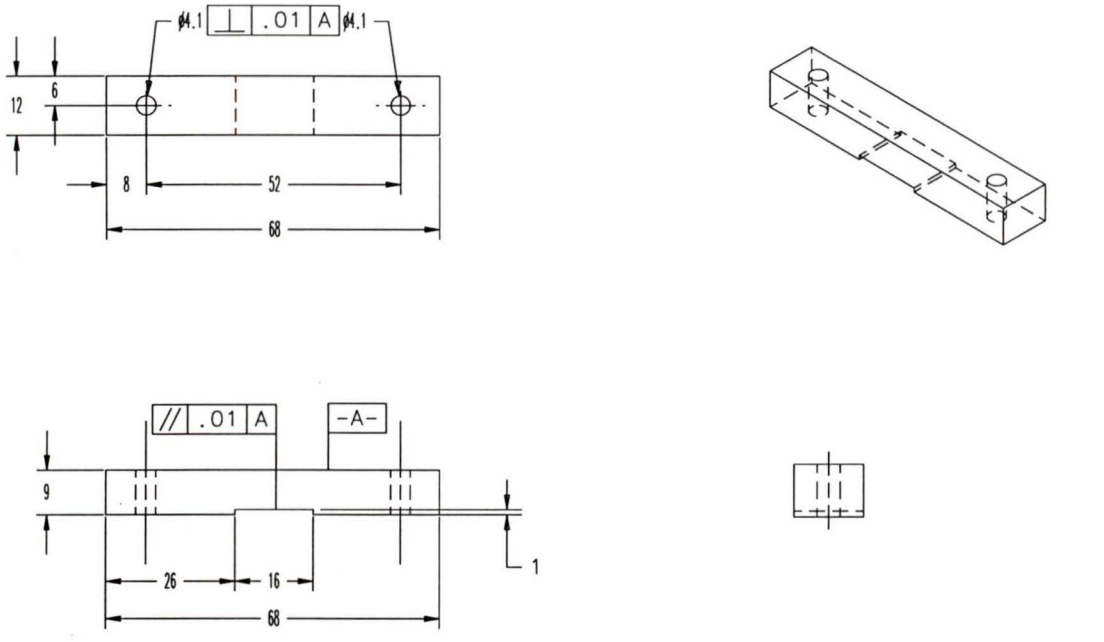

IRIS - Materials & Mechatronics Laboratory	
PROJECT CODE	IRIS-AMD4 - Actuator
PROJECT NAME	Piezoelectric Rotary Actuator
PART NAME / NUMBER	PZT Assembly beams / PZT-ACT:6
SCALE	1:1
MATERIAL	304 Stainless
QUANTITY	2
DESIGNED BY	Selcuk Gursan
DRAWN BY	Selcuk Gursan

Figure C.12: PZT assembly beams.

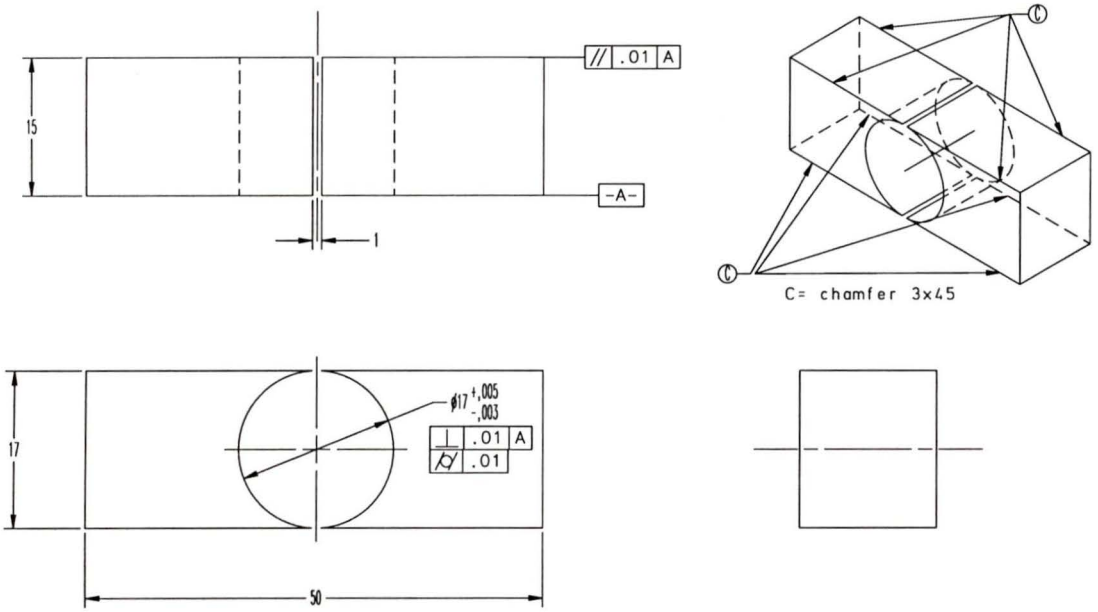

P.S. This drawing contains two seperate parts. They are shown as a single part for simplicity.

IRIS - Materials & Mechatronics Laboratory	
PROJECT CODE	IRIS-AMD4 - Actuator
PROJECT NAME	Piezoelectric Rotary Actuator
PART NAME / NUMBER	Clamping Shoes / PZT-ACT:7
SCALE	2:1
MATERIAL	6061 - T6
QUANTITY	1(Two pieces)
DESIGNED BY	Selcuk Gursan
DRAWN BY	Selcuk Gursan

Figure C.13: Clamping shoes.

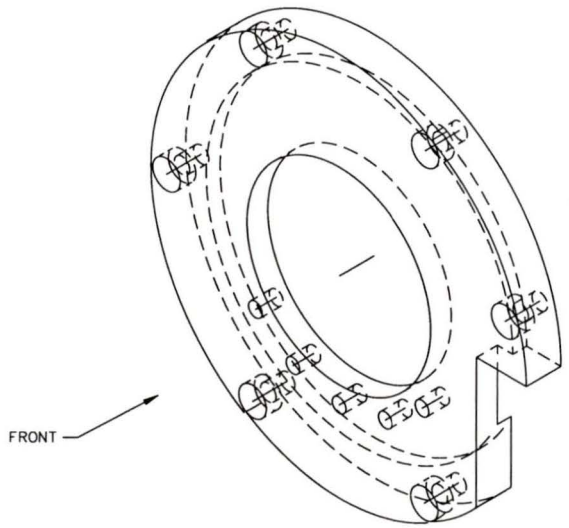

ROTATIONAL FLEXURE FLANGE (ISOMETRIC VIEW)

IRIS - Materials & Mechatronics Laboratory	
PROJECT CODE	IRIS-AMD4 - Actuator
PROJECT NAME	Piezoelectric Rotary Actuator
PART NAME / NUMBER	Rotational Flexure Flange / PZT-ACT:8
SCALE	1:1
MATERIAL	6061 - T6
QUANTITY	1
DESIGNED BY	Selcuk Gursan
DRAWN BY	Selcuk Gursan

Figure C.14: Rotational flexure flange (Isometric view).

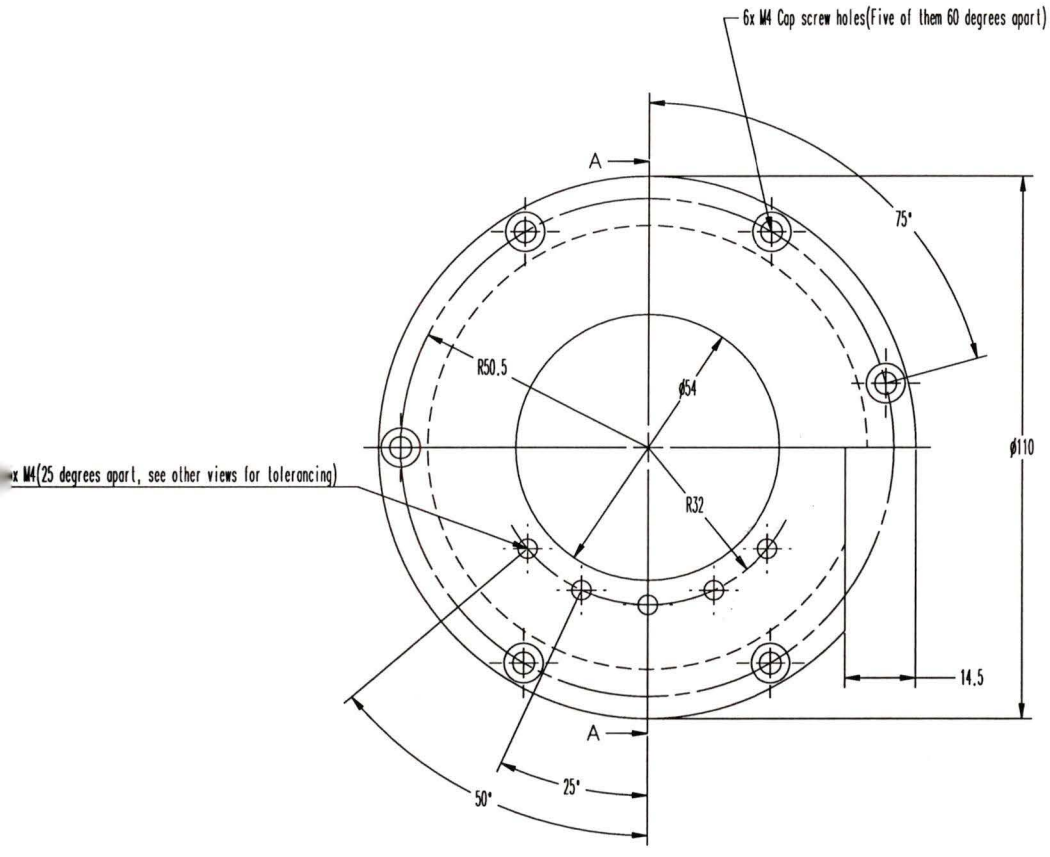

ROTATIONAL FLEXURE FLANGE (FRONT VIEW)

Figure C.15: Rotational flexure flange (Front view).

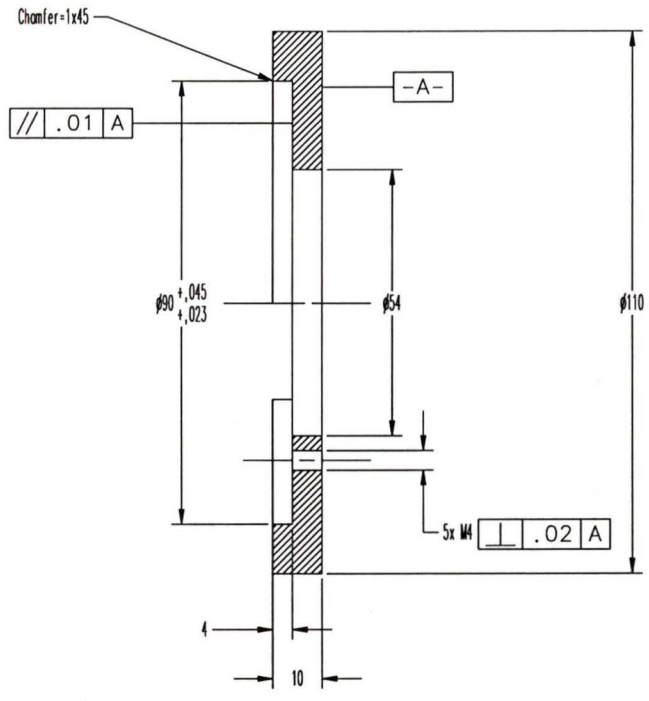

ROTATIONAL FLEXURE FLANGE (AA CROSS-SECTIONAL VIEW)

Figure C.16: Rotational flexure flange (AA Cross-sectional view).

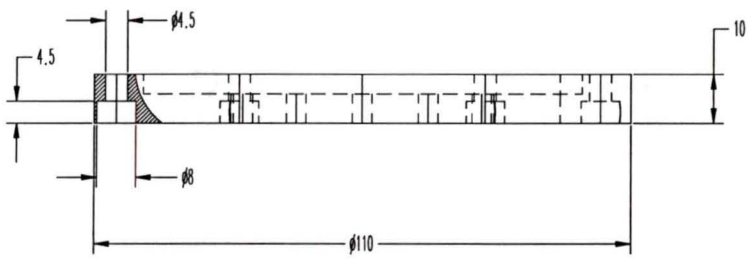

ROTATIONAL FLEXURE FLANGE (TOP VIEW)

Figure C.17: Rotational flexure flange (Top view).

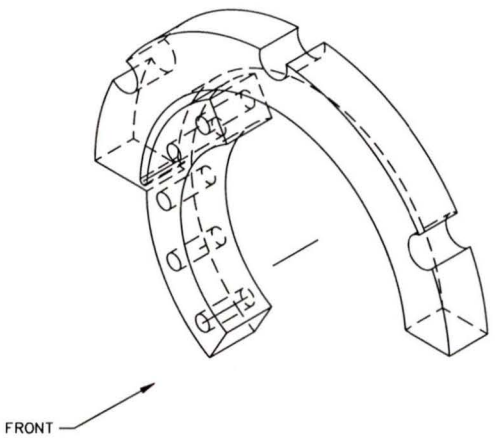

ROTATIONAL FLEXURE (ISOMETRIC VIEW)

IRIS - Materials & Mechatronics Laboratory	
PROJECT CODE	IRIS-AMD4 - Actuator
PROJECT NAME	Piezoelectric Rotary Actuator
PART NAME / NUMBER	Rotational Flexure / PZT-ACT:9
SCALE	1:1
MATERIAL	Grade 2 Titanium
QUANTITY	1
DESIGNED BY	Selcuk Gursan
DRAWN BY	Selcuk Gursan

Figure C.18: Rotational flexure (Isometric view).

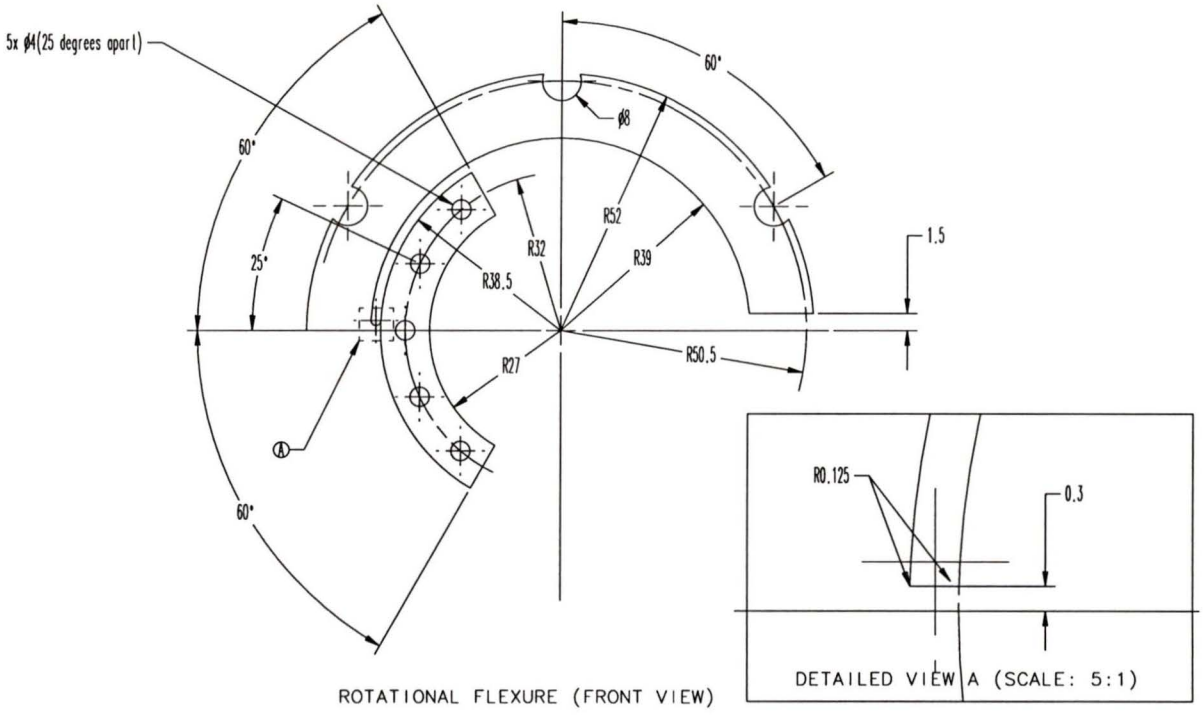

Figure C.19: Rotational flexure (Front view).

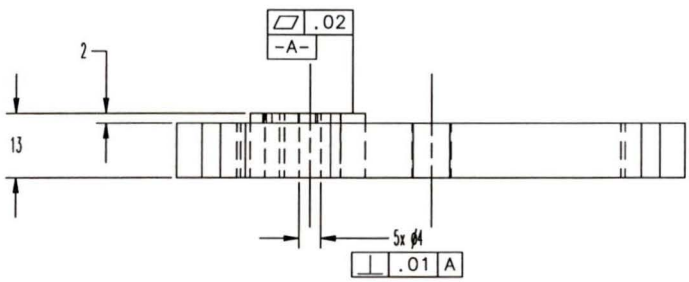

ROTATIONAL FLEXURE (TOP VIEW)

Figure C.20: Rotational flexure (Top view).

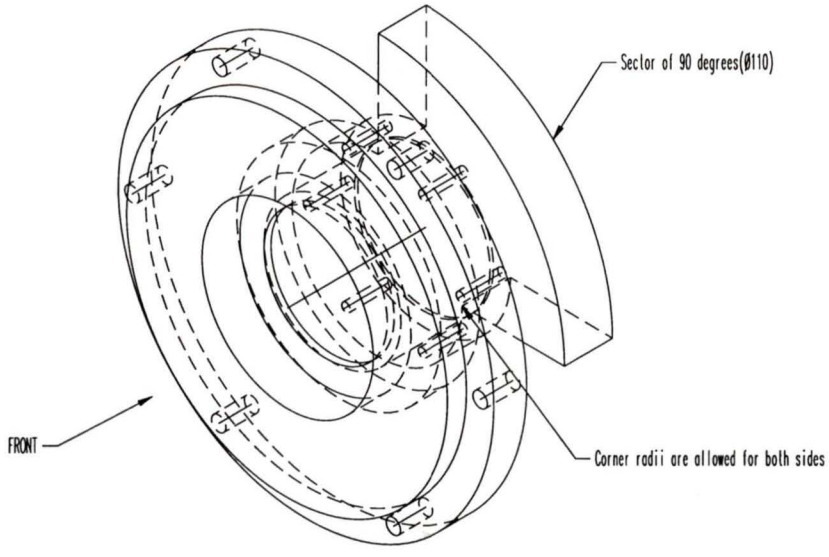

BEARING HOUSING UNIT (ISOMETRIC VIEW)

IRIS - Materials & Mechatronics Laboratory	
PROJECT CODE	IRIS-AMD4 - Actuator
PROJECT NAME	Piezoelectric Rotary Actuator
PART NAME / NUMBER	Bearing Housing Unit / PZT-ACT:10
SCALE	1:1
MATERIAL	6061 - T6
QUANTITY	1
DESIGNED BY	Selcuk Gursan
DRAWN BY	Selcuk Gursan

Figure C.21: Bearing housing unit (Isometric view).

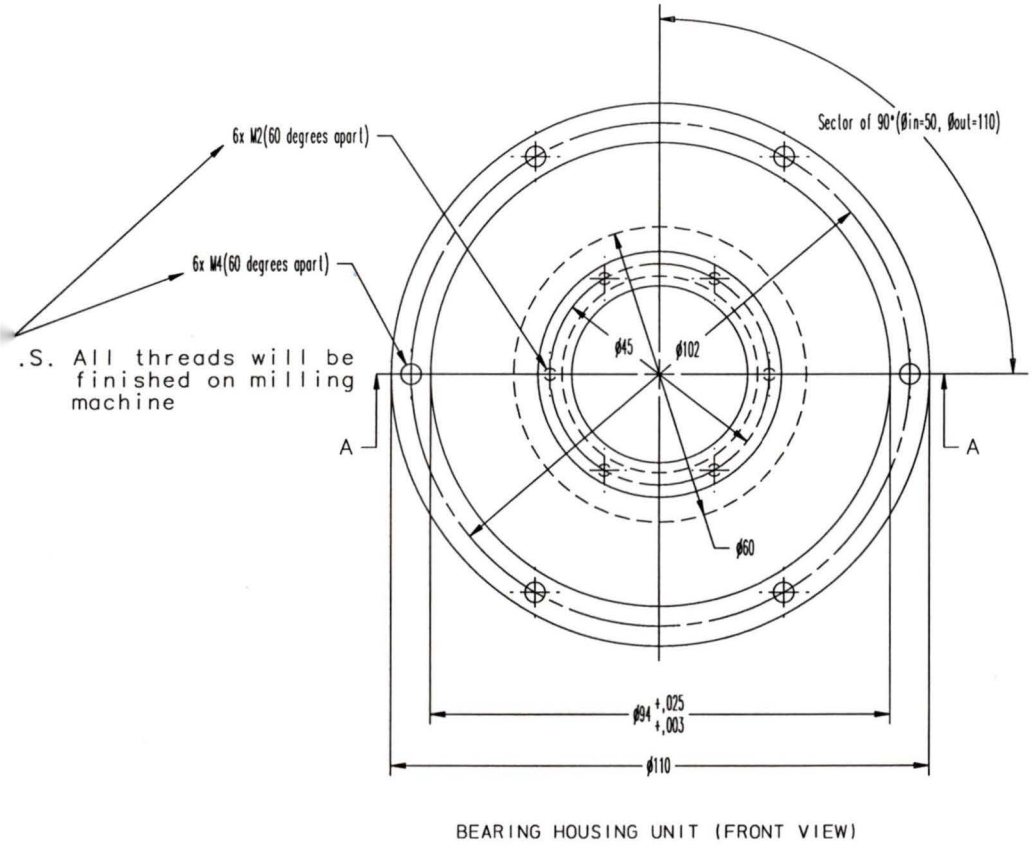

BEARING HOUSING UNIT (FRONT VIEW)

Figure C.22: Bearing housing unit (Front view).

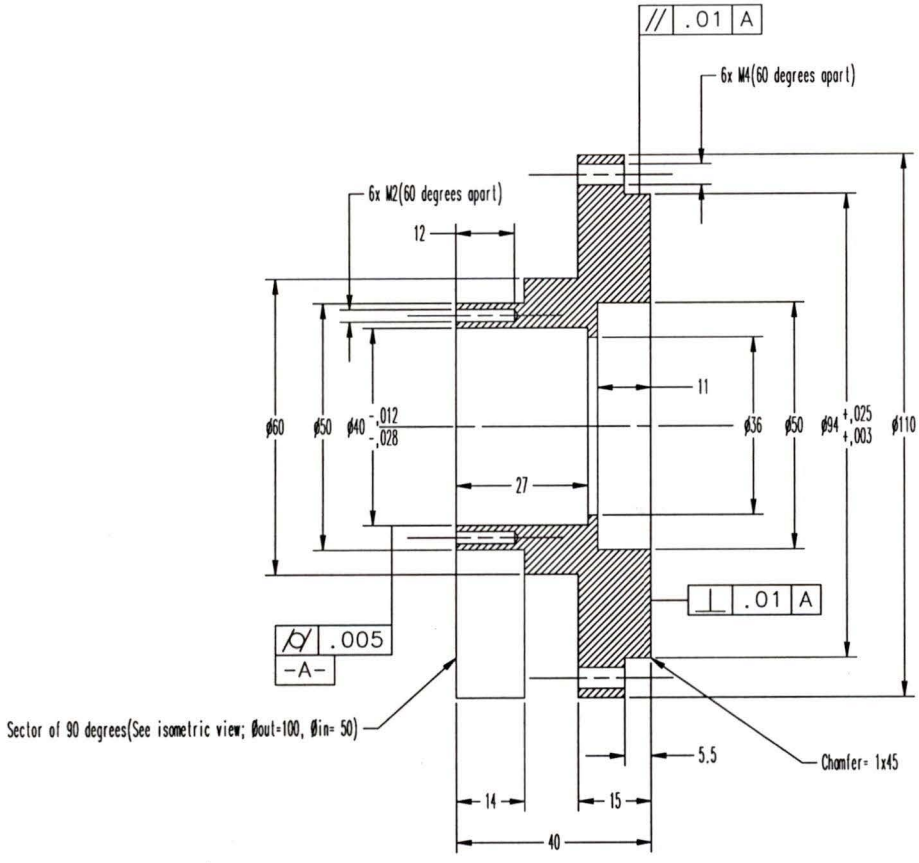

Figure C.23: Bearing housing unit (AA Cross-sectional view).

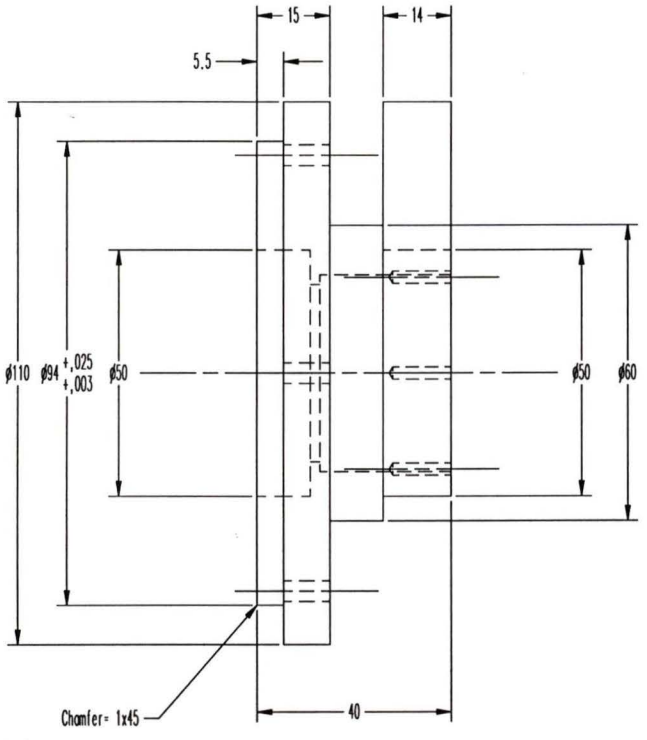

Figure C.24: Bearing housing unit (Right view).

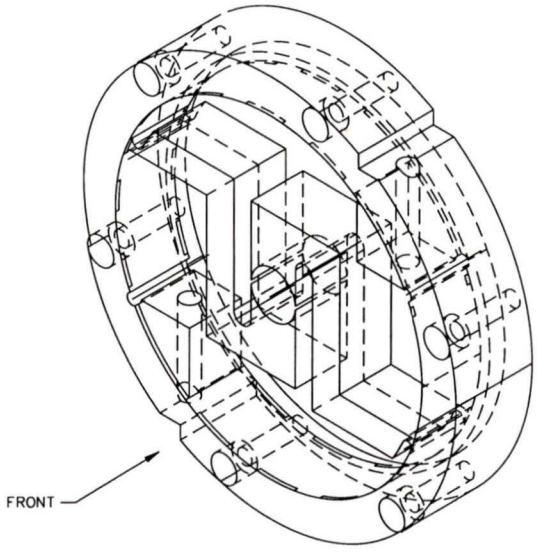

CLUTCH FLEXURE UNIT (ISOMETRIC VIEW)

IRIS - Materials & Mechatronics Laboratory	
PROJECT CODE	IRIS-AMD4 - Actuator
PROJECT NAME	Piezoelectric Rotary Actuator
PART NAME / NUMBER	Clutch Flexure Unit / PZT-ACT:11
SCALE	1:1
MATERIAL	Grade 2 Titanium
QUANTITY	1
DESIGNED BY	Selcuk Gursan
DRAWN BY	Selcuk Gursan

Figure C.25: Clutch flexure unit (Isometric view).

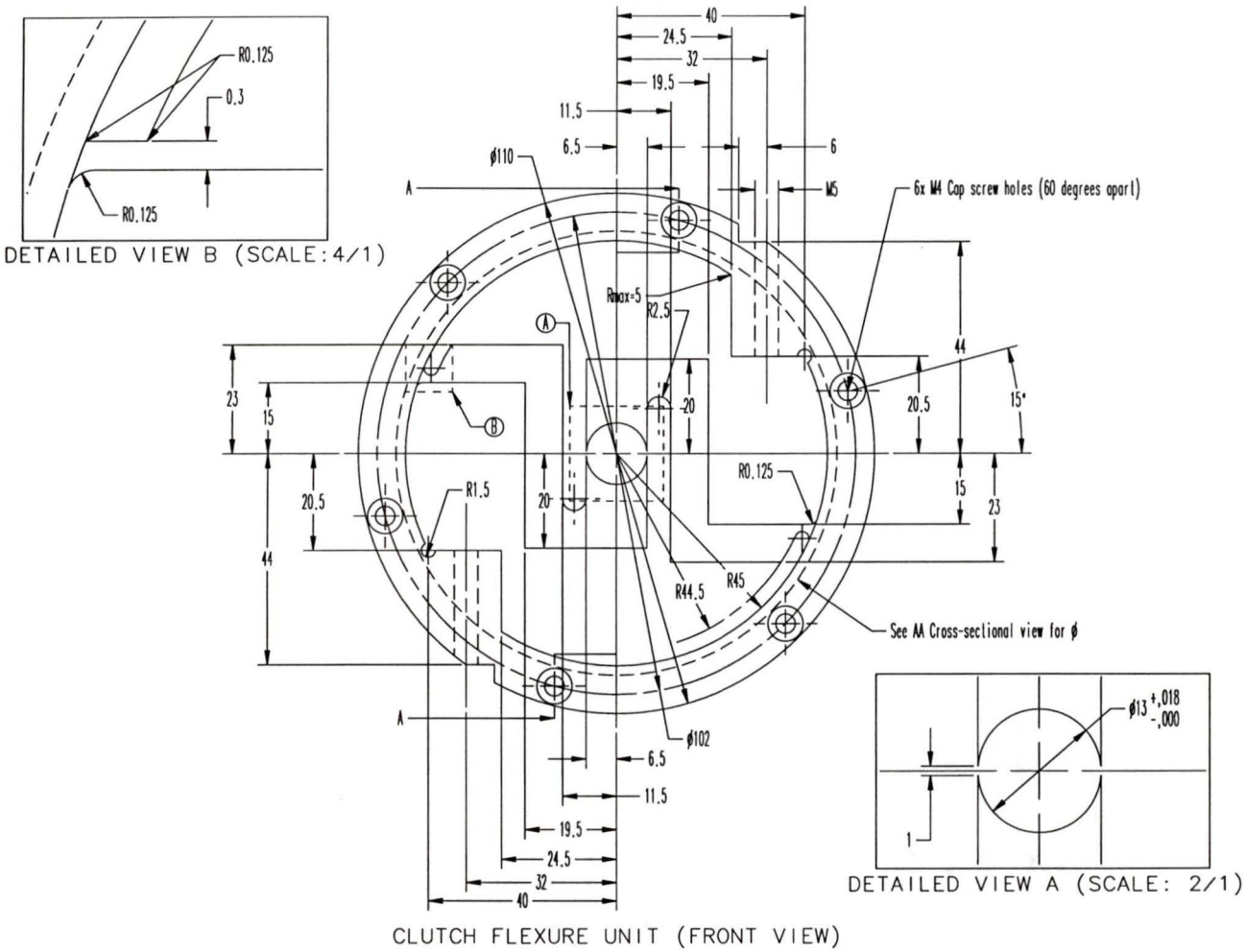

Figure C.26: Clutch flexure unit (Front view).

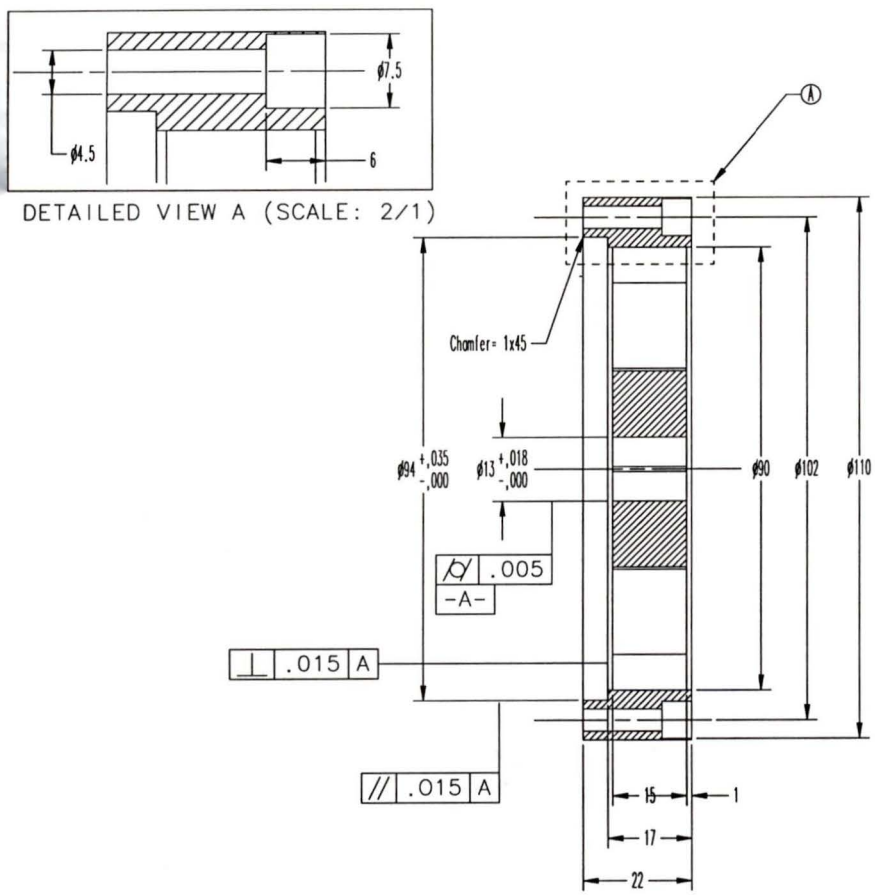

Figure C.27: Clutch flexure unit (AA Cross-sectional view).

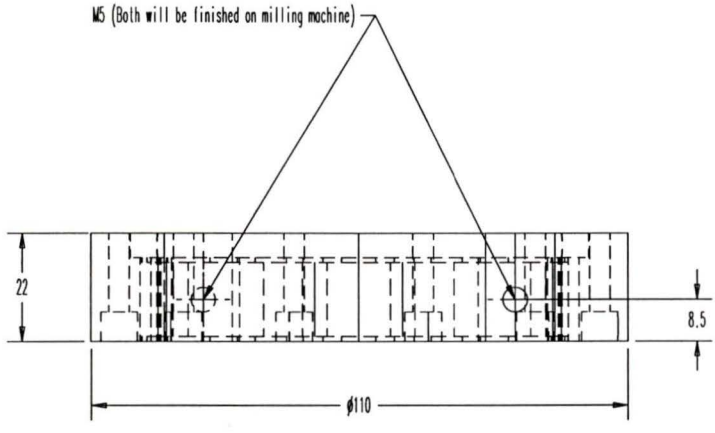

CLUTCH FLEXURE UNIT (TOP VIEW)

Figure C.28: Clutch flexure unit (Top view).

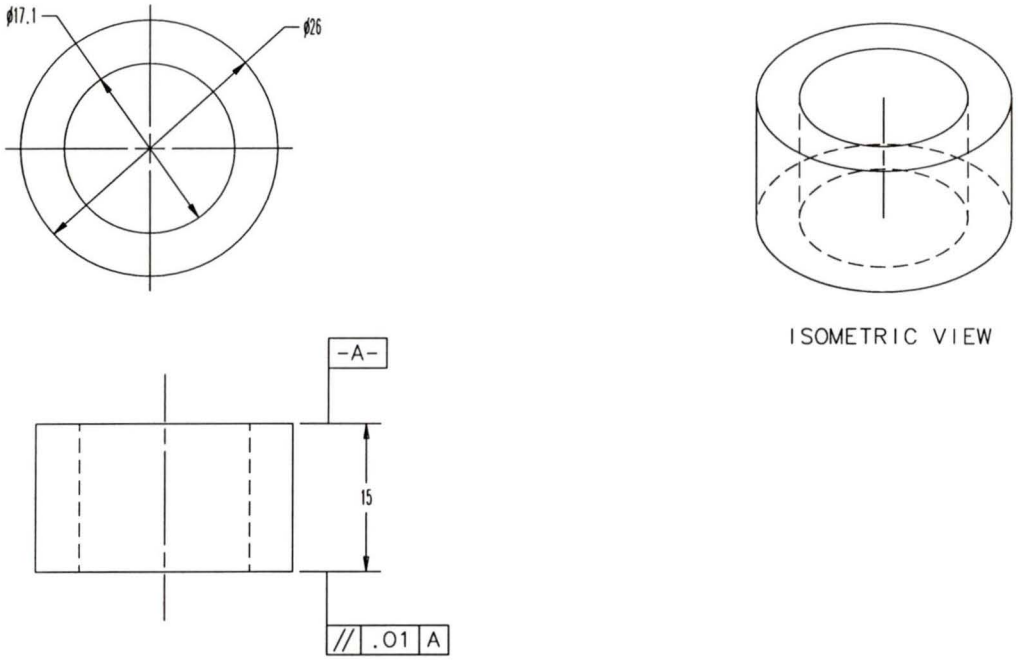

IRIS - Materials & Mechatronics Laboratory	
PROJECT CODE	IRIS-AMD4 - Actuator
PROJECT NAME	Piezoelectric Rotary Actuator
PART NAME / NUMBER	Spacer#1 / PZT-ACT:12
SCALE	2:1
MATERIAL	304 Stainless
QUANTITY	1
DESIGNED BY	Selcuk Gursan
DRAWN BY	Selcuk Gursan

Figure C.29: Spacer#1.

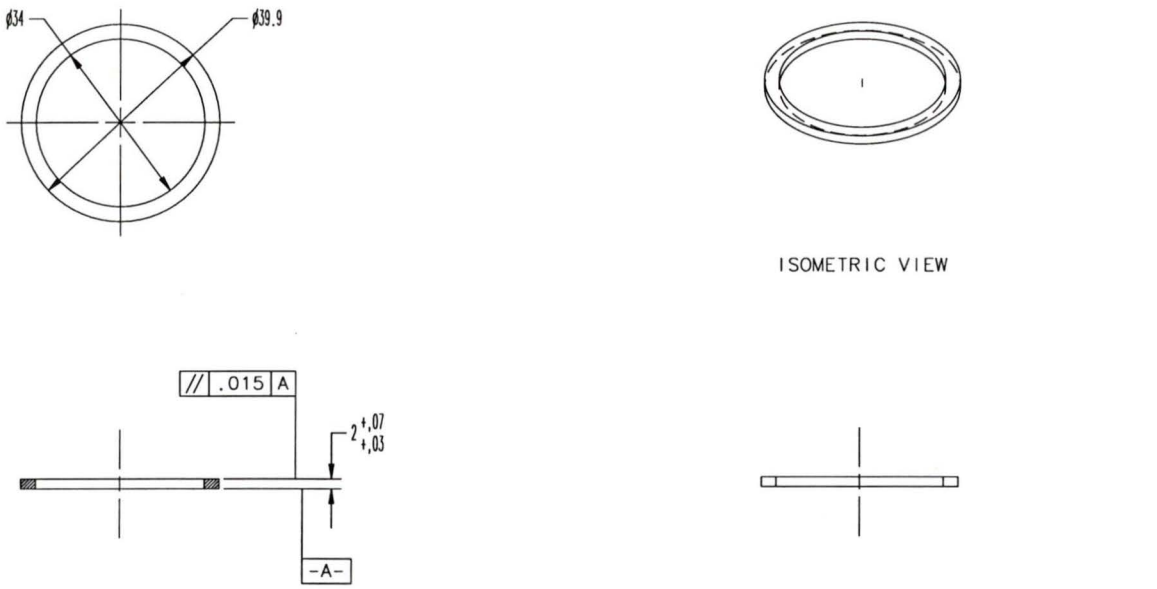

IRIS - Materials & Mechatronics Laboratory	
PROJECT CODE	IRIS-AMD4 - Actuator
PROJECT NAME	Piezoelectric Rotary Actuator
PART NAME / NUMBER	Spacer#2 / PZT-ACT:13
SCALE	2:1
MATERIAL	304 Stainless
QUANTITY	1
DESIGNED BY	Selcuk Gursan
DRAWN BY	Selcuk Gursan

Figure C.30: Spacer#2.

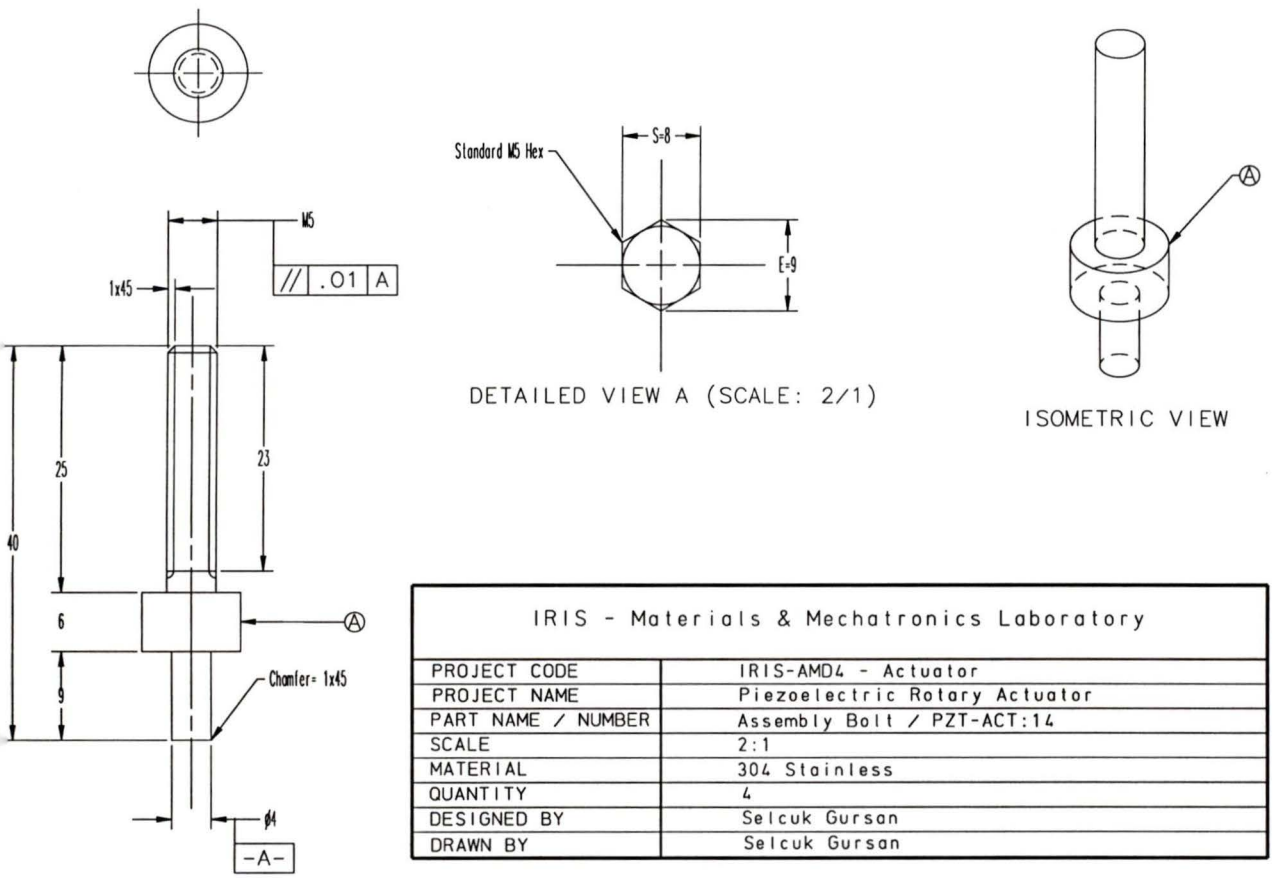

IRIS - Materials & Mechatronics Laboratory	
PROJECT CODE	IRIS-AMD4 - Actuator
PROJECT NAME	Piezoelectric Rotary Actuator
PART NAME / NUMBER	Assembly Bolt / PZT-ACT:14
SCALE	2:1
MATERIAL	304 Stainless
QUANTITY	4
DESIGNED BY	Selcuk Gursan
DRAWN BY	Selcuk Gursan

Figure C.31: Assembly bolt.

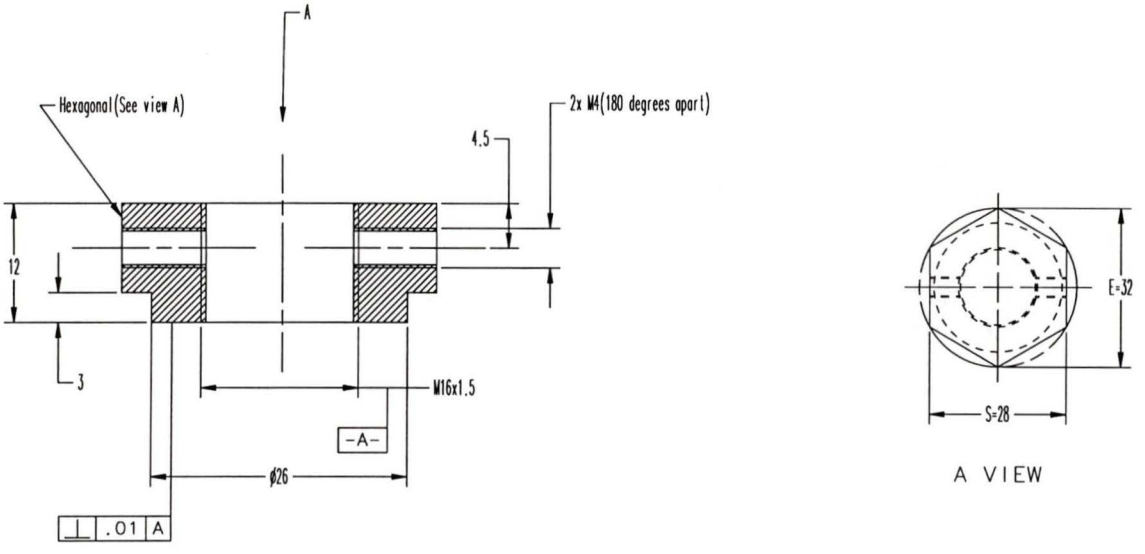

IRIS - Materials & Mechatronics Laboratory	
PROJECT CODE	IRIS-AMD4 - Actuator
PROJECT NAME	Piezoelectric Rotary Actuator
PART NAME / NUMBER	Bearing Preloading Nut / PZT-ACT:15
SCALE	2:1
MATERIAL	304 Stainless
QUANTITY	1
DESIGNED BY	Selcuk Gursan
DRAWN BY	Selcuk Gursan

Figure C.32: Bearing preloading nut.

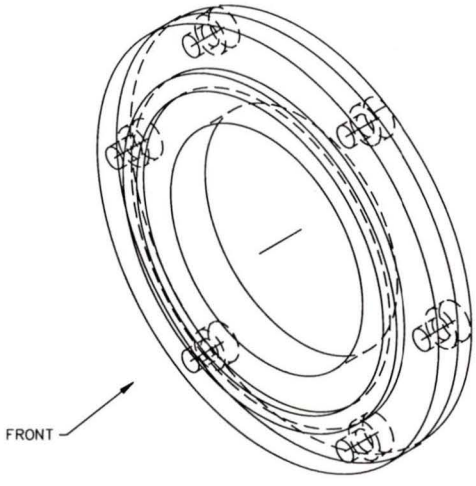

BEARING HOUSING UNIT CAP (ISOMETRIC VIEW)

IRIS - Materials & Mechatronics Laboratory	
PROJECT CODE	IRIS-AMD4 - Actuator
PROJECT NAME	Piezoelectric Rotary Actuator
PART NAME / NUMBER	Bearing Housing Cap / PZT-ACT:16
SCALE	2:1
MATERIAL	6061 - T6
QUANTITY	1
DESIGNED BY	Selcuk Gursan
DRAWN BY	Selcuk Gursan

Figure C.33: Bearing housing unit cap (Isometric view).

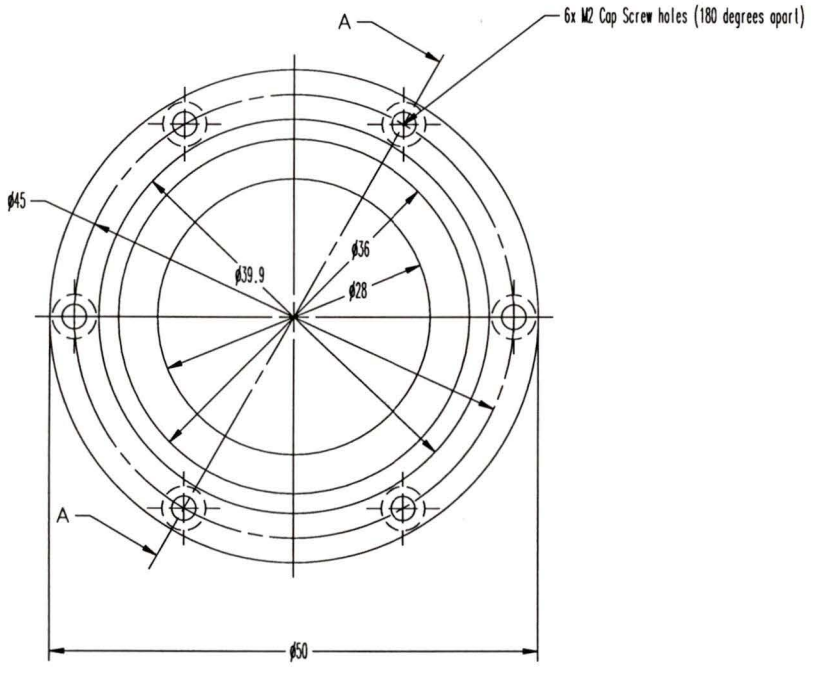

Figure C.34: Bearing housing unit cap (Front view).

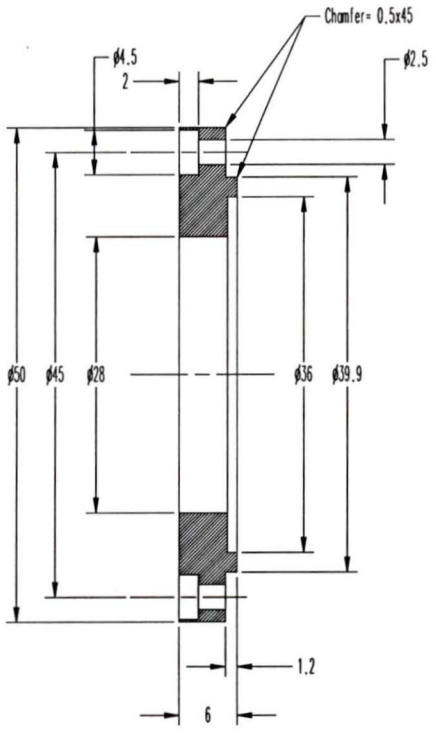

Figure C.35: Bearing housing unit cap (AA Cross-sectional view).

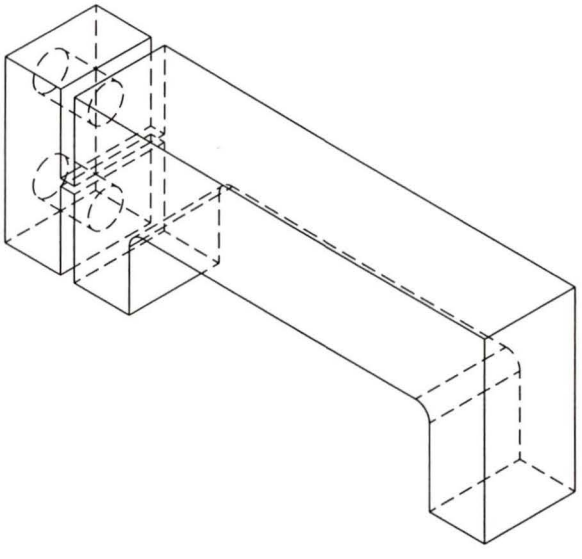

CLAMP FLEXURE (ISOMETRIC VIEW)

IRIS - Materials & Mechatronics Laboratory	
PROJECT CODE	IRIS-AMD4 - Actuator
PROJECT NAME	Piezoelectric Rotary Actuator
PART NAME / NUMBER	Clamp Flexure / PZT-ACT:17
SCALE	2:1
MATERIAL	Grade 2 Titanium
QUANTITY	2
DESIGNED BY	Selcuk Gursan
DRAWN BY	Selcuk Gursan

Figure C.36: Clamp flexure (Isometric view).

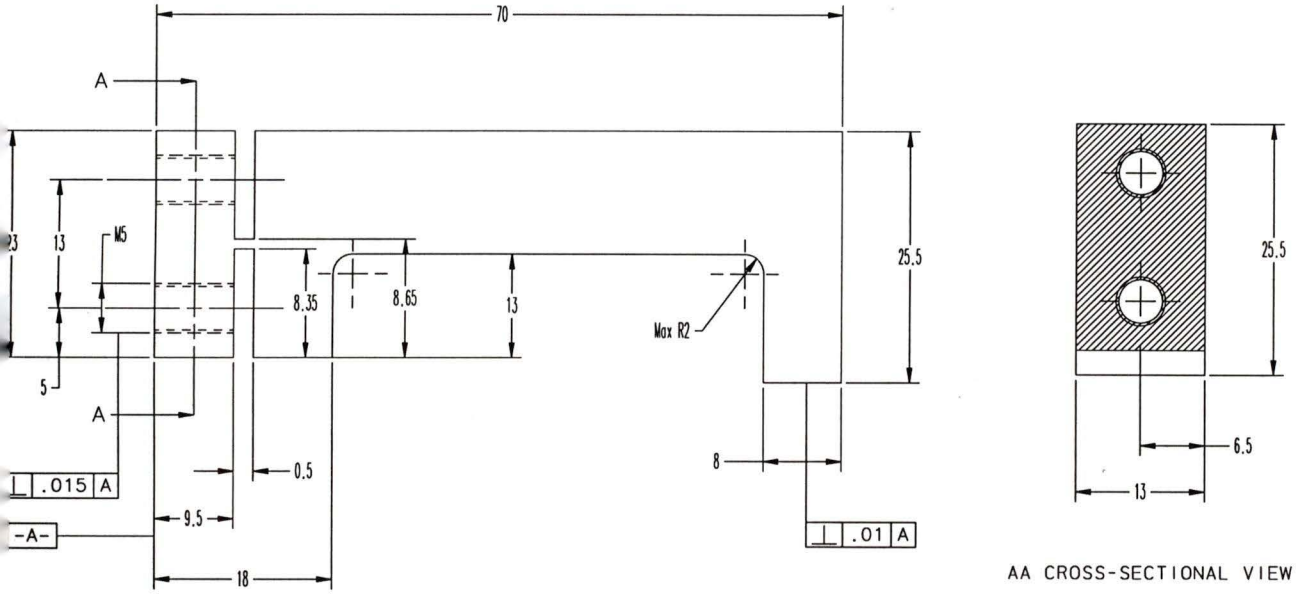

Figure C.37: Clamp flexure (Front view).

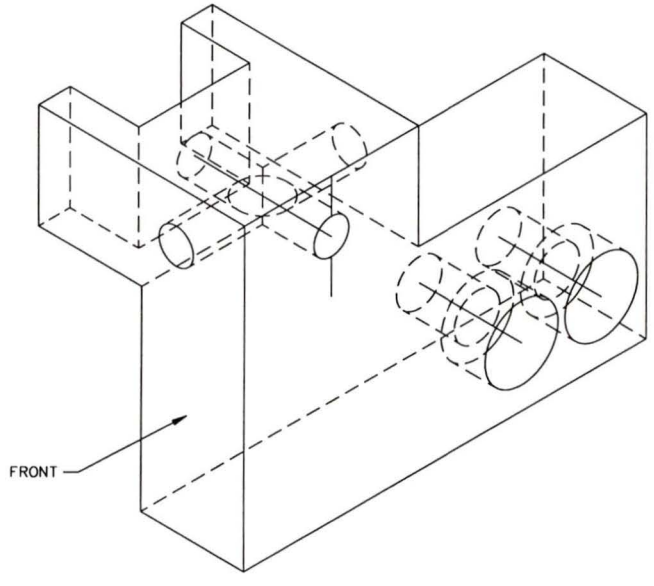

PZT HOLDER (ISOMETRIC VIEW)

IRIS - Materials & Mechatronics Laboratory	
PROJECT CODE	IRIS-AMD4 - Actuator
PROJECT NAME	Piezoelectric Rotary Actuator
PART NAME / NUMBER	PZT HOLDER / PZT-ACT:18
SCALE	2:1
MATERIAL	6061 - T6
QUANTITY	1
DESIGNED BY	Selcuk Gursan
DRAWN BY	Selcuk Gursan

Figure C.38: PZT holder (Isometric view).

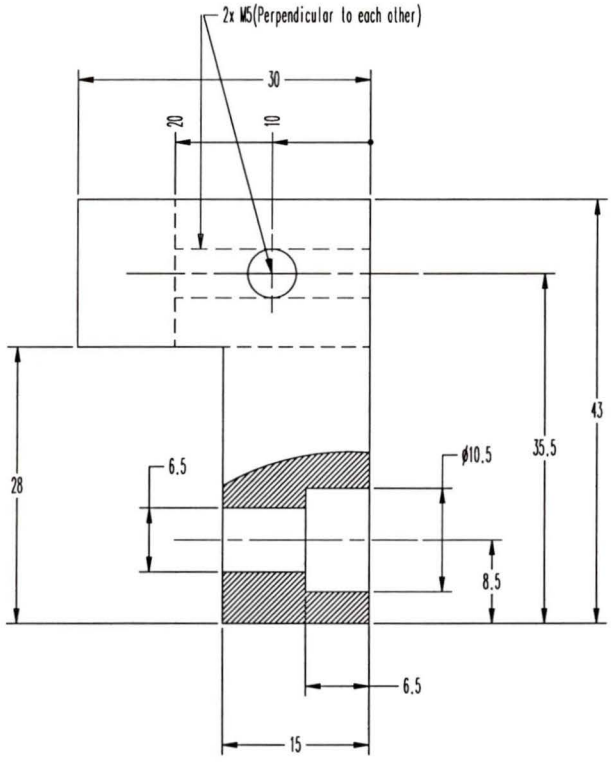

PZT HOLDER (FRONT VIEW)

Figure C.39: PZT holder (Front view).

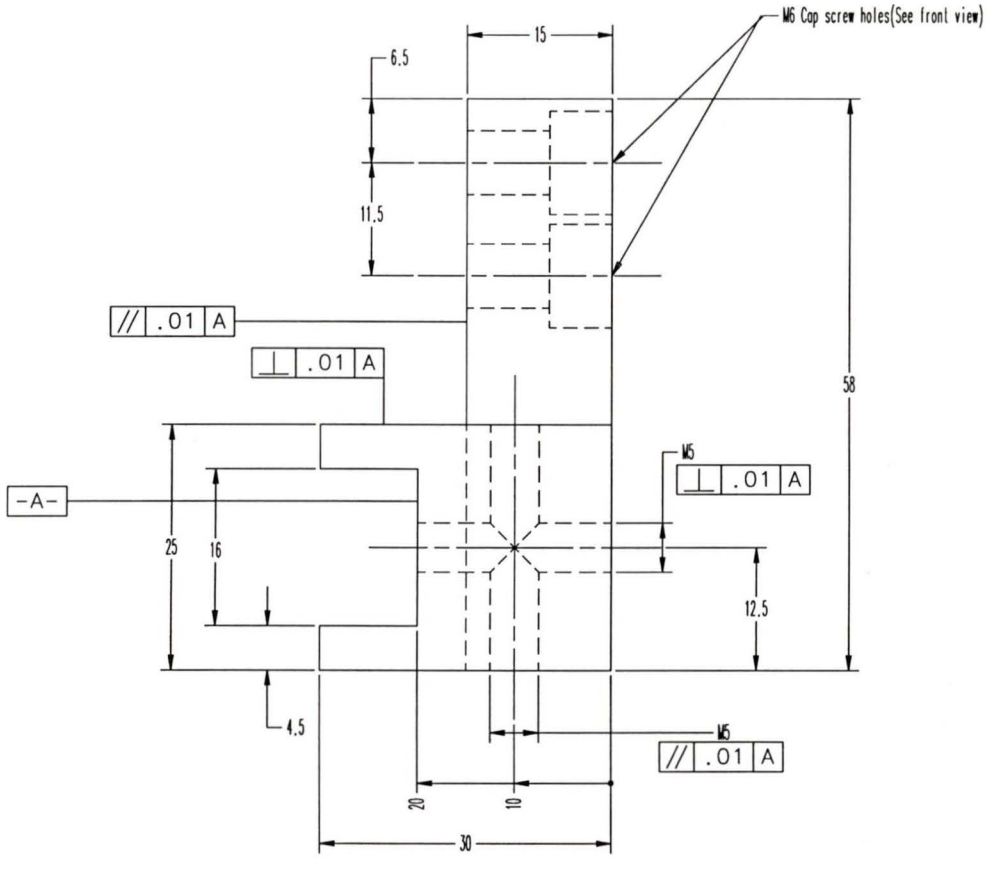

PZT HOLDER (TOP VIEW)

Figure C.40: PZT holder (Top view).

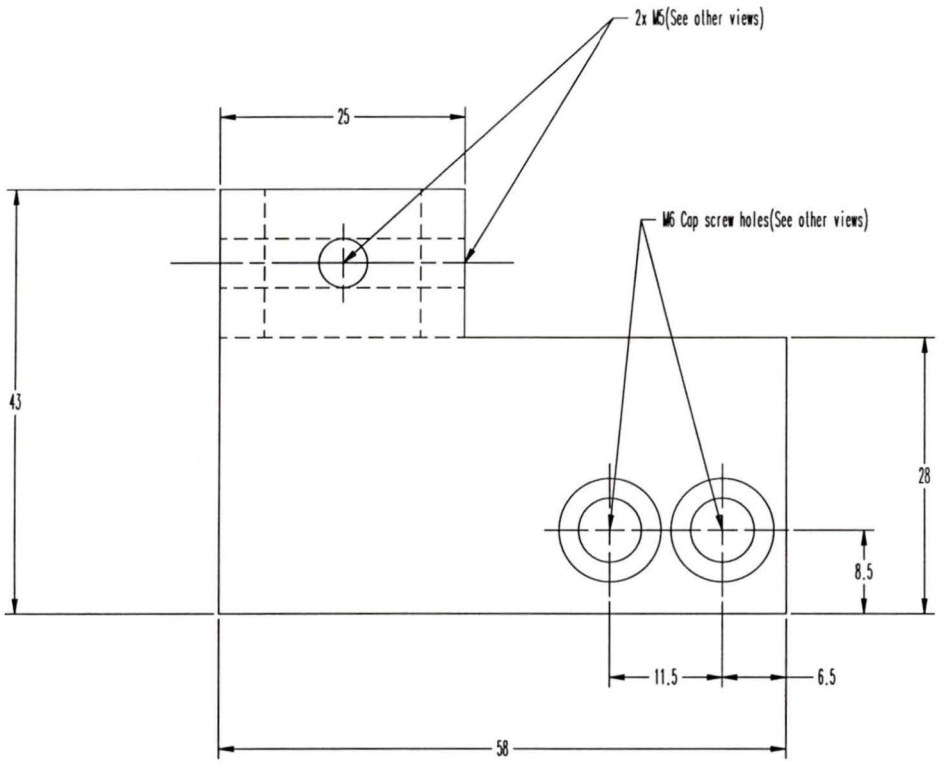

Figure C.41: PZT holder (Right view).

Appendix D

Supplementary Illustrations

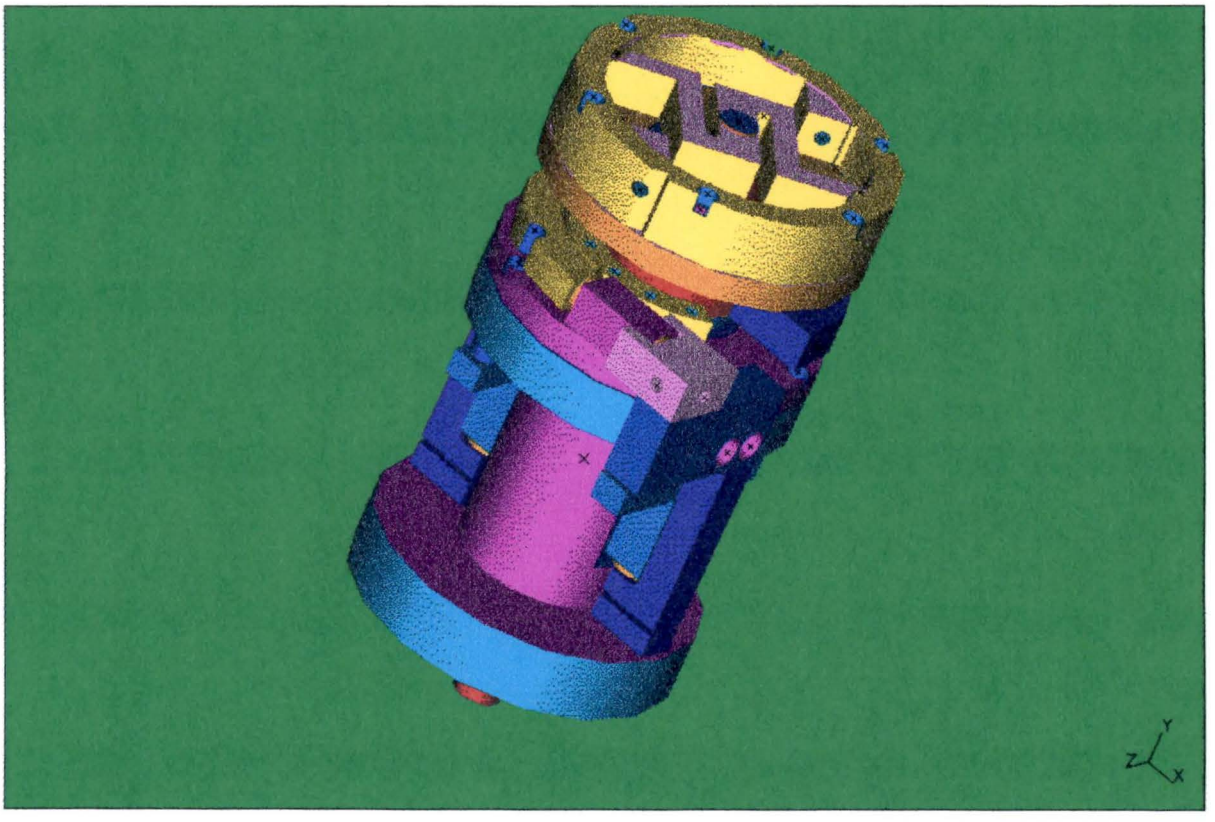

Figure D.1: Shaded image representation of the proposed actuator.

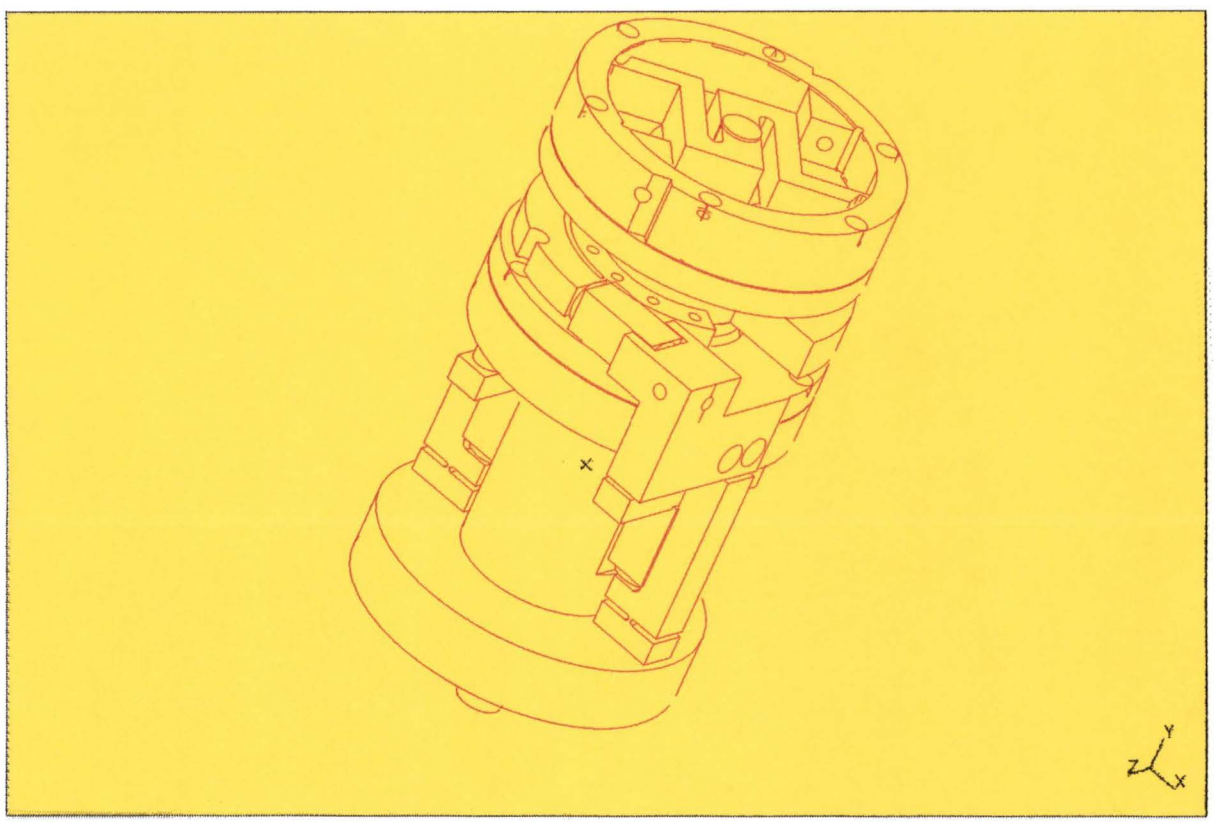

Figure D.2: Surface boundary representation of the proposed actuator.

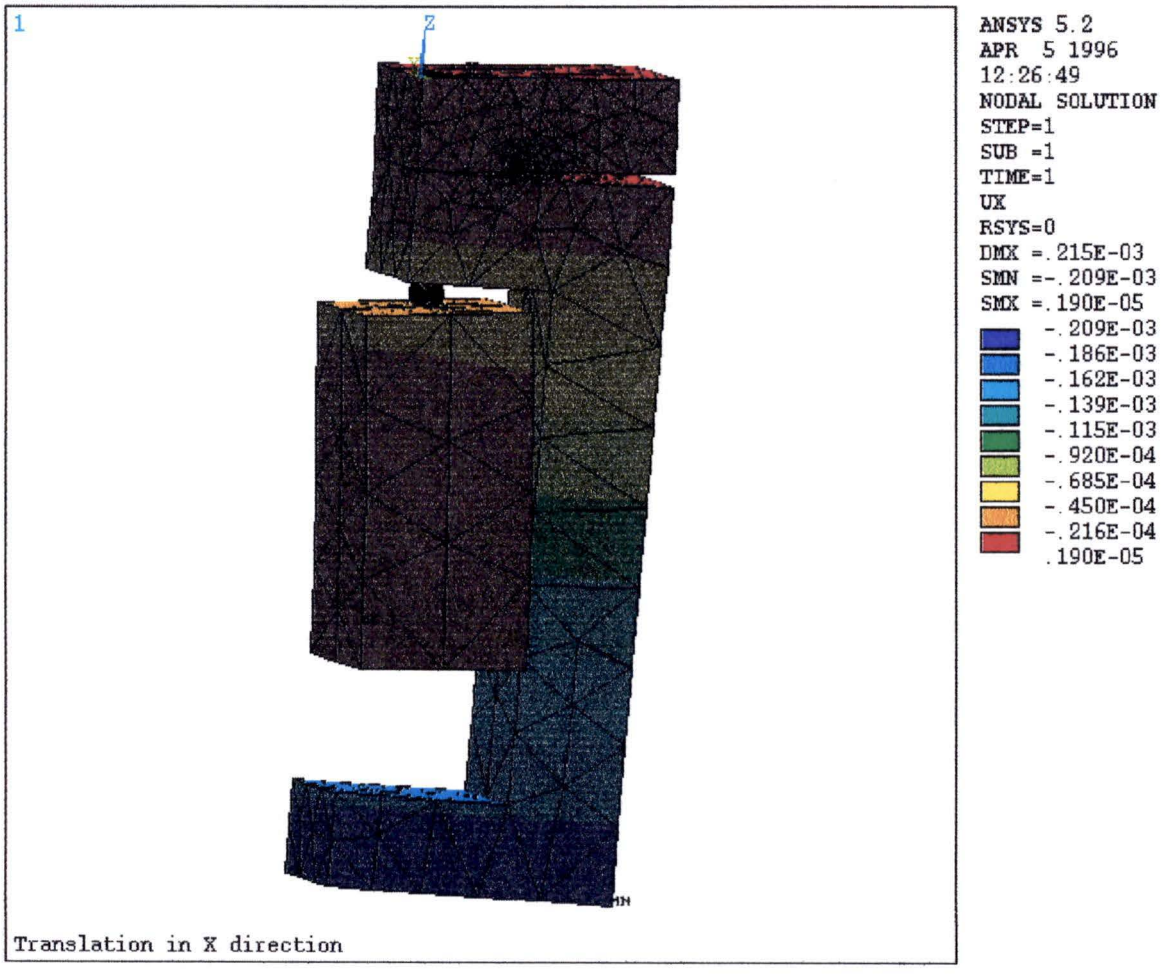

Figure D.3: Free deflection of clamp flexure.

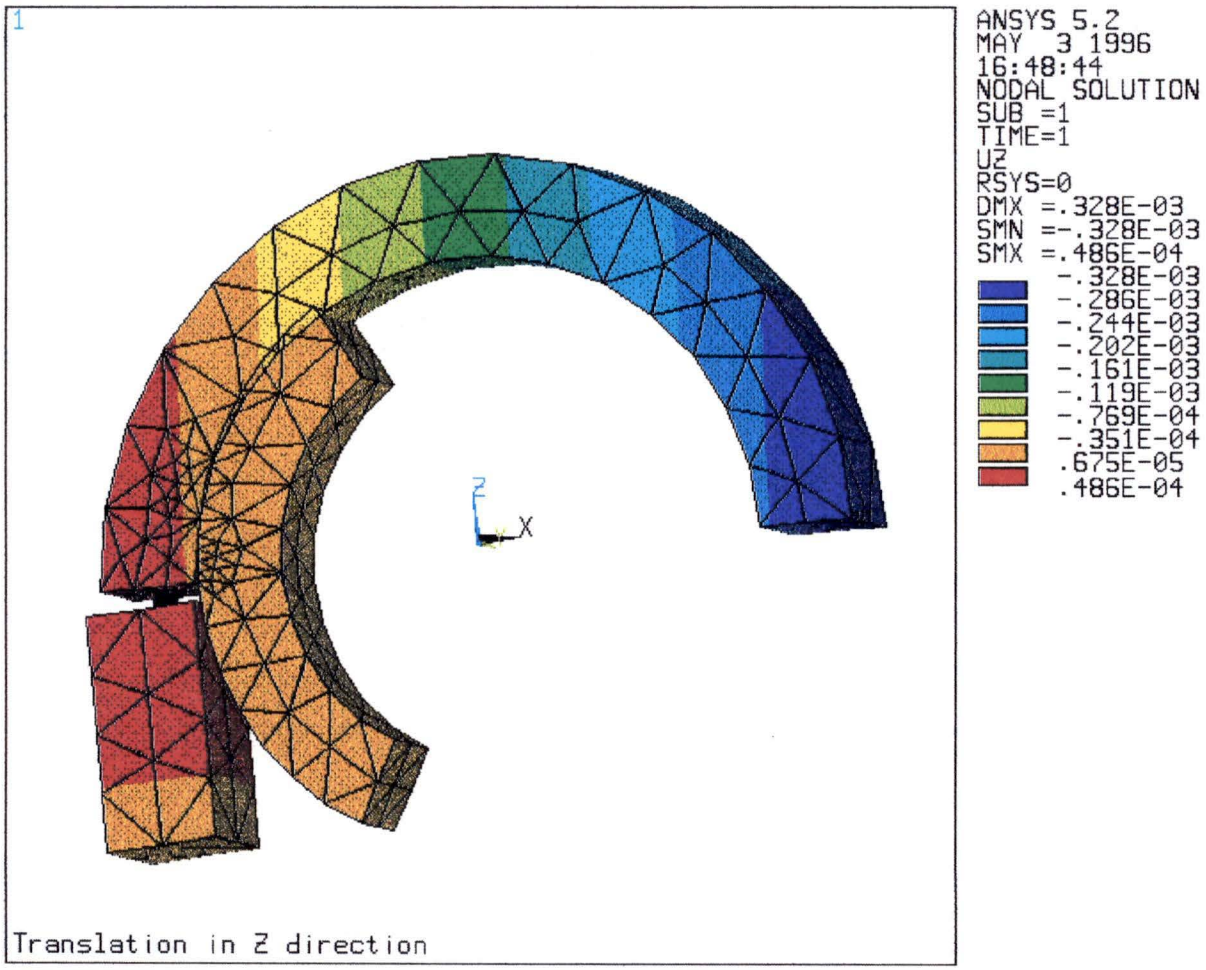

Figure D.4: Free deflection of rotational flexure.

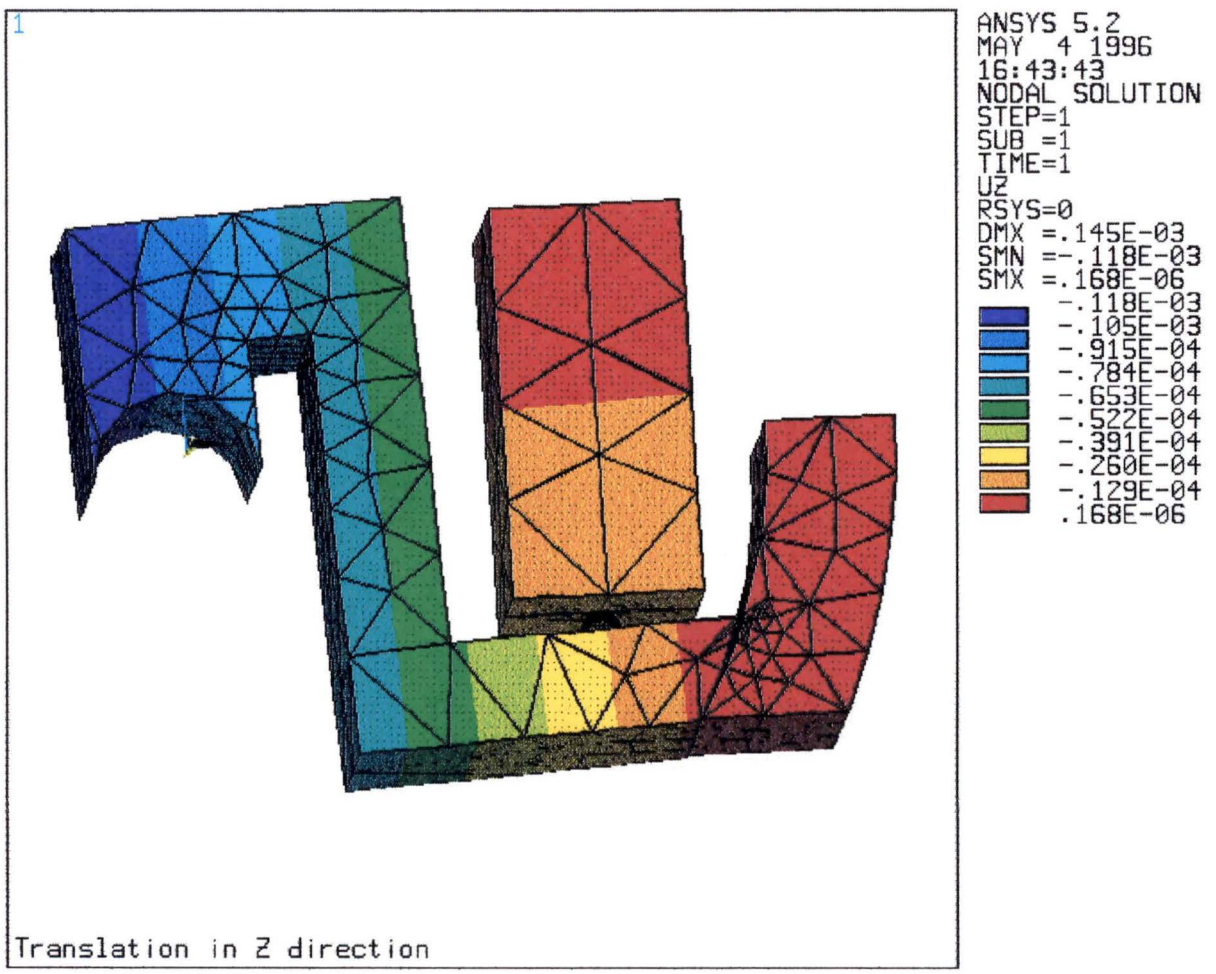

Figure D.5: Free deflection of clutch flexure.

Figure D.6: Experimental set-up.

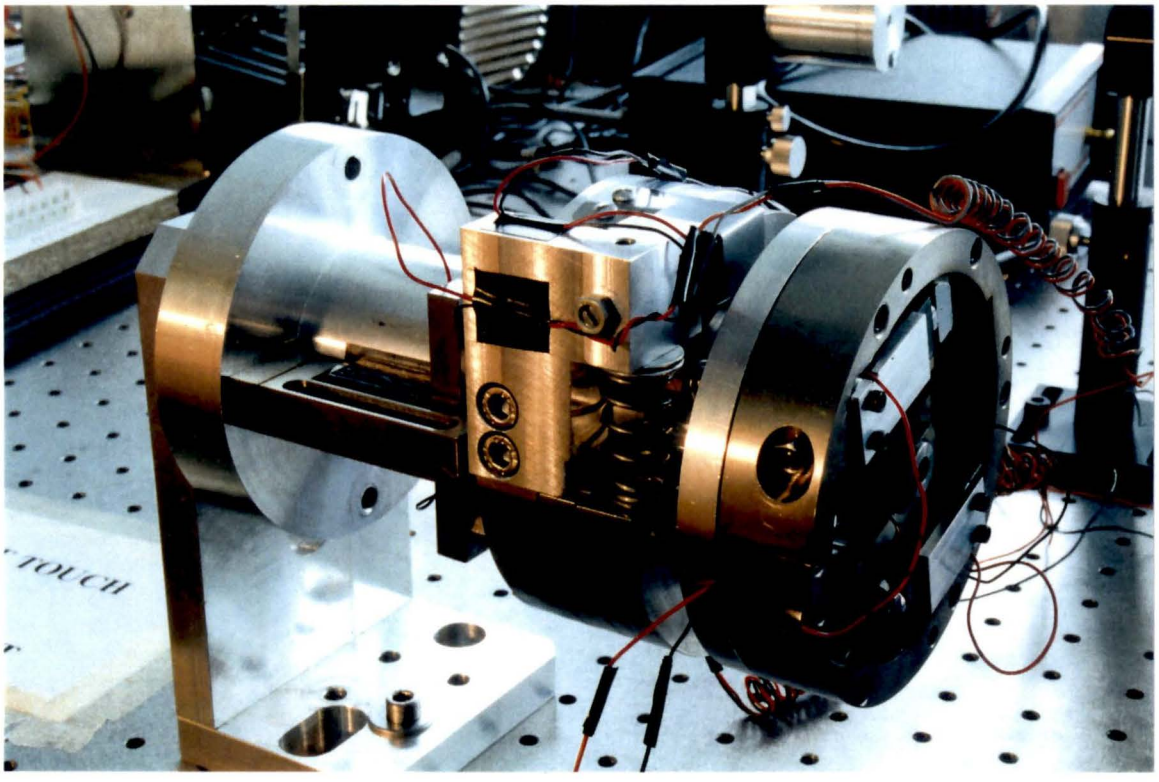

Figure D.7: Built prototype of the proposed piezoelectric rotary actuator.

VITA

Surname: Gursan | Given Names: Selcuk

Place of Birth: Erzurum, Turkey | Date of Birth: February 18, 1965

Educational Institutions Attended:

University of Victoria	1993 – 1996
Dokuz Eylul University	1983 – 1987

Degrees Awarded:

B.Sc. (Honours)	Dokuz Eylul University	1987

PARTIAL COPYRIGHT LICENSE

I hereby grant the right to lend my thesis to users of the University of Victoria Library, and to make single copies only for such users or in response to a request from the Library of any other university, or similar institution, on its behalf or for one of its users. I further agree that permission for extensive copying of this thesis for scholarly purposes may be granted by me or a member of the University designated by me. It is understood that copying or publication of this thesis for financial gain shall not be allowed without my written permission.

Title of Thesis:

Development of A Continuous-Motion Piezoelectric Rotary Actuator for Mechatronics and Micropositioning Applications

Author: [redacted]

Selcuk Gursan

October 28, 1996

Date